RESEARCH ACTIVITIES

PHOTODISSOCIATION DYNAMICS OF HCN IN 135 - 145 nm

T. Nagata, K. Kanda*, T. Kondow, A. Hiraya** and K. Shobatake**

Department of Chemistry, Faculty of Science,
The University of Tokyo, Bunkyo-ku, Tokyo 113
*Department of Fundamental Science, College of Science
and Engineering, Iwaki Meisei University, Iwaki, Fukushima 970
**Institute for Molecular Science, Myodaiji, Okazaki 444

Photodissociation of hydrogen cyanide, HCN, was studied by the measurements of the fluorescence excitation and the optical polarization of subsequent CN(B-X) emission in the wavelength range of 135 - 145 nm at the BL2A line of UVSOR. The synchrotron radiation dispersed by a 1-m Seya-Namioka monochromator was introduced through a LiF window into a flow cell containing HCN gas of ∿20 mTorr. Emission from the product CN(B) radical was collected at right angles to the incident radiation. The polarization anisotropy (R) of the emission was measured with reference to the electric vector of the synchrotron radiation by a polarimeter developed in the present work. Figure 1 shows the observed polarization anisotropy as a function of the excitation wavelength along with the fluorescence excitation spectrum. The prominent peaks appearing in the excitation spectrum were assignable to the ν_2 (bending mode) progression of the C - X transition. Non-zero base line of the specturm is owing to the underlying continuum. The R value was observed to be positive for the ν_2 progression, whereas negative for the continuum. This indicates that the C state belongs to A' symmetry and the continuum to A" symmetry. The vibrational structures observed in the polarization anisotropy are probably ascribed to the ($0\nu_2 1$) and the ($1\nu_2 0$) progressions, while they are not distinct in the excitation spectrum. A possible explanation for this observation is the operation of vibrationally-enhanced predissociation of these vibronic states. Careful examinations of the R value for the ($0\nu_2 0$) progression revealed that the predissociation from the K=1 levels proceeds much faster than that from the K=0 levels of the C state, indicating the heterogeneous predissociation.

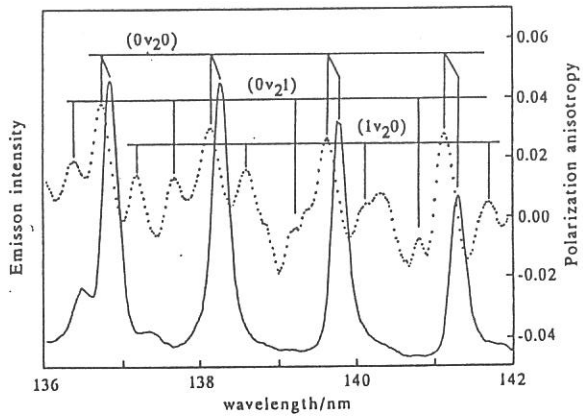

Fig. 1 Fluorescence excitation (solid line) and polarization spectra (dotted line) of HCN

PHOTOCHEMISTRY OF RARE GAS-DIHALOGEN VAN DER WAALS MOLECULES. I. Absorption and Fluorescence Excitation Spectra of Rg_n-Cl_2.

Kiyohiko TABAYASHI, Atsunari HIRAYA, and Kosuke SHOBATAKE
Institute for Molecular Science, Myodaiji, Okazaki 444

One of the merits for the application of SOR light to photochemistry of van der Waals molecules (VDWM) lies in that spectral measurements for both direct-absorption and fluorescence can be easily carried out in wide VUV regions. By studying photo-induced chemistry of rare gas-halogen VDWM systems, in which chemical processes such as excimer formation and predissociation are expected to occur following photo-excitation, it is hoped to pin down the potential energy surfaces relevant to the reaction dynamics. Here we report the preliminary results on the measurements of absorption and fluorescence excitation spectra for Rg_n-Cl_2 clusters generated in supersonic free jets of binary Cl_2/Rg gas mixtures.

Absorption and fluorescence spectra of Xe_n cluster in pure Xe jets have been studied in the wavelength region 1050 - 1550 Å, and the dimer and cluster excitation bands were reasonably assigned (**Figures 1a** and **2a**) [1]. As the amount of Cl_2 gas added to the Xe flow is increased, a strong and broad Xe_n feature gradually disappears and broad absorption bands grow in the whole energy region above 1550 Å. **Figures 1b** and **2b** show typical absorption and fluorescence excitation spectra obtained for a free jet of 6%Cl_2/Xe mixture (The fluorescence in the 180 ~ 650 nm region was detected). The depletion of the Xe_n bands and the growth of a new broad feature in absorption are Cl_2 concentration-dependent, therefore the new bands are assigned as Xe_n-Cl_2 absorption. Under the experimental condition of the $[Cl_2]/[Xe]$ ratio which gives rise to **Figure 1b**, we speculate that Xe-Cl_2 complex contributes much to the new broad feature, since weak Xe_n-Cl_2 ($n \geq 2$) bands are observed near atomic Xe lines in lower $[Cl_2]$ mixtures. In contrast to the absorption, fluorescence spectrum shown in **Figure 2b** has a rather flat and weak base line, indicative of low quantum yield for XeCl(*A*,*B*)

excimer formation channels.

Similar absorption and fluorescence results as above have also been observed in Kr/Cl_2 system.

[1] A. Hiraya and K. Shobatake, **UVSOR** Activity Report, **15**, 27 (1987).

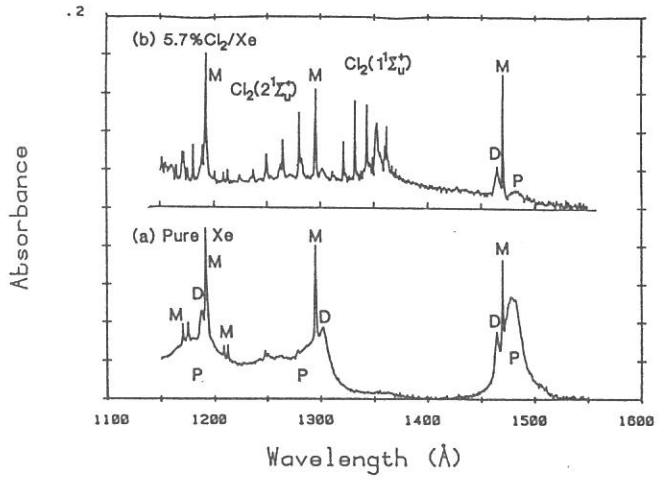

Figure 1. Absorption spectra of free jets of (a) pure Xe and (b) Cl_2/Xe gas mixture at a stagnation temperature T_0 = - 6 °C. Spectral resolution is 1.5 Å.
(a) Pure Xe at a stagnation pressure P_0 = 440 Torr.
(b) 5.7%Cl_2/Xe mixture at P_0 = 550 Torr.
Monomer (atomic), dimer, and cluster bands of Xe are indicated as M, D, and P.

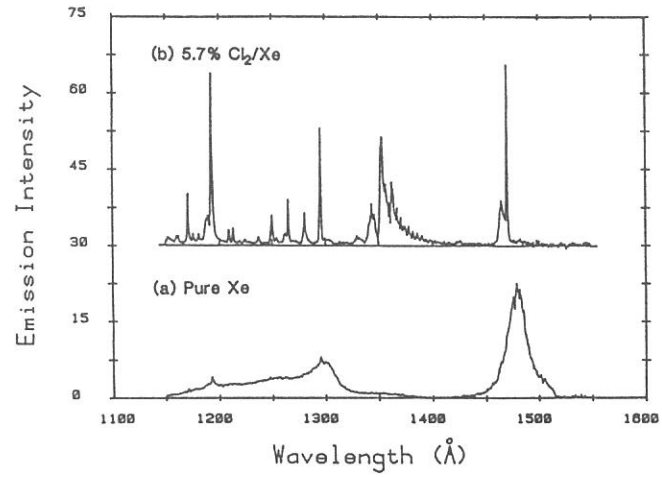

Figure 2. Fluorescence excitation spectra of free jets of (a) pure Xe and (b) 5.7%Cl_2/Xe gas mixture at the same stagnation conditions as described in Figure 1. Spectral resolution is 1.5 A.

PHOTOCHEMISTRY OF RARE GAS-DIHALOGEN VAN DER WAALS MOLECULES. II. VUV Excitation of Xenon Dichloride ($Xe\text{-}Cl_2$).

Kiyohiko TABAYASHI, Atsunari HIRAYA, and Kosuke SHOBATAKE
Institute for Molecular Science, Myodaiji, Okazaki 444

Absorption and fluorescence excitation spectra originated from (1:1) $Xe\text{-}Cl_2$ VDWM in the VUV region have been studied in free jets of regulated Cl_2/Xe/Ne mixtures. In rich Ne-diluent mixtures, possible formation for both Xe_n and $Xe_n\text{-}Cl_2$ can be minimized due to less interaction of Ne than Xe with Xe and Cl_2 molecules.

Figure 1 illustrates absorption spectra for some $[Cl_2]/[Xe]/[Ne]$ concentration conditions, in which the absorption bands due to free Cl_2 molecule are subtracted such that the sharp feature for the Cl_2 transitions disappears. In lean Xe and Cl_2 mixtures, two broad bands in the 1250 - 1550 Å region are intrinsic and its intensities are found to be proportional both to $[Cl_2]$ and [Xe], hence they are assigned to (1:1) $Xe\text{-}Cl_2$ VDWM excitation. In **Figure 2** we show typical fluorescence excitation spectra (with detection of 180 ~ 650 nm radiation) obtained in the region near the lowest atomic Xe (1469.60 Å) line. Although red-shaded band tail resulted from $Cl_2(X^1\Sigma^+_g\text{-}1^1\Sigma^+_u)$ excitation is superimposed in the lower spectral region, the broad feature of $Xe\text{-}Cl_2$ and a new banded system at ~ 1425 Å, which has not been found in the absorption probably due to the limited detection ability, are clearly seen in the figure. From the same consideration of $[Cl_2]$ dependence for the fluorescence intensity as described above for the absorption bands, 1425 Å band is also attributed to $Xe\text{-}Cl_2$ excited state. The broad bands are tentatively assigned to the transitions to charge-transfer states of $XeCl^+Cl^-$ and/or $Xe^+Cl_2^-$ entities, the presence of similar $RgCl^+Cl^-$ complex has been proposed in the environment of Cl_2 trapped in Ar/Ne matrices.[1] Further spectroscopic search for the photo-induced reactions for this VDWM system is under way to clarify the outcome of excited VDWM and the origin for the relevant chemiluminescent processes.

[1] P. Gurtler, H. Kunz, and J. Le Calve, J. Chem. Phys. **91**, 6020 (1989).

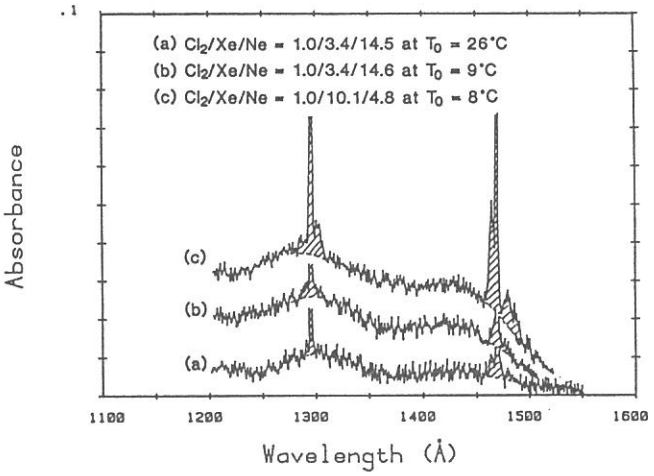

Figure 1. Absorption spectra of Xe-Cl_2 VDWM observed in free jets of Cl_2/Xe/Ne gas mixtures. Here, absorption bands of free Cl_2 are reasonably subtracted and those of $Xe_n(n\geq 1)$ (hatched bands) remain in the figure. Spectral resolution is 3 Å.
(a) $[Cl_2]/[Xe]/[Ne]$ ratio of 1.0/3.4/14.5 at P_0 = 560 Torr and T_0 = 26.4 °C.
(b) $[Cl_2]/[Xe]/[Ne]$ = 1.0/3.4/14.6 at P_0 = 530 Torr and T_0 = 9 °C.
(c) $[Cl_2]/[Xe]/[Ne]$ = 1.0/10.1/4.8 at P_0 = 590 Torr and T_0 = 8 °C.

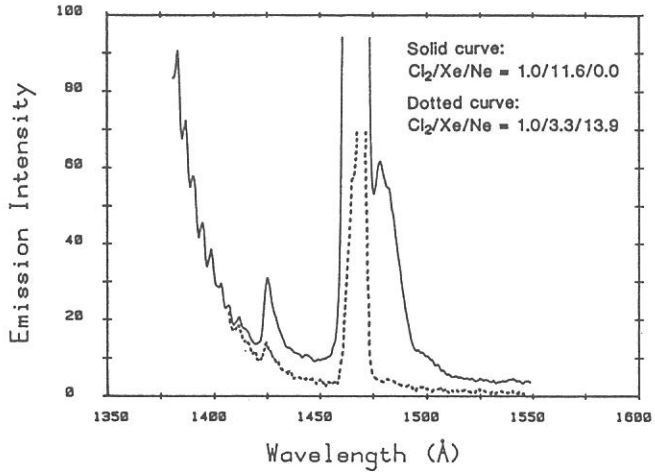

Figure 2. Fluorescence excitation spectra of free jets of Cl_2/Xe/Ne gas mixtures at T_0 = 1 °C. Spectral resolution is 3 Å.
Solid curve: $[Cl_2]/[Xe]/[Ne]$ = 1.0/11.6/0.0 at P_0 = 500 Torr.
Dotted curve: $[Cl_2]/[Xe]/[Ne]$ = 1.0/3.3/13.9 at P_0 = 480 Torr.

Decay of the 4d hole states of Xe studied by
photoelectron-photoelectron coincidence spectroscopy

K. Okuyama, J.H.D. Eland, and K. Kimura

Institute for Molecular Science (IMS), Okazaki 444 Japan

The formation of Xe^{2+} by decay of 4d hole states in xenon has been investigated by observing both the $N_{4,5}OO$ normal Auger spectra and the resonantly excited spectra using synchrotron radiation and a new form of electron-electron coincidence spectroscopy involving a magnetic-bottle time-of-flight analyzer. Direct double Auger processes from the resonance populate all accessible states of Xe^{2+} while indirect processes via superexcited Xe^{+} levels populate ground and lower excited states of Xe^{2+} preferentially.

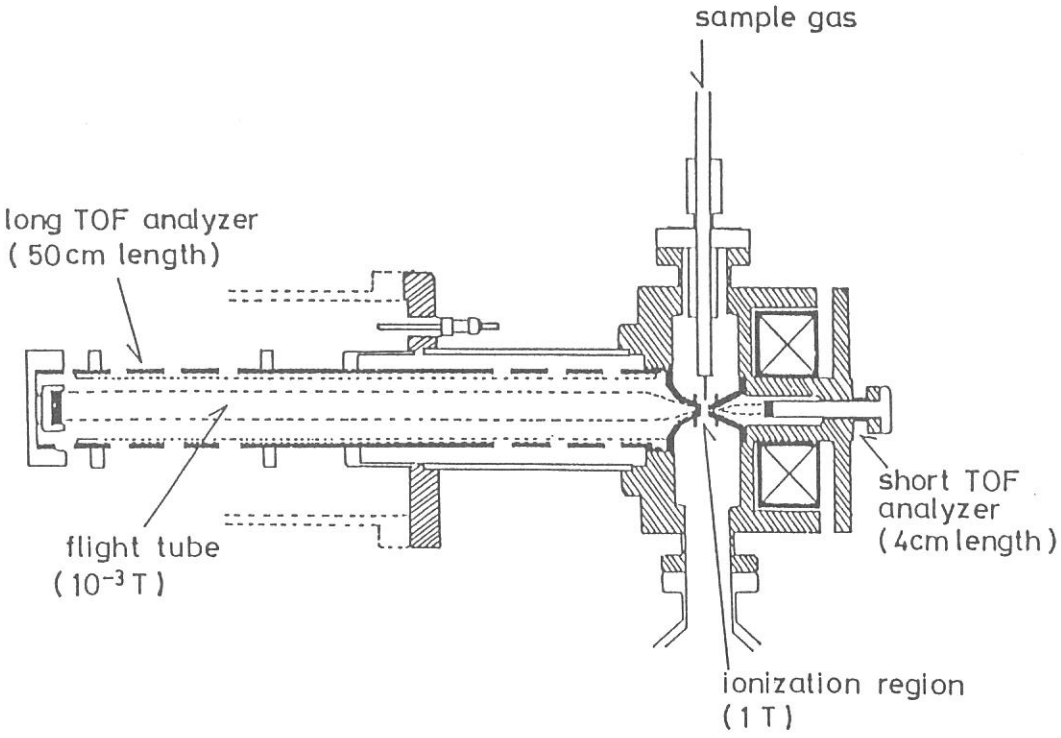

Figure 1. Schematic diagram of the apparatus. External high permeability shields are used to eliminate the geomagnetic field and stray fields from the bending magnets of the stotage ring.

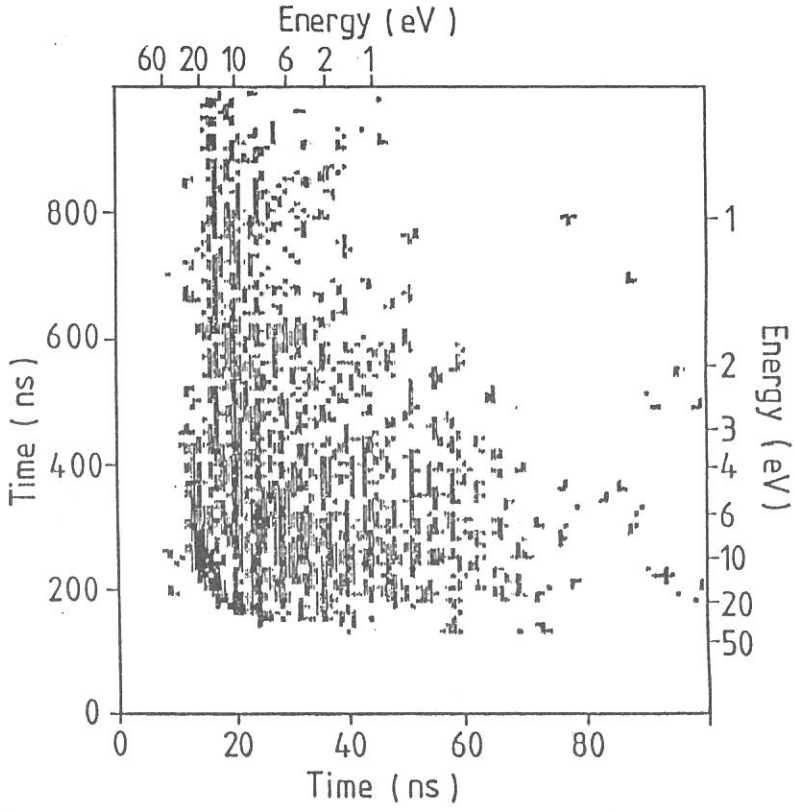

Figure 2. PEPECO spectrum of xenon at 190.4 Å (65.1 eV) on the peak of the $4d^9 5s^2 5p^6 6p$ resonance, with intensities coded as dot density. Times of flight in the short and long analyzers (horizontal and vertical axes, respectively) are on a linear scale, as measured. Single isolated counts have been suppressed to improve contrast for display.

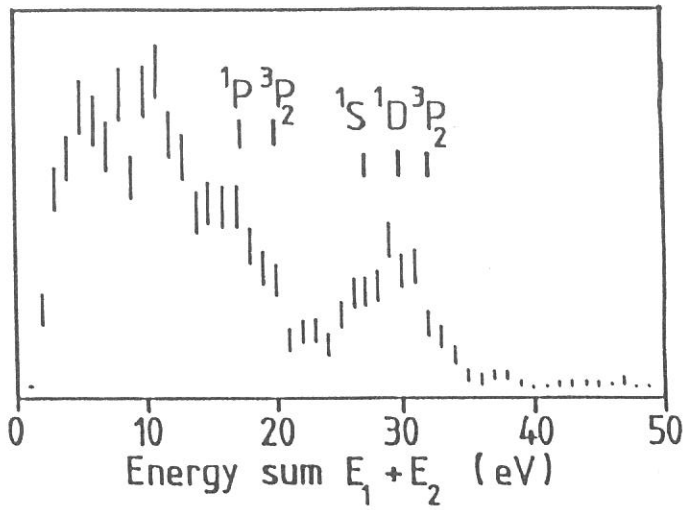

Figure 3. Spectrum of the energy sum $E_1 + E_2$ derived from the 190.4 Å PEPECO spectrum in Figure 2, showing data as error bars two standard dviations long. The positions of some final states of Xe^{2+} are indicated.

Dissociative-ionization processes of CO_2 and CH_4

Yasuhiro Sakai, Byong Soo Min, Takao Mori, Toshinobu Takayanagi,
Takato Hirayama*, Shin-ichi Nagaoka**, and Katsumi Kimura+

Department of Physics, Sophia University, Chiyodaku, Tokyo 102
*Department of Physics, Gakushuin University, Toshimaku, Tokyo 171
**Department of Chemistry, Ehime University, Matuyama 790
+Institute for Molecular Science, Myodaiji, Okazaki 444

The study of dissociative-ionization processes of CO_2 and CH_4 is going on by synchrotron radiation using a technique of threshold-electron photo-ion coincidence(TEPICO) spectroscopy on the beam line BL2B2 with a 1m Seya-Namioka monochromator in the UVSOR facility.

In this study we have adopted an angular discrimination technique using a capillary array plate (CAP) for the threshold electron detection, and the method of time-of-flight (TOF) mass spectroscopy for photo-ion.[1)]

In figure 1, we show the threshold-electron spectrum of CO_2 in the wavelength region between 600 and 660 A.

The highest peak at 639.4 A is for the $C^2\Sigma_g^+$ (0,0,0) state of CO_2^+. Some peaks of the vibrational excited levels of the $C^2\Sigma_g^+$ state are known,[2)] but those peaks are not clear in this spectrum except for the (0,1,0) state.

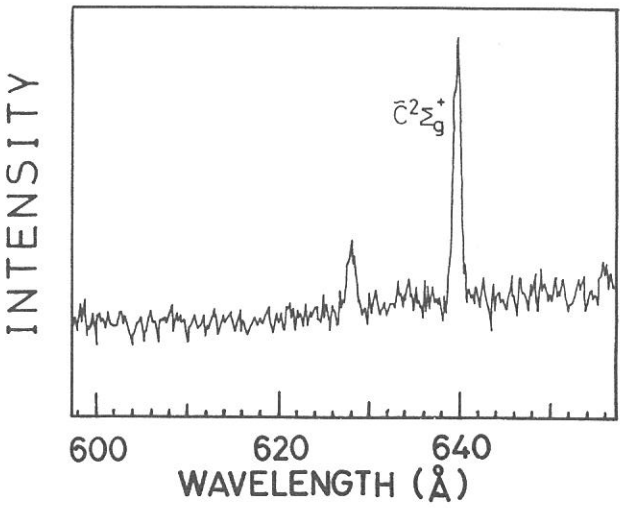

Figure 1. Threshold electron spectrum of CO_2 in the region of 600 - 660 A.

Because the $C^2\Sigma_g^+$ is fully dissociative,[3)] we measured two kinds of ion TOF spectrum at the wavelength 639.4 A.

One is a simple TOF mass spectrum without coincidence, and the other is

a spectrum measured by the TEPICO method.

These spectra are shown in figure 2.

There are four main peaks in the spectrum without coincidence. The largest peak is for the CO_2^+ ion that comes from ionization of the outer valence electrons. There are only two peaks in the TEPICO spectrum. The peak of CO_2^+ becomes notably small compared with the peak in the simple TOF.

These measurements are consistent with the fact that the $C^2\Sigma_g^+(0,0,0)$ state of CO_2^+ is fully dissociative into O^+ and CO.

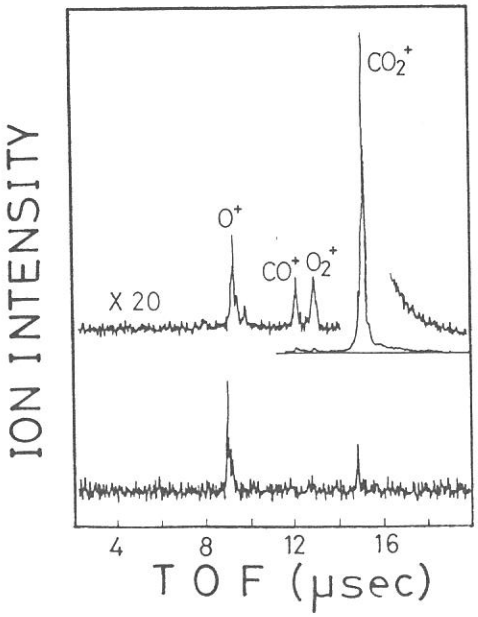

Figure 2. TOF spectra of CO_2 at 639.4 A. Top: without coincidence Bottom: with coincidence

Recently, the results of the TEPICO measurements for CO_2 has been reported by Morioka et al. independently.[4)]

Similar measurements will be done for the $2a_1$ electron ionization of CH_4.

References

1) T.Hirayama, S.Nagaoka and K.Kimura, Atomic Collision Research in Japan (Progress Report), 14, 148(1988).
2) T.Bear and P.M.Guyon, J.Chem.Phys, 85, 4765(1986).
3) J.H.Eland and J.Berkowitz, J.Chem.Phys, 67, 2782(1977).
4) Y.Morioka, T.Matsumoto, T.Endow, T.Hayashi, K.Tanaka and K.Ito, P.F.Activity Report, 6, 260(1988).

SELECTIVE PHOTOIONIZATION OF O_2 IN A FRAMEWORK OF VAN DER WAALS MOLECULES*)

Masatoshi UKAI, Kosei KAMETA, Kyoji SHINSAKA, and Yoshihiko HATANO
Department of Chemistry, Tokyo Institute of Technology, Meguro-ku, Tokyo 152
and
Takato HIRAYAMA, Shin-ichi NAGAOKA, and Katsumi KIMURA
Institute for Molecular Science,
Myodaiji, Okazaki 444, Japan.

Photoionization of binary clusters or van der Waals molecules offers an important opportunity to investigate ionization processes concerning intermolecular process within an intramolecular framework of a cluster. The difference between two distinct components of a cluster give rise to internal energy transfer processes such as intramolecular chemi-ionization and intramolecular charge transfer: the dissociation of the clusters corresponds to the half collisions of ion-molecule reactions. Furthermore, in case where an excited state of neutral or ionizaed molecule involved in the van der Waals complex is unstable, a collision process is only observable in a intramolecular framework of van der Waals molecules.

In this report, we present dissociative photoionization of van der Waals molecules $(O_2)_2$ and ArO_2. In production of O_3^+ ions, an atomic rearrangement was observed to be quite effective. Ionic product of ArO^+ was observed for the first time in such a gas phase collision process, which was not obtained in a "full" ion-molecule reaction. Furthermore, among various ionic states of O_2^+, the $O_2^+(b^4\Sigma_g^-)$ state involved in the ArO_2^+ complex produce the ArO^+ ion preferentially.

The experimental apparatus employed in the present experiment was the same as described in the previous papers [1]. The monochromatized VUV photon beam dispersed by a 1m Seya-Namioka monochromator installed at the beam line BL2-B2 intersected a supersonic nozzle beam at right angle. Ionic products were extracted perpendicularly to both of the photon and the molecular beams, and then mass-analyzed using a quadrupole mass-analyzer. Van der Waals clusters were produced in an expansion of 1:1 gas mixture of O_2 and Ar via a $50\mu m\phi$ nozzle at -100°.

The photoionization efficiency (PIE) curves for O^+ and O_3^+ ions are shown in fig.1. The curve for O^+ was quite similar to the previous measurement [2]. The thresholod structure of the PIE curve for O_3^+ was not identical to that of O^+ [3], which was interpreted as the intramolecular rearrangement or the so-called ion-molecule half-reaction of $O_2^+(a^4\Pi_u, v' \geq 5)\cdot O \rightarrow O_3^+ + O$. However, the overview of O_3^+ curve was not identical to the partial ionization cross section of the $O_2^+(a^4\Pi_u)$ state but rather similar to the total

ionization cross section of O_2 in the higher energy region. It is shown that intramolecular rearrangement occurs after formation of parent ion $(O_2)_2^+$ to give a main contribution to O_3^+ formation.

As mentioned above, ArO^+ was observed for the first time in the present experiment. The PIE curve of ArO^+ is shown in fig.2. The gross feature of the spectrum was completely different from the curve of O^+ or O_3^+. The onset located around 68 nm appearing between those for O^+ and O_3^+. However, it is not due to the molecular rearrangement in less interactive frame between O_2 and Ar. In this region, photoionization into the $O_2^+(b^4\Sigma_g^-)$ state is the most dominant channel. The partial ionization cross section into the $O_2^+(b^4\Sigma_g^-)$ state is also shown in fig.2. The two spectra were identical in this region within experimental error suggesting that the ArO^+ ion is preferentially populated in dissociative ionization of $ArO_2+h\nu\rightarrow ArO_2^+(b^4\Sigma_g^-)+e^-\rightarrow ArO^++O$. This reaction was not observed in a full ion-molecule reaction because of a short lifetime of the $O_2^+(b^4\Sigma_g^-)$ state of about 3×10^{-7}s.

*) to be appeared in *Chem. Phys. Lett.* (in press)

[1] H. Shiromaru et al., *Chem. Phys. Lett.*, 141, 7(1987); K. Kimura et al., *Rev. Sci. Instrum.*, 60, 2205(1989).
[2] T. Hayaishi et al., *J. Phys.*, B19, 2861(1986).
[3] S. H. Linn et al., *J. Chem. Phys.*, 74, 3348(1981).

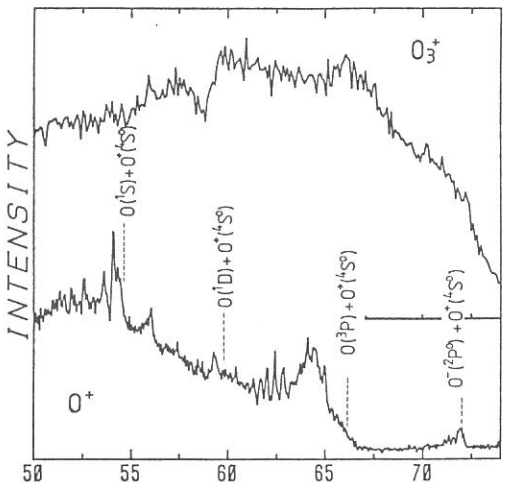

fig.1 PIE curves for O^+ and O_3^+.

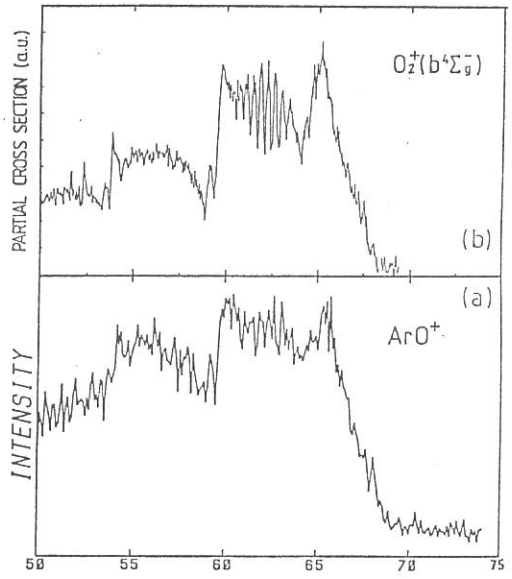

fig.2 PIE curve for ArO^+ (a) and partial ionization cross section of the $O_2^+(b^4\Sigma_g^-)$ state (b).

NEGATIVE-ION MASS SPECTROMETRIC STUDY OF ION PAIR FORMATION IN THE VACUUM ULTRAVIOLET

Koichiro MITSUKE,* Shinzo SUZUKI, Takashi IMAMURA, and Inosuke KOYANO

Institute for Molecular Science, Myodaiji, Okazaki 444
*Department of Chemistry, College of Arts and Sciences,
The University of Tokyo, Komaba, Meguro-ku, Tokyo 153

Ion pair formation from photoexcitation of OCS, CO_2 and N_2O has been studied by mass spectroscopy using synchrotron radiation in the 15 - 40 eV photon energy range.[1,2] A molecular beam apparatus is installed on the beam line BL3B of UVSOR. Negative ions, S^- and O^- from OCS, O^- from CO_2, and O^- from N_2O have been observed as shown in Figs. 1-3. The lowest onset energy of the photodissociation efficiency curve for each ion is in good agreement with the thermochemical threshold for the formation of a pair of a negative ion in the ground ^2P_u state and a counterpart positive ion in the ground $^2\Sigma^+_{(g)}$ state. There exist narrow peaks with medium intensities in the efficiency curves of S^- from OCS and O^- from CO_2; they are identified as resulting from predissociation of the Rydberg states converging to OCS^+ ($\tilde{B}\,^2\Sigma^+$) and CO_2^+ ($\tilde{C}\,^2\Sigma^+_g$), respectively. Broad peaks centered at 18.4 eV (~675 Å) in the efficiency curves for both S^- and O^- produced from OCS are considered to result from the intravalence $9\sigma \rightarrow 10\sigma$ transition and subsequent predissociation of the excited state thus formed (Fig. 1, panels a and b). In addition, a broad band feature is present in the wavelength range of 400 - 610 Å in the O^- efficiency curve (Fig. 1b). A suitable candidate for the corresponding doorway state is the two electron excited state of the neutral OCS formed by simultaneous $9\sigma \rightarrow 10\sigma$ and $3\pi \rightarrow 4\pi$ transitions. In the case of the O^- efficiency curve from CO_2, two maxima observed at 21.4 eV (580 Å) and 23.0 eV (538 Å) are explained as the $3\sigma_u \rightarrow 5\sigma_g$ intravalence transition to the excited valence state which effectively couples with the ion pair continuum (Fig. 2). Several series of peaks in the O^- efficiency curve from N_2O (Fig. 3) are assigned as resulting from predissociation of the Rydberg states

converging to N_2O^+ ($\tilde{A}\,^2\Sigma^+$, $\tilde{B}\,^2\Pi$, and $\tilde{C}\,^2\Sigma^+$). Two Rydberg series, $nd\sigma$ and $nd\pi$, converging to the vibrational ground state of N_2O^+ ($\tilde{C}\,^2\Sigma^+$) are observed most prominently. In contrast, only the members of the $nd\pi$ series can be found among the Rydberg states converging to N_2O^+ [$\tilde{A}\,^2\Sigma^+(0,0,0)$ and $(1,0,0)$].

1) K. Mitsuke, S. Suzuki, T. Imamura, and I. Koyano, *J. Chem. Phys.*, in press.

2) K. Mitsuke, S. Suzuki, T. Imamura, and I. Koyano, *J. Chem. Phys.*, submitted.

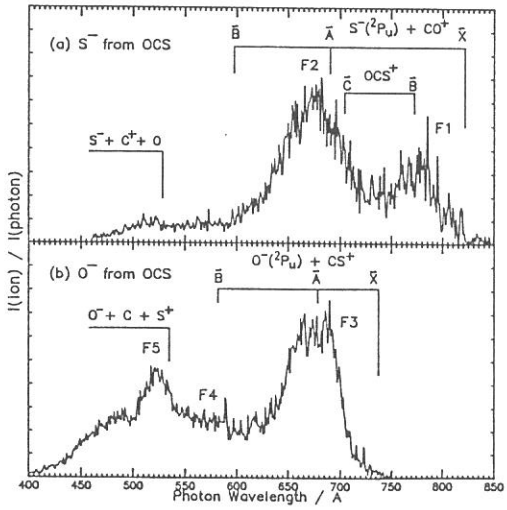

Figure 1. Photodissociation efficiency curves for S^- (panel a) and O^- (panel b) produced from OCS taken at a wavelength resolution (fwhm) of 0.8 Å and wavelength intervals of 1 Å. The vertical lines indicate the thermochemical thresholds for the formation of $S^-(^2P_u) + CO^+$ ($\tilde{X}$, $\tilde{A}$, and $\tilde{B}$), $O^-(^2P_u) + CS^+$ ($\tilde{X}$, $\tilde{A}$, and $\tilde{B}$), $S^-(^2P_u) + C^+(^2P_u) + O$, and $O^-(^2P_u) + C + S^+(^4S_u)$, and the ionization limits for the vibrational ground states of OCS^+ ($\tilde{B}\,^2\Sigma^+$ and $\tilde{C}\,^2\Sigma^+$).

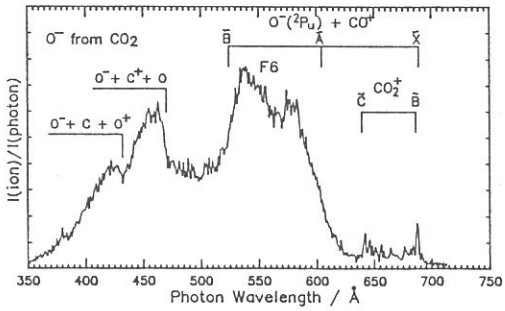

Figure 2. Photodissociation efficiency curve for O^- produced from CO_2 taken at a wavelength resolution (fwhm) of 0.8 Å and wavelength intervals of 1 Å. The vertical lines indicate the thermochemical thresholds for the formation of $O^-(^2P_u) + CO^+$ ($\tilde{X}$, $\tilde{A}$, and $\tilde{B}$), $O^-(^2P_u) + C^+(^2P_u) + O$, and $O^-(^2P_u) + C + O^+(^4S_u)$, and the ionization limits for the vibrational ground states of CO_2^+ ($\tilde{B}\,^2\Sigma_u^+$ and $\tilde{C}\,^2\Sigma_g^+$).

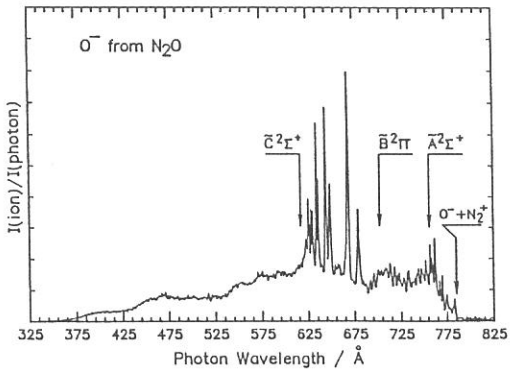

Figure 3. Photodissociation efficiency curve for O^- produced from N_2O taken at a wavelength resolution (fwhm) of 0.8 Å and wavelength intervals of 1 Å. The vertical lines indicate the thermochemical threshold for the formation of $O^-(^2P_u) + N_2^+(\tilde{X}\,^2\Sigma_g^+)$ and the ionization limits for the vibrational ground states of N_2O^+ ($\tilde{A}\,^2\Sigma^+$, $\tilde{B}\,^2\Pi$, and $\tilde{C}\,^2\Sigma^+$).

THE STUDY OF THE ION-PAIR PROCESS SF_6 --> F^- + SF_5^+ USING SYNCHROTRON RADIATION

Shinzo SUZUKI, Koichiro MITSUKE*, Takashi IMAMURA and Inosuke KOYANO

Institute for Molecular Science, Myodaiji, Okazaki 444
*Department of Chemistry, College of Arts and Sciences, The University of Tokyo, Komaba, Meguro-ku, Tokyo 153

The study of ion-pair formation from photoexcitation of molecules gives information about the interaction between the ion-pair states and the excited valence or Rydberg states of molecules.[1)]

In the present paper, the ion-pair process SF_6 --> F^- + SF_5^+ has been studied by measuring the efficiency curve for the formation of F^- in the 400-1000 Å wavelength range at BL3B of UVSOR. Figures 1 and 2 show the efficiency curves of F^- in the 400-700 Å and 700-1000 Å wavelength range, respectively. There exists three distinct peaks in the wavelength range 450-510 Å. The positions and the spacings of these peaks agree well with those of the Rydberg transitions of SF_6 observed in the VUV absorption spectrum by K. Codling.[2)]

In addition, several structures were observed in the wavelength range 510-700 Å and 700-1000 Å. Based on the discussion by Sasanuma et al.[3)], the position of the allowed transitions from a valence orbital to a virtual orbital of SF_6 are indicated by hatched rectangles in Figures 1 and 2. The four broad bands in the wavelength range 700-1000 Å and the band around 620 Å are then reasonably attributed to the F^- ion

formation following these intravalence transitions. However, no clear peaks are assignable to the known Rydberg transitions in the 550-650 A wavelength range and the valence transitions in the 450-510 Å wavelength range, as also indicated in Figure 1. These findings suggest the occurrence of some selectivities concerning the transitions between the ion-pair states and the excited valence or Rydberg states of SF_6.

REFERENCES

1) K. Mitsuke, S. Suzuki, T. Imamura, and I. Koyano, UVSOR Activity Report 1989 and references cited therein
2) K. Codling, J. Chem. Phys., 44, 4401(1966)
3) M. Sasanuma, E. Ishiguro, H. Masuko, Y. Morioka, and M. Nakamura, J. Phys. B, 11, 3655(1978)

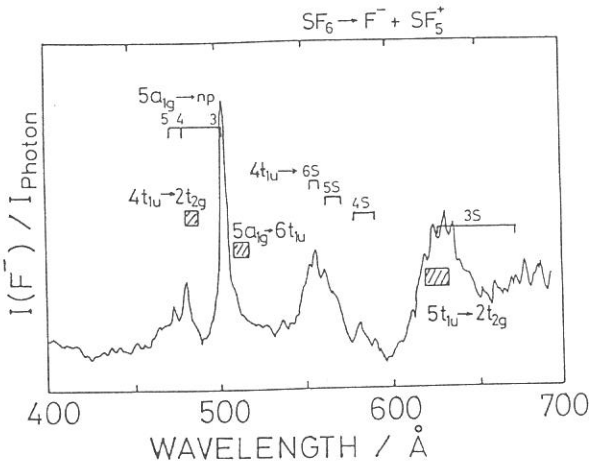

Figure 1

The efficiency curve for F^- in the wavelength range 400-700 A

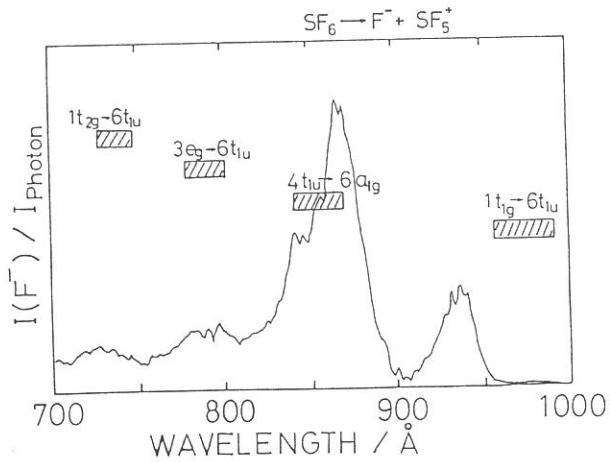

Figure 2

The efficiency curve for F^- in the wavelength range 700-1000 A

THE STUDY OF THE ION-MOLECULE REACTION $Ne^+(^2P_{3/2})$ + OCS USING DODECAPOLE ION BEAM GUIDE.

Shinzo SUZUKI, Kazuhiko OKUNO*, Takashi IMAMURA and Inosuke KOYANO

Institute for Molecular Science, Myodaiji, Okazaki 444
*Department of Physics, Faculty of Science, Tokyo Metropolitan University, Setagaya-ku, Tokyo 158

For obtaining absolute cross sections of ion-molecule reactions, high and equal collecting efficiency is necessary for all product ions. A dodecapole ion-beam guide has been installed as a reaction chamber in the TEPSICO-II apparatus[1] at beam line BL3B of UVSOR because of its almost hundred percent collecting efficiency for a wide range of kinetic energies of primary and secondary ions.[2]

Its performance has been examined utilizing Ne^+ ions produced by photoionization of Ne at the $^2P_{3/2}$ threshold.[3] Figure 1 shows the pressure dependences of the relative intensities of all product ions of the ion-molecule reaction $Ne^+(^2P_{3/2})$ + OCS at 1.7 eV center-of-mass collision energy. The solid line indicates the relation $I = I_0 n\sigma l$, where I_0, n, l, and σ denote the intensity of Ne^+ with no reactant gas, the number density of neutral reactant in the dodecapole collision chamber, the length of the dodecapole collision chamber (9cm), and the partial cross section for each product ion, respectively. Table 1 gives a summary of the cross sections for the individual product channels, determined from the plot of Figure 1. It is seen that the agreement between the sum of the partial cross sections and

the attenuation cross section (σ_{att}) of Ne^+ is excellent.

Figure 2 shows the dependence of the attenuation cross section for $Ne^+(^2P_{3/2})$ + OCS on the collision energy. It seems that the collision energy dependence deviates from $\sigma_{att} \propto E_{cm}^{-1/2}$ (shown by the dotted line), which was derived from the expression of the classical orbiting cross section for resonant charge transfer reactions, above 1 eV collision energy.

REFERENCES

1) S. Suzuki, S. Nagaoka, I. Koyano, K. Tanaka, and T. Kato, Z. Phys. D4, 111(1986)
2) S. Suzuki, T. Imamura, I. Koyano, and K. Okuno, UVSOR Activity Report 1988, p.15
3) S. Suzuki, T. Imamura, I. Koyano, and K. Okuno, Rev. Sci. Instrum., 60, 2186(1989)

Figure 1

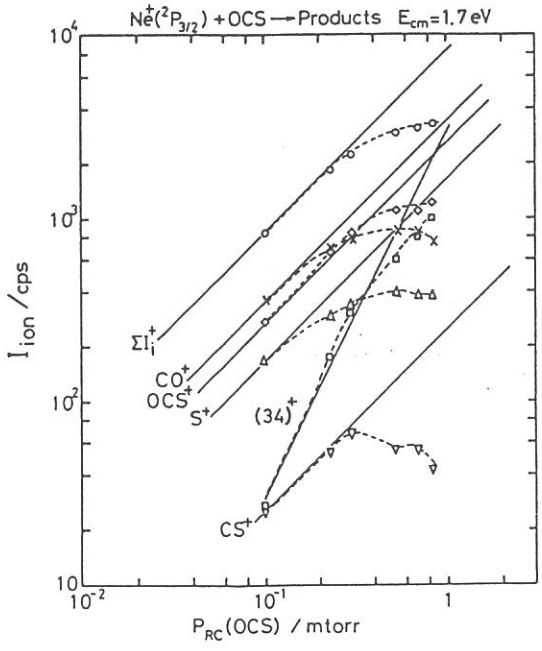

TABLE I. Partial cross sections and the attenuation cross section in the ion–molecule reaction Ne^+ + OCS at 1.7 eV c.m. collision energy.

σ_{CO}^+	18.6 Å²
σ_{OCS}^+	15.3 Å²
σ_{S}^+	9.3 Å²
σ_{CS}^+	1.3 Å²
$\sigma_{\Sigma i}^+$	45.5 Å²
σ_{att}	46.2 Å²

Figure 2

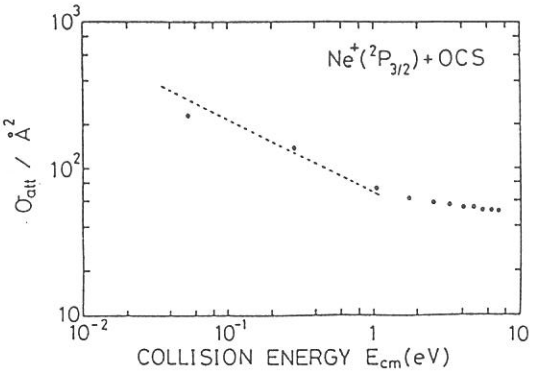

ANGULAR DISTRIBUTION OF POSITIVE-ION PAIRS PRODUCED BY DISSOCIATIVE DOUBLE PHOTOIONIZATION OF OCS

Toshio MASUOKA and Inosuke KOYANO*

Department of Physics, Osaka City University, Sumiyoshi, Osaka 558
* Institute for Molecular Science, Myodaiji, Okazaki 444

The angular distribution of photodissociation products is an important source of information on the symmetry of the dissociating parent state(s)[1,2]. We report here the first observation of angle-dependent dissociation of OCS^{2+} produced by direct (not via Auger decay) double photoionization.

Figure 1 shows an example of the PIPICO (photoion-photoion coincidence) spectrum of OCS, taken at 70 eV of photon energy and in the direction of the electric vector of the polarized incident photons. Five dissociation channels have been identified as indicated in the figure (also given in the preceding report). Such spectra were measured as a function of photon energy in two directions, horizontal and vertical, corresponding respectively to the parallel and perpendicular directions to the electric vector of the incident photons. The results for the four dissociation channels are summarized in Fig. 2 in the form of the ratio of the PIPICO fractions obtained in the vertical direction to those obtained in the horizontal direction.

The figure clearly shows that the dissociation channels fall into three types in the context of the angular distribution of the ionic fragments: Type (1) in which ion-pairs are scattered more strongly in the vertical direction (the channel $CS^+ + O^+$), Type (2) in which ion-pairs are scattered more strongly in the horizontal direction (the channel $O^+ + S^+ + C$), and Type (3) in which ion-pairs are scattered almost equally in both directions (the channels $CO^+ +$

S^+ and $C^+ + S^+ + O$). It is interesting to note that only the channel $CS^+ + O^+$ shows photon energy dependence of the ratio. The anisotropy parameter β for the channel $O^+ + CS^+$ (at 70 eV, for example) and for the channle $O^+ + S^+ + C$ (at atll energies) are estimated to be about -0.2 and 0.7, respectively. It is worth mentioning here that the nondissociative ions OCS^+ and OCS^{2+} also show anisotropy in the TOF mass spectra. This evidently reflects the anisotropy of photoelectrons used for gating the TOF measurements.

The analysis of these results, which is under way, is complicated by the fact that the angular distribution is not simply determined by the relation between the initial and the fifnal ionic states but we have to consider the symmetry of the total final state, consisting of molecular dication and two ejected electrons.

References

1) R. N. Zare, Mol. Photochem. 4, 1 (1972)
2) J. L. Dehmer and D. Dill, Phys. Rev. A 18, 164 (1978)

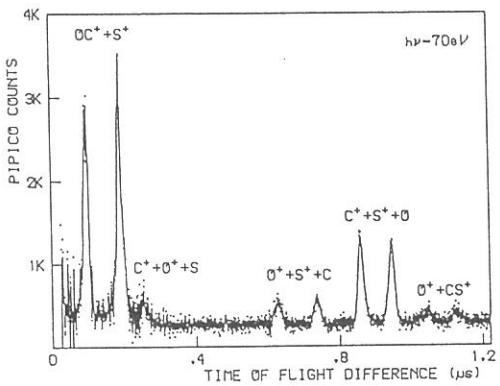

Fig. 1 PIPICO spectrum of OCS measured in the horizontal direction at 70 eV of the incident photon.

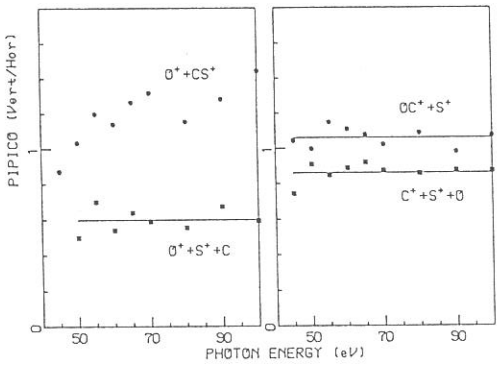

Fig. 2 Angular dependence of the intensities of the four PIPICO peaks as a function of photon energy.

DISSOCIATIVE DOUBLE PHOTOIONIZATION OF CH_3F STUDIED BY PHOTOION-PHOTOION COINCIDENCE METHOD

Toshio MASUOKA and Inosuke KOYANO*

Department of Applied Physics, Osaka City University, Sumiyoshi, Osaka 558
*Institute for Molecular Science, Okazaki, Aichi 444

Double photoionization of gas molecules takes place when they absorb enough photon energy for two-electron ejection. Because of the Coulomb repulsion between two positive holes, the doubly charged parent ions are not particularly stable and subsequently dissociate into two ionic fragments after a very short lifetime. Only little information on the doubly charged ion CH_3F^{2+} has been reported.[1-3] In the present study, we report the dissociative double photoionization of CH_3F examined by use of synchrotron radiation, mass spectrometry, and photoion-photoion coincidence (PIPICO) method.[4]

Stable CH_3F^{2+} was not observed in the whole energy range studied in a μsec time scale. This means that all the doubly charged parent ions break up into fragments without a barrier. A PIPICO spectrum measured at a photon energy of 97.2 eV (Fig. 1) shows that at least four types of dissociation processes occur: $CH_3F^{2+} \rightarrow H^+ + CH_nF^+ + n.f.$ (n=0-2) (1), $H_2^+ + CHF^+$ (2), $H^+ + CH_n^+ + n.f.$ (n=0-2) (3), and $H^+ + F^+ + n.f.$ (4). Here n.f. stands for neutral fragment(s). At low energies below about 39 eV, only the four channels are open, i.e., the C-H bond breakage (1) and a rearrangement reaction (2) (Fig. 2). These two types of processes are due to two-electron ejection from the outermost 2e orbital. The lowest-energy channel is $H^+ + CH_2F^+$ with a threshold at about 35 eV. As the photon energy increases, high vibrational modes of the electronic states ^1E, $^1A_1$ $(2e)^{-2}$ are excited and other three dissociation channels appear.

The fragmentation into $H^+ + CH_n^+ + n.f.$ (the C-F as well as C-H bond breakage) starts to occur at about 39.6 eV because of two-electron ejection such as $(5a_1 2e)^{-1}$ and $(1e2e)^{-1}$, where $5a_1$ and 1e orbitals are related to the C-F bond. Process (4) is due to two-step dissociation, $CH_3F^{2+} \rightarrow CH_3^+ + F^+$, $CH_3^+ \rightarrow H^+ + n.f.$, and is probablly related to the electron configu-

ration $(3a_1 2e)^{-1}$ and $(3a_1 4a_1)^{-1}$. The observed dissociation channels are correlated with the electronic states of CH_3F^{2+} measured experimentally[2,3] and calculated by the Green's function method.[1] From an analysis of the PIPICO spectra, kinetic energies released in the dissociation processes are deduced. Anisotropic distributions of fragment ions produced in process (4) have been observed, representing the first case for the direct double photoionization from valence orbitals. This result is reported separately.[5]

References

1) C. M. Liegener, Chem. Phys. 151, 83 (1988).

2) W. E. Moddeman, Auger spectroscopy of simple gaseous molecules, Dissertation, University of Tennesee (1970). Oak Ridge Nat. Lab. Rep. No. ORNL-TM-3013.

3) W. J. Griffiths and F. M. Harris, Int. J. Mass Spectrom. 85, 69 (1988).

4) T. Masuoka, T. Horigome, and I. Koyano, Rev. Sci. Instrum. 60 2179 (1989).

5) T. Masuoka and I. Koyano, in this report.

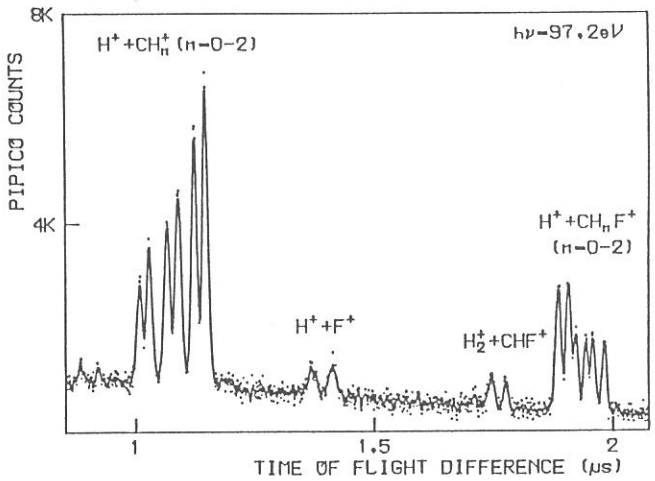

Fig. 1. PIPICO spectrum measured at 97.2 eV showing four dissociation processes.

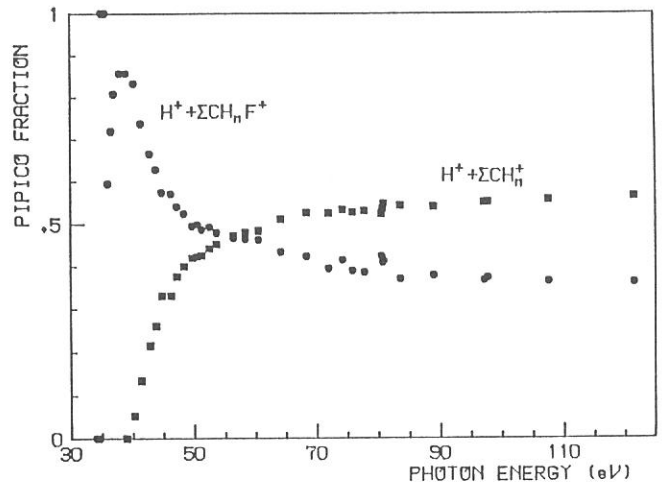

Fig. 2. Fractional abundance of C-H bond breakage (●) and C-F and C-H bond breakage (■).

ANISOTROPIC ANGULAR DISTRIBUTION OF FRAGMENT IONS IN DISSOCIATIVE DOUBLE PHOTOIONIZATION OF CH_3F

Toshio MASUOKA and Inosuke KOYANO*

Department of Applied Physics, Osaka City University, Sumiyoshi, Osaka 558
*Institute for Molecular Science, Okazaki, Aichi 444

Angular distributions of the neutral and ionic fragments produced in molecular photodissociation[1] and photoionization[2] are closely related to the symmetry and the dynamics of the processes involved. Although the same symmetry-characteristic-dissociation may occur also in the direct double ionization (not from Auger decay), anisotropy of fragment ions has not yet been examined by photoion-photoion coincidence (PIPICO) spectroscopy.[3] In order to study this subject, angle resolved PIPICO spectra were measured for a symmetric top molecule CH_3F in the energy region of the valence orbitals by use of linearly polarized synchrotron radiation and a time-of-flight mass spectrometer.[4]

The two PIPICO spectra shown in Fig. 1, measured horizontally and vertically at 90 eV, clearly indicate anisotropic angular distribution of the ionic fragments in the dissociation channel $H^+ + F^+ + n.f.$ Here n.f. stands for neutral fragments. The anisotropy parameter is estimated to be about -0.8 at 90 eV. The observed anisotropy probablly depends on the particular dissociation mechanism, in which the breakup occurs in two steps , $CH_3F^{2+} \rightarrow CH_3^+ + F^+$, $CH_3^+ \rightarrow H^+ + n.f.$, with negligibly small energy release in the second step. In this mechanism, the direction of the C-F axis at the moment of the molecular photoabsorption is the same with that of the final dissociation products H^+ and F^+. The electronic configurations related to the channel $H^+ + F^+ + n.f.$ are inferred to be $(3a_1 2e)^{-1}$ and $(3a_1 4a_1)^{-1}$. The analysis of the symmetry of the final states, including both the ionic states and two ejected electrons, shows that the Σ-Π transitions are dominant for the electron configurations $(3a_1 2e)^{-1}$ and $(3a_1 4a_1)^{-1}$. On the other hand, in the case of two-electron ejection from the outermost orbital 2e, both the parallel- and perpendicular-type transitions[1] such as Σ-Σ and Σ-Π are involved in addition to other type

transitions. Furthermore, the C_{3v} symmetry smears out anisotropy even if it exists in the C-H bond breakage. Consequently, it is quite reasonable that anisotropy was not observed in the other dissociation channels, $H^+ + CH_2F^+$, $H^+ + CHF^+ + n.f.$, $H^+ + CF^+ + n.f.$, $H_2^+ + CHF^+$, $H^+ + CH_2^+ + n.f.$, $H^+ + CH^+ + n.f.$, and $H^+ + C^+ + n.f.$[5] Thus, the above consideration confirms that the anisotropy observed in this study for the first time in the case of direct two-electron-ejection processes is also explained in terms of the symmetry and the dynamics of the processes involved.

References

1) R. N. Zare, Mol. Photochem. 4, 1 (1972).

2) J. L. Dehmer and D. Dill, Phys. Rev. A 18, 164 (1978).

3) see for example J. H. D. Eland, Mol. Phys. 61, 725 (1987).

4) T. Masuoka, T. Horigome, and I. Koyano, Rev. Sci. Instrum. 60, 2179 (1989).

5) T. Masuoka and I. Koyano, in this report, to be published.

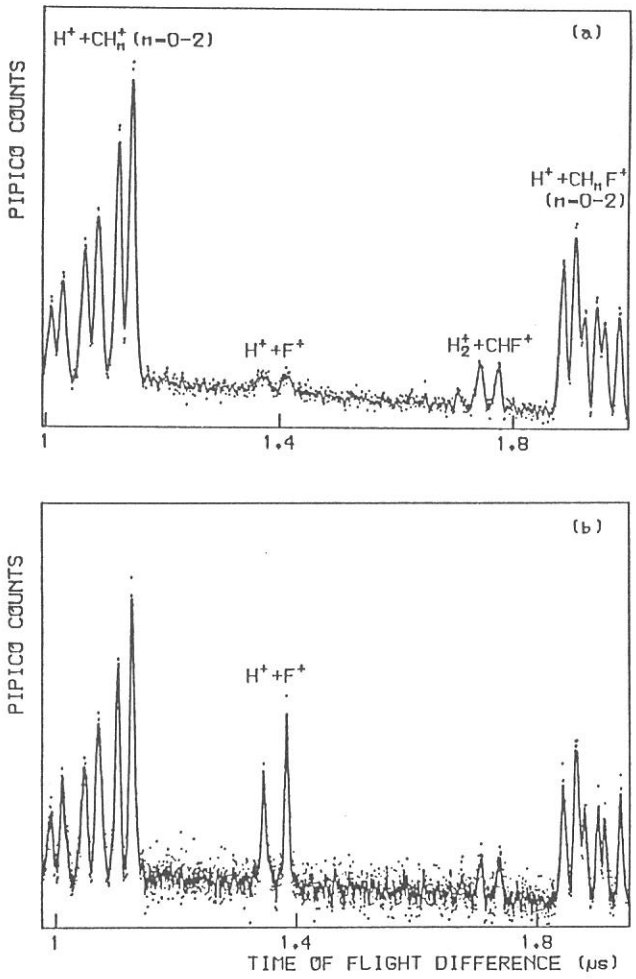

Fig. 1. Photoion-photoion coincidence spectra measured (a) in parallel and (b) perpendicularly with respect to the electric vector of the polarized radiation. The anisotropy of the fragment ions is observed in only the dissociation channel $H^+ + F^+ + n.f.$

DISSOCIATIVE DOUBLE PHOTOIONIZATION OF OCS STUDIED BY MASS SPECTROMETRY AND COINCIDENCE METHOD

Toshio MASUOKA and Inosuke KOYANO*

Department of Applied Physics, Osaka City University, Sumiyoshi, Osaka 558
*Institute for Molecular Science, Okazaki, Aichi 444

The study of double photoionization of gasous molecules is becoming a growing research field in recent years because of physical and chemical interests, development of a variety of experimental methods such as photo-ion-photoion, photoelectron-photoelectron, and photoelectron-photoion-photoion coincidence experiments, and relatively easy access to the synchrotron radiation. We have studied dissociative double photoionization in OCS by use of linearly polarized synchrotron radiation, the time-of-flight mass spectrometry, and the photoion-photoion coincidence (PIPICO) technique[1] in the photon energy range 16-100 eV.

The singly and doubly charged parent ions, OCS^+ and OCS^{2+}, as well as all the posssible fragment ions, C^+, O^+, S^+, OC^+, CS^+, were detected. The observation of metastable OCS^{2+} in a μsec or longer time scale suggests that the ground electronic state of OCS^{2+} is bound. The nondissociating state is derived from the π_g^{-2} configuration. The fractional abundance of OCS^{2+} starts to rise at about 31 eV in accordance with other experimental measurements[2,3] and stays almost constant (6 % or 10 %, when measured horizontally or vertically, respectively) above $\sim$36 eV.[5]

The five dissociation channels, $OC^+ + S^+$, $C^+ + O^+ + S$, $O^+ + S^+ + C$, $C^+ + S^+ + O$, and $O^+ + CS^+$, were observed, all of which are possible from the linear triatomic molecules. The fractional abundance of the two strongest dissociation channels, $OC^+ + S^+$ and $C^+ + S^+ + O$, is shown in Fig. 1 in comparison with other measurements.[4] The agreement is seen to be fairly good. The dissociation products in these channels show almost spherically symmetric distributions,[5] as can be seen from the figure. The observed dissociation channels are correlated with the electronic states of OCS^{2+}.[4]

Kinetic energies of the dissociation products give information on the internal energy of the dissociating parent states, so that the PIPICO spec-

tra of the four dissociation channels were analyzed. An example is shown in Fig. 2, which represents the released energy carried by the two ionic fragments, excluding that carried by the neutral fragment. The figure shows that the energy distribution changes markedly as the photon energy increases, in contrast to the cases of other dissociation channels.

References

1) T. Masuoka, T. Horigome, and I. Koyano, Rev. Sci. Instrum. 60, 2179 (1989).

2) R. G. Cooks, D. T. Terwilliger, and J. H. Bynon, J. Chem. Phys. 61, 1208 (1974).

3) W. J. Griffiths and F. M. Harris, Int. J. Mass Spectrom. 87, 349 (1989).

4) P. Millie et al., J. Chem. Phys. 84, 1259 (1986).

5) T. Masuoka and I. Koyano, in this report, to be published.

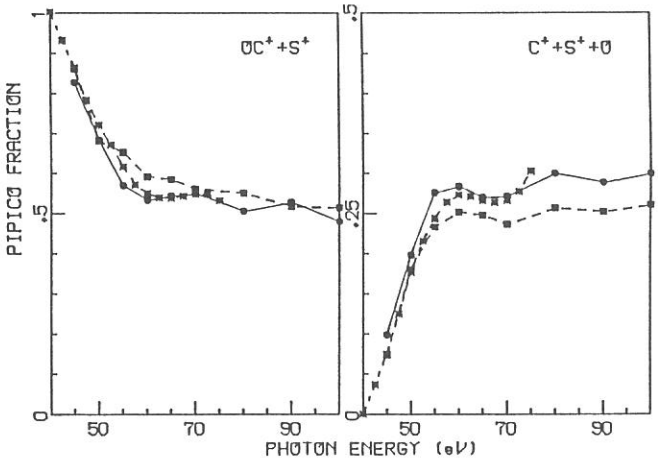

Fig. 1. Fractional abundance of the dissociation channels, $OC^+ + S^+$ and $C^+ + S^+$, measured horizontally (●) and vertically (■). * (ref. 4).

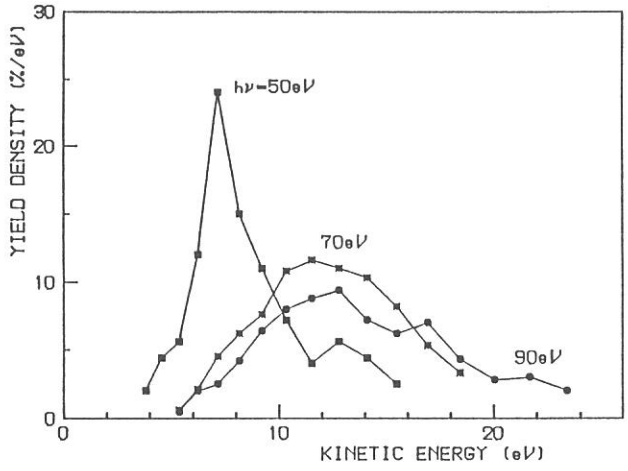

Fig. 2. Kinetic energy distributions of the fragment ions for the channel $O^+ + S^+$, which show remarkable changes as photon energy increases.

DISSOCIATIVE DOUBLE IONIZATION FOLLOWING VALENCE AND Al:2P CORE LEVEL PHOTOEXCITATION OF $Al(CH_3)_3$

Shin-ichi NAGAOKA,* Inosuke KOYANO, and Toshio MASUOKA+

Institute for Molecular Science, Okazaki 444, Japan
+Department of Applied Physics, Osaka City University, Sumiyoshi, Osaka 558, Japan

In recent years, relaxation processes following core excitation in molecules have been a topic of much interest. We have investigated the dissociation processes following double photoionization of $Al(CH_3)_3$ (TMA) in the range of valence and Al:2p core-level ionization by means of the photoelectron-photoion and photoion-photoion coincidence methods (PEPICO and PIPICO methods, respectively).[1] The experiments were performed using a time-of-flight (TOF) spectrometer with variable path length, coupled to a constant-deviation grazing incidence monochromator installed at the BL3A2 beam line of the UVSOR synchrotron radiation facility in Okazaki.[2]

Figures 1 and 2 show examples of the TOF mass spectra in the PEPICO mode and of the PIPICO spectra of TMA taken at 81.3 eV, respectively. Figures 3 and 4 show plots of the ratios of the integrated intensities of the various ions and ion-pairs in the TOF mass and PIPICO spectra to the total photoionization efficiency ($I_{ion}/I_{tot-ion}$) and to the total double-photoionization efficiency ($I_{PIPICO}/I_{tot-PIPICO}$), respectively, as functions of photon energy. The double-ionization threshold and the Al:2p core-ionization threshold are estimated to be about 30 and 80 eV, respectively. The relative yields of the H^+-Al^+ and H^+-$CH_{m'}^+$ (m'=0–3) ion pairs are enhanced around the Al:2p core-ionization threshold. The fragmentation scheme leading to the production of the H^+-Al^+ and H^+-$CH_{m'}^+$ (m'=0–3) ion pairs in TMA may be described as follows:

$$Al_2(CH_3)_6 + h\nu \rightarrow Al_2(CH_3)_6^+ + e \qquad \text{(Al:2p ionization)}$$

$$\rightarrow Al_2(CH_3)_6^{2+} + e \qquad \text{(LVV Auger)}$$
$$\rightarrow Al^+ + H^+ + n.p.$$
$$\rightarrow H^+ + CH_{m'}^+ + n.p. \quad (m'=0-3)$$

*Present address: Department of Chemistry, Faculty of Science, Ehime University, Matsuyama 790, Japan.

1. S. Nagaoka, I. Koyano, and T. Masuoka, Phys. Scr., in press.
2. T. Masuoka, T. Horigome, and I. Koyano, Rev. Sci. Instr. 60, 2179 (1989); E. Ishiguro, M. Suzui, J. Yamazaki, E. Nakamura, K. Sakai, O. Matsudo, N. Mizutani, K. Fukui, and M. Watanabe, Rev. Sci. Instr. 60, 2105 (1989).

Fig. 1 TOF mass spectrum

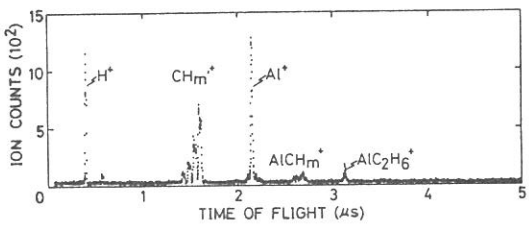

Fig. 2 PIPICO spectrum

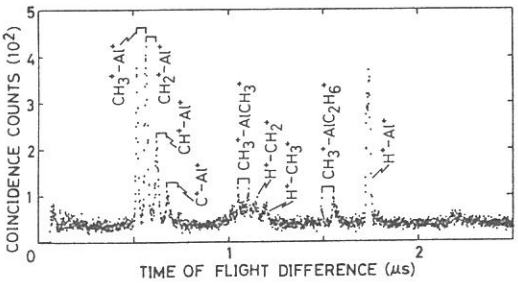

Fig. 3 Ratios of integrated intensities of various ions in TOF mass spectrum to total photoionization efficiency as a function of photon energy

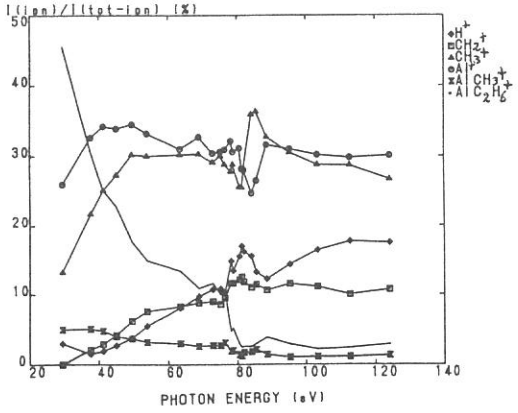

Fig. 4 Ratios of integrated intensities of various ion pairs in PIPICO spectrum to total double-photoionization efficiency as a function of photon energy

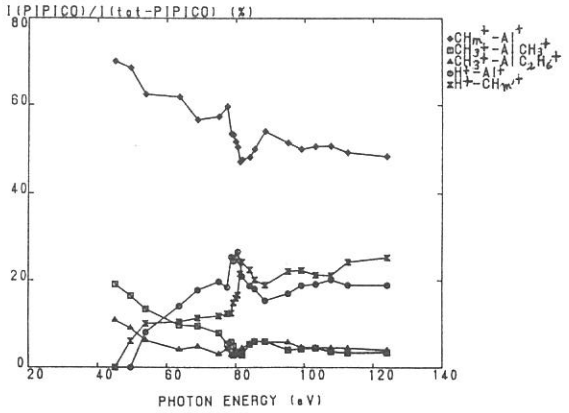

CAUSE OF EXCIMER LASER INDUCED 4.8 EV OPTICAL ABSORPTION AND 1.9 EV LUMINESCENCE IN HIGH PURITY SiO_2 GLASSES

Koichi AWAZU, Hiroshi KAWAZOE and Masayuki YAMANE
Department of Inorganic Materials, Tokyo Institute of Technology, Meguroku, Tokyo 152

There have been several reports dealing with an optical absorption peak at 4.8 eV(255 nm) and a photoluminescence peak at 1.9 eV in high purity silica glasses.[1),2)] No satisfactory model which can explain the optical properities seems to be established. We found that both the 4.8 eV absorption band and the 1.9 eV luminescence band could be observed simultaneously in O2 rich SiO_2 glasses referred to as SiO_{2+x}; X 0). Therefore SiO_{2+x} glasses were produced with VAD technique(Vaporphase Axial Deposition)[3)] to study the cause of the absorption band and photoluminescence. In the VAD process, the ratio of O_2 and He gases of sintering atmosphere was changed as O_2/He=0, 1/10, 3/10, 7/10 and 10/10, and the samples are abbreviated as VAD0, VAD1, VAD3, VAD7 and VAD10, respectively.

Fig.1 shows the absorption spectrum of these samples in VUV region. It is noticed that the optical absorption in the region above 7 eV increases according to the increase of the O_2 partial pressure of sintering atmosphere. Fig.2 shows the absorption spectrum in UV-VIS region before and after an irradiation of ArF excimer laser radiation (100mJ, 100Hz, 3min.). After the irradiation the new absorption bands peaking at 4.8 eV and around VUV region were generated except for VAD0 sample. The intensitiy of the induced band was larger in order of O_2 partial pressure. Moreover, all samples which have 4.8 eV absorption band gave a luminescence band at 1.9 eV.

We propose that O_2 molecule treated in the network of silica glass is the precursor for the absorption band and luminescence peak. It is well-known about the photochemistry O_2 molecule in the gas phase;[4)]

$$O_2 \xrightarrow{h\nu} O + O \quad (h\nu > 5.1 \text{ eV}) \qquad (1)$$

$$O + O_2 \rightarrow O_3 \qquad (2)$$

(ozone gas which has an absorption band peaking at 4.8 eV, namely Hartley bands)

$$O_3 \xrightarrow{h\nu} O(^1\Delta) + O_2 \rightarrow O(^3\pi) + O_2 + 1.9 \text{ eV} \quad (h\nu > 4 \text{ eV}) \qquad (3)$$

Refering to these reactions, we propose the same chain reactions are occuring in the silica glass containing O_2 molecule.

References;

1) G.W. Arnold and W.D. Compton, Phys. Rev. 116, 802 (1959) (1961)

2) J.H. Stathis and M.A. Kastner, Phil. Mag.B49, 357 (1984)

3) P.C. Schultz, Fiber optics eds. B. Bendow and S.S. Mitra (Plenum Press, New York and London, 1979), Vol.3

4)H.Okabe, Photochemistry of Small Molecules, John Wiley Sons(1978)

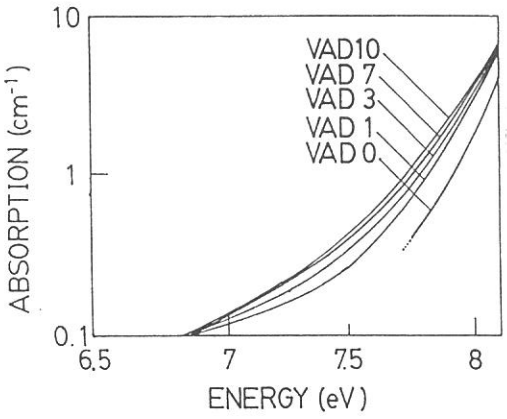

Fig.1 The absorption spectrum in VUV region.

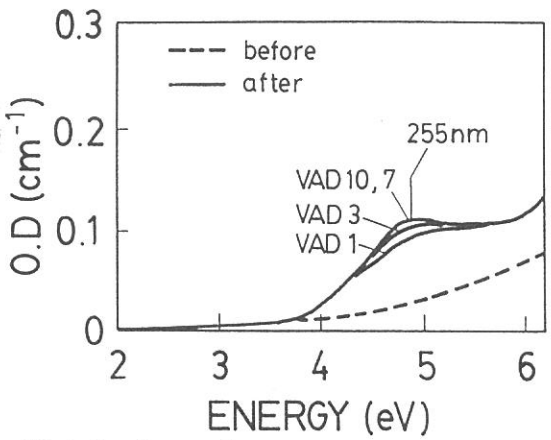

Fig.2 The absorption spectrum in UV-VIS region before and after ArF eximer laser radiation

VUV Laser-Induced Oxygen Desorption in SiO_2

Kou KUROSAWA and Yasuo TAKIGAWA*

Department of Electronics, University of Osaka Prefecture
Mozu-Umemachi, Sakai, Osaka 591
*Department of Solid State Electronics, Osaka Electro-Communication University, Hatsuchou,, Neyagawa, Osaka 572

Electronic excitation has been wellknown to result in defect formation and/or desorption in some semiconductors and insulators. In case of SiO_2 glass, self-traped excitons have been considered to be included in such phenomena [1]. On the course of the developing high power rare gas excimer lasers [2], we have observed beam patterns on the SiO_2 mirror surfaces after they were used as cavity reflectors for the Ar and Kr excimer laser. The transmission and reflectance spectra have been measured for the SiO_2 mirrors, in order to clarify the characteristics of the laser damages. The radiation fluence is around 200mJ/cm2 for respective shots, and the observed damages were formed by several shots.

In Fig. 1 are shown transmission spectra for SiO_2 glass (a-SiO_2) and natural crystalline quartz (c-SiO_2) by curves 1 and 2, respectively. In spite of the fundamental band gap energies of 9eV for a-SiO_2 and 9.4eV for c-SiO_2, the optical band gap energies are 165nm and 150nm, respectively, being much smaller than those of the fundamental ones. This is because of electronic levels in the band gap caused by impurities or structural defects. Therefore, the Ar and Kr excimer laser photons are fully absorbed by these SiO_2. The curves 3 and 4 show transmission spectra of the SiO_2 irradiated by the Ar excimer laser. The transmittance decreases to large extent, since the mirror surfaces are roughened by the laser irradiation.

More distinct features are seen in their reflectance spectra in the VUV and UV regions. Fig. 2 shows the spectra of a-SiO_2, in which curve 1 shows that of the virgin SiO_2 mirror, curve 2 that of the Ar excimer laser radiation damaged SiO_2, and curve 3 that of the Kr excimer laser radiation damaged SiO_2. For the case of the Kr excimer laser radiation, the reflectivity decreases to some extent by the mirror surface roughness. On the contrary, the Ar excimer laser radiation acts as if the irradiation makes the reflectivity increase, in particular in the range around 200nm. The specrtal feature resembles that of the Si single crystals. It is just agreement with the results of X-ray photoelectron spectroscopy [3]. The same result is found in the case of c-SiO_2 (Fig. 3). It can be concluded that Si-O bonds have been broken in a-SiO_2 and c-SiO_2 by the Ar excimer laser radiation, but not by the Kr excimer laser radiation.

From the thermal considerations, the temperature of the mirror surfaces rises beyond the melting temperature only by one laser shot. Therefore, the Si-O bond breaking or oxygen desorption is inferred to be caused by a combined effect of the band-to-band excitation and melting.

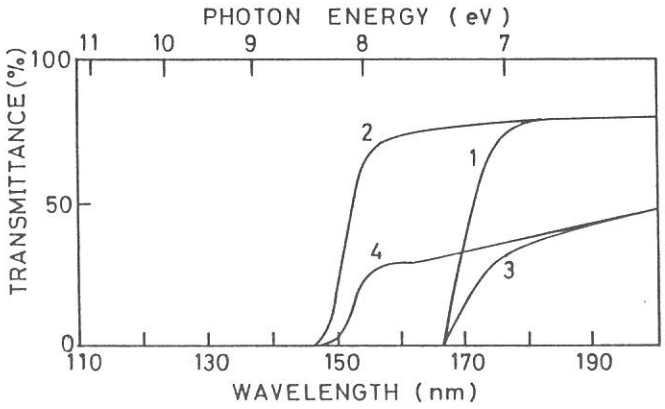

Fig.1
Transmission spectra of $a\text{-}SiO_2$ and $c\text{-}SiO_2$: curve 1 is taken from a virgin $a\text{-}SiO_2$, 2 from a virgin $c\text{-}SiO_2$, 3 from an Ar excimer laser irradiated $a\text{-}SiO_2$, and 4 from a Kr excimer laser irradiated $c\text{-}SiO_2$.

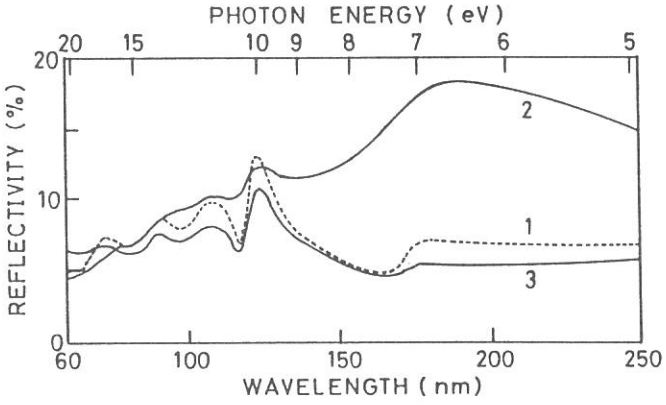

Fig.2
Reflectance spectra of $a\text{-}SiO_2$: curve 1 is taken from a non-irradiated part, 2 from an Ar excimer laser irradiated part, and 3 from a Kr excimer laser irradiated part.

Fig.3
Reflectance spectra of $c\text{-}SiO_2$: curve 1 is taken from a non-irradiated part and 2 from an Ar excimer laser irradiated part.

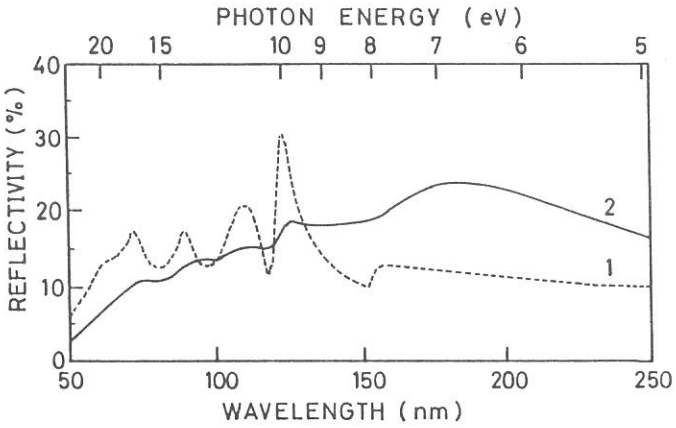

References
[1] N.Itoh, K.Tanimura, and C.Itoh: Solid Sate Physics, 22, 1000(1987).
[2] W. Sasaki and K. Kurosawa: Rev. Laser Engin., 16, 200(1988).
[2] Y. Takigawa et al.: J. Non-Cryst. Solids (in print).

Luminescence Process of O_2^- center in Alkali Halides

Sadato Hongo, Hiroshi Murata, and Riso Kato

Department of Physics, Faculty of Science
Kyoto University, Kyoto 606

It is well known that O_2^- ions substituted for halogen ions in various alkali halides show strong luminescence which consists of a series of sharp zero-phonon lines acccompanied by phonon sidebands.[1,2] In recent years, superradiance and laser action are reported in KCl:O_2^-.[3,4] Motivated by these interesting phenomena, we have investigated the temperature dependence of the luminescence intensity and the decay time of O_2^- centers in various alkali halides.

Specimens were grown from melts containing about 1 mol% of KO_2 or Na_2O_2. Decay time of the luminescence was measured under the excitation of uv(250~350 nm) light pulse from UVSOR in the temperature range from 10 K to 500 K. The luminescence spectra and intensity were measured under the excitation with uv light from a high pressure mercury lamp in the same temperature range.

Figure 1 shows typical luminescence spectra of KCl:O_2^- at 4.5 K and 77 K. The decay time and the luminescence intensity shows similar temperature dependence (Fig. 2). They are almost constant below 250 K, above which they drop rapidly. Their temperature dependence is described by the following equations:

$$\tau^{-1}(T) = \tau_R^{-1} + \nu \exp(-\Delta E/kT)$$
$$I(T)/I(0) = \tau(T)/\tau_R$$

Solid lines in Fig. 2 are theoreticl curves calculated by eqs. (1) and (2). This relation expresses the thermal quenching of luminescence due to thermally activated non-radiative decay process. Radiative decay time τ_R, frequency factor ν, and activation energy ΔE are obtained from curve fitting analysis. These values obtained for various host crystals are summarized in Table 1. The values of ν's and ΔE's for three systems are of

the same order of magnitude, while τ_R for NaCl:O_2^- is one order of magnitude smaller than that for the others. The luminescence yield in NaCl:O_2^- at low temperature is also smaller than the others. These features suggest that the tunnelling decay process is important at low temperature in NaCl:O_2^-.

References:

1) M.Ikezawa and J.Rolfe: J. Chem. Phys. **58** (1973) 2024

2) J.Rolfe, F.R.Lipsett, and W.J.King: Phys. Rev. **123** (1961) 447

3) R.Florian, L.O.Schwan, and D.Schmid: Phys. Rev. A**29** (1984) 2709

4) S.R.Wilk, R.W.Boyd, and K.J.Teegarden: Opt. Commun. **47** (1983) 404

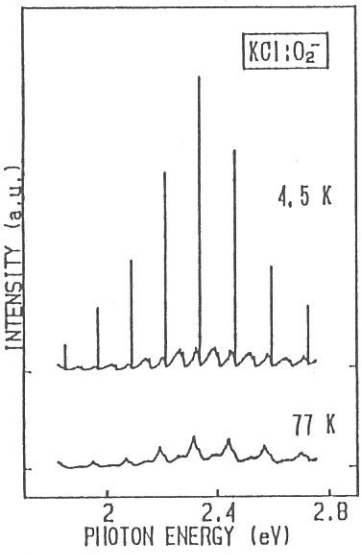

Fig.1

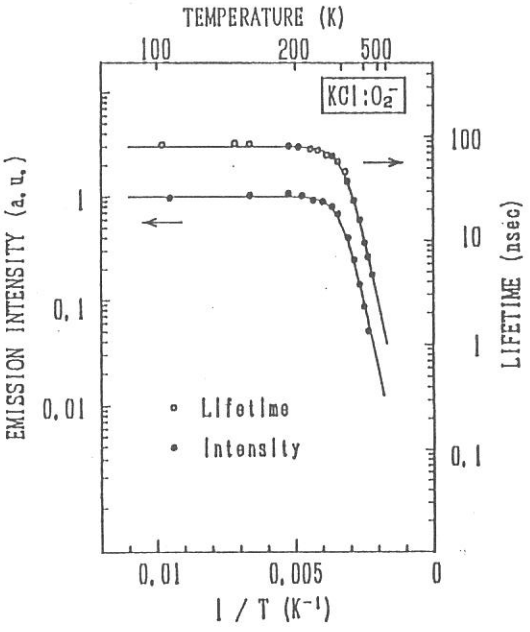

Fig.2

Table 1

	τ_R (nsec)	ν (10^{11} s^{-1})	ΔE (meV)
KCl:O_2^-	79.8	1.32	253
KBr:O_2^-	92.7	3.32	241
NaCl:O_2^-	8.8	1.50	252

Stability of Free-Holes in LiBr

Koji FUJIWARA, Sadao TANAKA, Shunji NAGATA, Masaaki NAKAYAMA,
Hitoshi NISHIMURA, Teruo KOMATSU* and Satoshi HASHIMOTO**

Department of Applied Physics, Osaka City University, Sumiyoshi-ku Osaka 558
* Department of Physics, Osaka City University, Sumiyoshi-ku Osaka 558
** Kyoto University of Education, Fushimi-ku Kyoto 612

Characteristics of the self-trapped excitons (STE's) in alkali halides are classified with a stability parameter for the exciton-phonon coupling, which is defined by r^-/d (r^-: anion radius, d: distance between adjacent anions). For LiBr, the parameter is the largest ($\sim$0.5), and the valence band width calculated by Kunz[1] is very broad (1.9 eV), so that the free hole state as well as the free exciton state is expected to be fairly stable. In other words, the potential barrier heights for self-trapping of free holes and excitons seem to be larger in LiBr than in other alkali halides with small stability parameters and with small valence band widths. Figure 1 shows a luminescence spectrum of a LiBr crystal excited in the exciton absorption region (163 nm). The 3.95 and 5.4 eV bands have been attributed to the self-trapped excitons (STE's) and unknown impurities, respectively.[2] The 3.95 eV band whose decay time is 4 μs at 5 K is due to the STE triplet state. So called σ luminescence band due to the STE singlet state is absent in LiBr.[2] The excitation spectra of the 3.95 and 5.4 eV bands, which are corrected for the reflection loss of the incident light, are shown in Fig. 2. It is obvious that the 5.4 eV impurity band is excited in the interband transition region as well as in the exciton absorption region. The 5.4 and 3.95 eV bands appear also by the 400 nm light irradiation on a x-rayed sample. In this process, electrons must be released from the traps that may be F centers, and recombined with STH's and/or holes trapped by impurities. These results indicate that holes are mobile for a moment after creation, and part of them are captured by the impurity before self-trapped, and then recombined with free electron to emit the 5.4 eV impurity luminescence. The rest of the free holes are self-trapped and recombined with free electrons to emit the 3.95 eV STE luminescence.

The intensities of the 3.95 and 5.4 eV bands are shown in Fig. 3 as a function of temperature. As temperature rises, the 5.4 eV impurity band is quenched and contrary the 3.95 eV STE band is enhanced, suggesting that free holes are self-trapped at these temperatures over the potential energy bar-

rier existing between the free hole state and the STH state. From this result, the barrier height is estimated to be 7 meV. Toyozawa has proposed[3] that the potential barrier for free holes is given by $(4/27)B^3/(E_{LR}^{ac})^2(1-3E_{LR}^{ac}E_{LR}^{op}/B^2)^{3/2}$, where B is the half value of the valence band width, and E_{LR}^{ac} and E_{LR}^{op} are the acoustic phonon mode and optical phonon mode contributions to the energy of lattice relaxation around the localized hole. This relation indicates that the barrier height is large for the material with broad valence band width. According to Kunz's calculations,[1,4] the valence band widths are broad in LiBr (1.9 eV), LiI (1.6eV), NaI (0.82 eV) and NaBr (1.5 eV) in which the stability parameters (r^-/d) are large ($\sim$0.5). Therefore, it is reasonable that the potential barrier heights for free holes are large in LiBr (7 meV) and in NaI (3 meV[5]).

References

1) Kunz, A. B., Phys. Rev. B26, 2056 (1982).
2) Fujiwara, K., Nishimura, H., Nakayama, M., Komatsu, T. and Hashimoto, S., UVSOR Intern. Rep. UVSOR-16, 48 (1989).
3) Toyozawa, Y., Excitonic Processes in Solids, ed. by P. Fulde, Springer Ser. Solid-state Sci., vol. 60, p249.
4) Kunz, A. B., Phys. Rev. 180, 934 (1969).
5) Nagata, S., Fujiwara, K. and Nishimura, H., to be contributed.

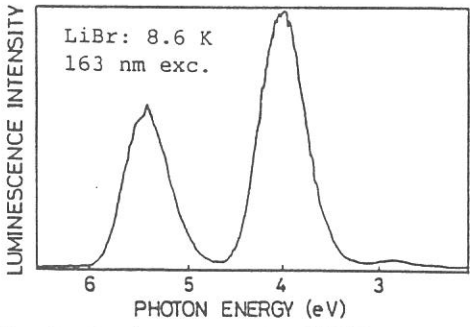

Fig.1. Luminescence spectrum of LiBr.

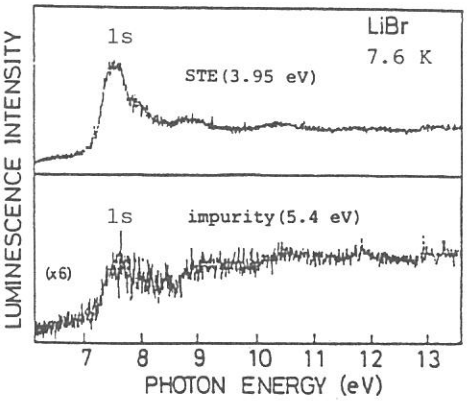

Fig.2. Excitation spectra of the 3.95 and 5.4 eV bands. The 1s exciton peak energy is shown by 1s.

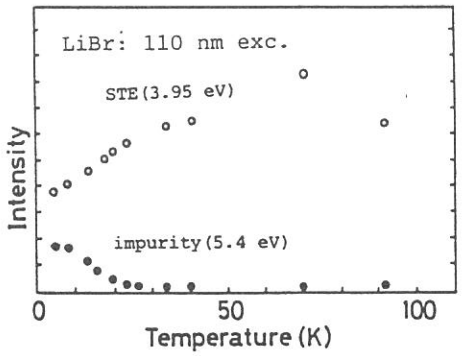

Fig.3. Temperature dependence of luminescence intensities.

SELF-TRAPPED EXCITON LUMINESCENCE IN $Na_{1-x}K_xI$ AND $K_{1-x}Rb_xI$ MIXED CRYSTALS

Minoru ITOH, Satoshi HASHIMOTO* and Nobuhito OHNO**

Faculty of Engineering, Shinshu University, Nagano 380
**Kyoto University of Education, Fushimi-ku, Kyoto 612*
***Faculty of Engineering, Osaka Electro-Communication University, Neyagawa, Osaka 572*

The self-trapped exciton (STE) luminescence of alkali halides consists of two different types of emission bands; high-energy band is σ polarized, short-lived, and due to the decay of singlet states, while the low-energy band is π polarized, relatively long-lived, and due to triplet states. Although these features are explained on the basis of the "on-center" V_K + e model for the STE, recent theoretical studies have suggested that an "off-center" STE state is stable in alkali halides, from which the π polarized luminescence occurs.[1] The off-center motion of the STE is easy or hard depending on whether the value of a geometric ratio S/D (Rabin-Klick parameter) is large or small. The quantity S/D is a measure of the space available to a halogen atom for insertion between two halide ions along a face diagonal. Accordingly, it would be expected that the STE luminescence shows a considerable change in alkali-substituted alkali halides, since the space between adjacent halide ions varies upon alloying.

In the present study we investigated the STE luminescence in $Na_{1-x}K_xI$ and $K_{1-x}Rb_xI$ mixed crystals. Lifetime measurements were carried out by the TAC method under single-bunch operation in which one can utilize the pulsed VUV light of 450 ps width with 178 ns interval. Figure 1 shows the luminescence spectra of $Na_{1-x}K_xI$ with x = 0.2, 0.5 and 0.8 measured by the excitation with 7.7 eV photons at 11 K. As clearly seen, the π emission band (4.2 eV) in NaI is not connected to the π band (3.3 eV) in KI but to the σ band (4.1 eV) in changing x. It has already been known that the decay curve of the 4.2 eV band in NaI consists not only of a long-lived triplet component but also of a fast singlet component.[2] In Fig. 2 are shown the decay curves of the 4.1 eV band of $Na_{1-x}K_xI$ system. It is evident that the triplet component decreases in intensity with increasing x, while the singlet one grows. We thus conclude that the 4.2 eV band in NaI does not belong to the family of π emission but to that of σ emission. The same situation has been found in the case of NaBr.[2] In Fig. 1, a new luminescence appears around 2.9 eV and becomes intense as $x \rightarrow 0.8$. This band may be ascribed to the triplet STE state of the off-center configuration which results from an expansion in the lattice constant due to the substitution of K^+ ions into NaI matrix, although further studies will be necessary.

In $K_{1-x}Rb_xI$ system, the σ emission band (4.1 eV) in KI is connected to the σ band (3.9 eV) in RbI.[3] In fact, it was found that the lifetime of the σ band changes continuously

from 2 ns in KI to 4 ns in RbI. Such a change will be mainly due to the wavefunction overlap between V_K center and electron which would decrease with x, i.e., the lattice constant.

1) K.S. Song *et al.*: J. Phys.: Condens. Matter **1** (1989) 683.
2) K. Kan'no *et al.*: Physica Scripta (in press).
3) Unpublished data.

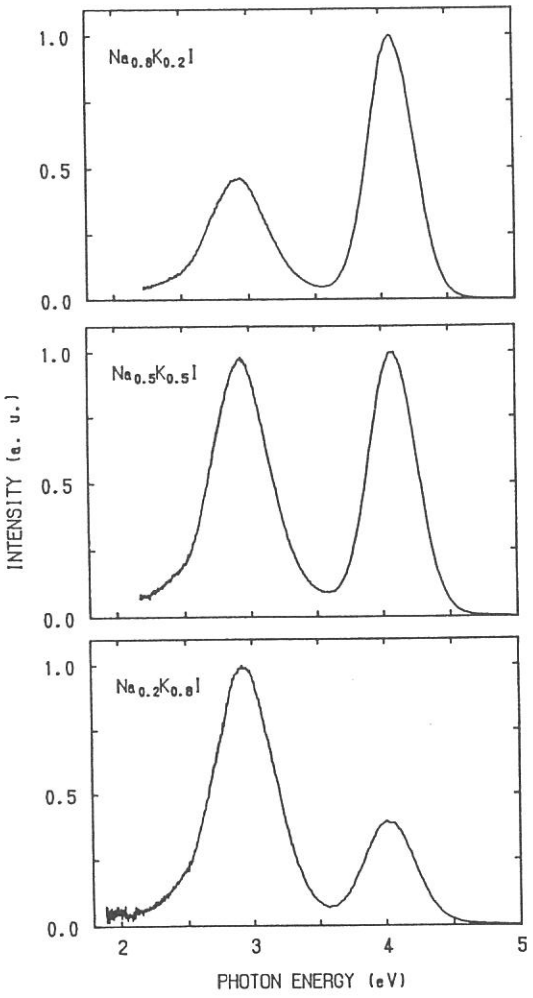

Fig. 1

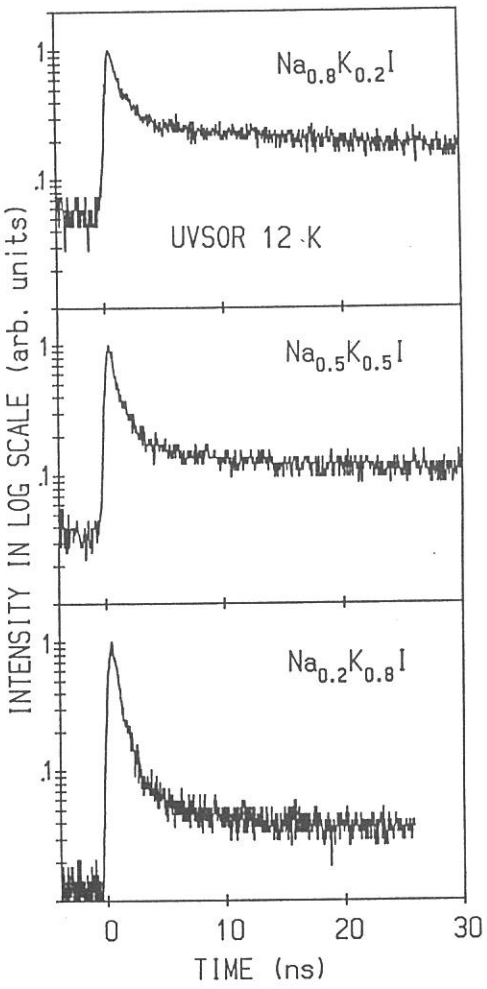

Fig. 2

LUMINESCENCE FROM SELF-TRAPPED EXCITONS IN NaBr AND KBr

Ken-ichi KAN'NO, Koichiro TANAKA, Hideo KOSAKA**, Yoshio NAKAI and Koichi TOYODA*

Department of Physics, Kyoto University, Kyoto 606, Japan
*) Department of Physics, Osaka Dental University, Hirakata, Osaka 573, Japan
**) Present address: Opto-Electronics Research Laboratories, NEC Co., Tsukuba 305, Japan

Two emission bands (σ and π) are known to arise in general from radiative decay of self-trapped excitons (STE) in alkali halides. NaBr and NaI, however, have only one emission band which has so far been classified as the family of the π emission on the basis of its long lifetime and its perpendicular polarization with respect to the STE axis. Excitation of these bands can be made efficiently in the lowest (n=1) exciton absorption band. This is also consistent with the commonly accepted classification as the π emission. But, the peak energies of these bands (NaBr: 4.62 eV, NaI:4.19 eV) are unusually higher than those of the π emission bands in other crystals (*e.g.*, KBr: 2.27 eV, KI: 3.29 eV), and are in the ultraviolet region where the σ emission with the short lifetime is usually observed (KBr: 4.45 eV, KI: 4.15 eV). Moreover, lifetime measurements[1] using single-bunched light pulses from UVSOR revealed that a weak component with the short lifetime (NaBr:1.5 ns, NaI:1.0 ns) coexists with the triplet component of the long lifetime (NaBr:470 ns, NaI:95 ns) in these π emission. Thus, the nature of the π emission bands in NaBr and NaI seem to be markedly different from that of the π emission bands in other crystals.

In the present study, interrelation between the emission spectrum of NaBr and that of KBr has been examined. Emission spectra and their decay profiles were measured in various $Na_{1-x}K_xBr$ mixed crystals at 10 K under excitation into the interband transition with the 7.7 eV light. As x is increased from 0 to 1, the π emission of NaBr continuously changes itself into the σ emission of KBr with keeping its band-width unchanged, as seen in Fig. 1(A). Its decay profile changes as shown in Fig. 1(B). The main triplet component decreases, and finally in KBr (x=1), the singlet component becomes a major part. For x>0.6, composite emission bands appear in the visible region. One of them around 2.8 eV, which diminishes in the limit of x=1, seems to have a close connection with the π_A emission[2] from STE's perturbed by Na^+ impurity ions in KBr. The other emission band in the lower energy region (hatched) is finally connected with the π emission band in KBr.

Figure 2 shows excitation spectra for the triplet (crosses) and the singlet (closed circles) components obtained by the time-resolved analysis of the π emission in NaBr, along with the absorption spectrum obtained for a thin film of NaBr by Teegarden and Baldini (solid line).[3] It is seen that both excitation spectra are different each other in the absorption range between the n=1 peak due to the $\Gamma(3/2,1/2)$ exciton at 6.75 eV and the n=1 peak due to the $\Gamma(1/2,1/2)$ exciton at 7.28 eV: The spectrum for the triplet component has a maximum around 6.9 eV, i.e., just below the n=2 peak of the $\Gamma(3/2,1/2)$

exciton (shown by the arrow),[4] while the one for the singlet component has a dip at the same position and a peak on the high energy side. It should also be noted that the singlet component as well as the triplet component can be appreciably stimulated even in the region of the n=1 exciton absorption. This suggests that the so-called π emission of NaBr comes from the radiative decay of STE's in the lowest triplet and singlet states with the 1s electronic orbitals slightly split by the exchange interaction.

So far, the σ emission has been generally believed to originate from the higher excited singlet STE with an orbital of s-like symmetry different from the lowest 1s orbital from which the π emission occurs. The present results, however, have revealed that an electronic orbital and a lattice configuration of the initial state of the σ emission in KBr are essentially the same as those of the π emission in NaBr. This means that not only the π emission but also the σ emission in KBr arise from the STE's with the lowest electronic orbitals. The large σ-π splitting in KBr and only one band in NaBr will be explained in terms of on-center and off-center distortion of STE's in the lowest singlet and the triplet states.[5,6]

1. Kan'no, K., Tanaka, K., Kosaka, H., Mukai, T., Nakai, Y., Itoh, M., Miyanaga, T., Fukui, T. and Watanabe, M., Physica Scripta (1989 in press).
2. Toyoda, K., Nakamura, K. and Nakai, Y., J. Phys. Soc. Jpn. **52**, 3254 (1983).
3. Teegarden, K. and Baldini, G., Phys. Rev. **155**, 896 (1967).
4. Miyata, T., J. Phys. Soc. Jpn. **31**, 529 (1971).
5. Tanaka, T., Kosaka, H., Kan'no, K. and Nakai, Y., Solid State Commun. **71**, 903 (1989).
6. Kan'no, K., Tanaka, K. and Hayashi, T., submitted to the Proceedings of U.S.-Japan Joint Seminar, Nagoya, Sept. 11-15, 1989, (ed. by Itoh N., World Scientific).

Fig. 1.

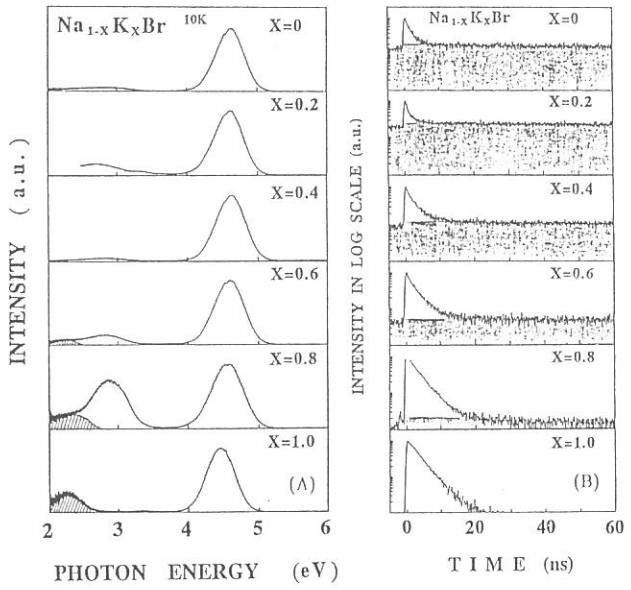

Fig. 2.

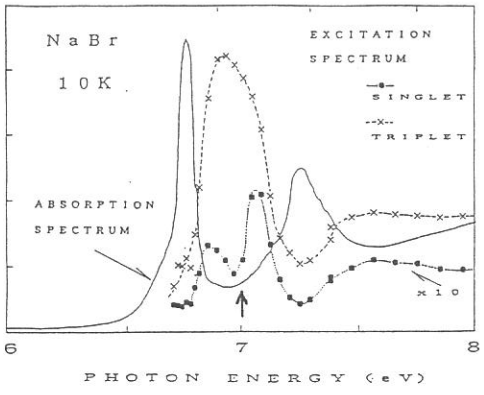

Photophysical Processes in Poly(N-vinylcarbazole)

Akira ITAYA and Hisashi SAKAI

Department of Polymer Science and Engineering,
Kyoto Institute of Technology,
Matsugasaki, Sakyo-ku, Kyoto 606

Considerable data on the fluorescence properties of poly(N-vinylcarbazole)(abbreviated hereafter as PVCz) have been accumulated because of an interest in its photoconductive properties, two spectrally distinct excimer fluorescences, and a clear relation between photophysical properties and tacticity.[1] One excimer, with an emission maximum at 420 nm, is attributed to a normal sandwich structure formed between neighboring carbazolyl groups in a totally eclipsed conformation. The other excimer, with a maximum at 370 nm, is due to a partial overlap structure formed between two carbazolyl groups in the TT conformation of the syndiotactic chain and is called the second excimer. We have already revealed, using a time-correlated single-photon counting technique with picosecond time resolution, that the partial overlap excimer fluorescence was observed immediately after excitation, while the sandwich excimer fluorescence showed delayed formation process.[2]

Considering the photoconductive properties of PVCz films, it is of interest to investigate the fluorescence dynamics under the excitation light of very short wavelength, where the intrinsic carrier-photogeneration due to the autoionization is possible. Time-resolved fluorescence spectra of films of PVCz prepared by the radical and cationic polymerizations (abbreviated as PVCz(r) and PVCz(c), respectively) have been measured with the excitation light of 295 and 180 nm, and compared with each other.

Time-resolved fluorescence spectra of PVCz(c) films are shown in Fig. 1, where each spectrum is normalized at the maximum intensity. In the early-gated spectrum, a structureless fluorescence with a peak at ca. 370 nm, due to the second excimer, was observed mainly under the both excitation conditions. At gate times of -0.54 - 0.54 ns, the sandwich excimer fluorescence appeared and its intensity increased with time. The build-up of the sandwich excimer fluorescence is slightly faster when PVCz(c) films were excited with 180 nm light than with 295 nm. Similar behavior was

obtained for PVCz(r) films.

Recently, we have found, by using the time-resolved total internal reflection fluorescence spectroscopy, that an aggregate state of pyrene in poly(methyl methacrylate) films is different between the vicinity of the interface and the bulk.[3] Therefore concentration of the excimer-forming sites in PVCz films may be also different between the vicinity of the polymer surface and the bulk. The depth where the fluorescence is observed is thinner when PVCz films were excited with 180 nm light than with 295 nm, Now, we cannot reject the possibility that the difference in the build-up of the sandwich excimer fluorescence is attributed to the small difference between concentration of the excimer-forming site. It is necessary to measure the time-resolved fluorescence spectra under the total internal condition by using the excitation light of 295 nm.

References
1) A. Itaya, H. Sakai, H. Masuhara, Chem. Phys. Lett., 146, 570 (1988) and references cited therein.
2) A. Itaya, H. Sakai, H. Masuhara, Chem. Phys. Lett., 138, 231 (1987).
3) A. Itaya, T Yamada, K. Tokuda, H. Masuhara, to be published.

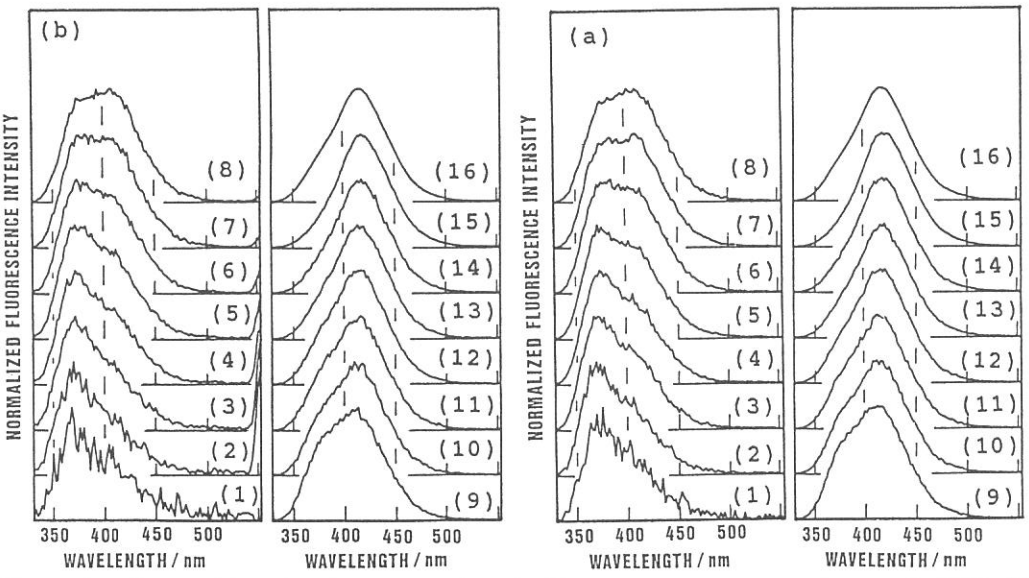

Fig. 1 Normalized time-resolved fluorescence spectra of PVCz(c) film. Excitation wavelength : (a) 180 nm and (b) 295 nm. Time window : (1) -0.72～-0.54, (2) -0.54～-0.36, (3) -0.36～-0.18, (4) -0.18～0, (5) 0～0.18, (6) 0.18～0.36, (7) 0.36～0.54, (8) 0.54～0.72, (9) 1.26～1.62, (10) 1.98～2.34, (11) 3.1～3.4, (12) 4.9～5.8, (13) 8.5～9.4, (14) 14～15, (15) 30～37 ns, and (16) total.

Lifetimes and Luminescences of p-Terphenyl Crystals

Kenji Uchida, Sadayosi Sato, Yoshihiro Takahashi[+] and Eiji Ishiguro[++]

Fukui Institute of Technology, Gakuen, Fukui 910
+ Aichi Institute of Technology, Yakusa, Toyoda 590-02
++ Department of Technology, Osaka City University, Osaka 558

Para-terphenyl molecule consists of three phenyl-rings joined by single bond, giving two possible internal angles. In general, it is believed that the polyphenyl molecules in solution have a non-planar configuration in its ground state and planar in the first excited state. Therefore, the molecules show broad and structureless absorption spectra and structured emission spectra. Meanwhile, in the crystalline state, a single phase transition takes place at 192 K. In the high temperature phase, the molecules are planar due to the libration of the central ring of the molecules. In the low temperature phase, the molecules are non-planar, since the central ring of each molecule is stabilized in one of the two bottoms of a double-well potential[1,2].

In the present study, we measured time dependences of emissions in order to study emission processes in para-terphenyl crystals. The excitation light was obtained from the storage ring under the single bunch operation of UVSOR, by using 1m Seya-Namioka type monochromator at BL7B beam line. The fluorescence was detected by a MCP photomultiplier (HAMAMATU R1564U) combined with a time-correlated single-photon counting system(EG&G Ltd.).

Figure 1 shows the emission spectra of para-terphenyl crystals under the various excitation wavelength. As wavelength of excitation increases, the vibrational structures of the fluorescence spectra become steeper and the fluorescence intensity in the region of shorter wavelength of emission spectra become weaker. Figure 2 shows the time dependences of emissions under the excitation wavelength of 200 nm, 230 m and 300 nm. The emission

decay curve under the excitation wavelength of 300 nm follows a single-exponential, but that under that of 200 nm shows multi-exponetial decay curves. These results seem to indicate that excimers of para-terphenyl are formed under the excitation of 200 nm.

1) P.J.L.Baudour and H.Cailleau, Acta Cryst. B33(1977)1773

2) K.Uchida and Y.Takahashi, J.Luminescence 40/41(1988)292

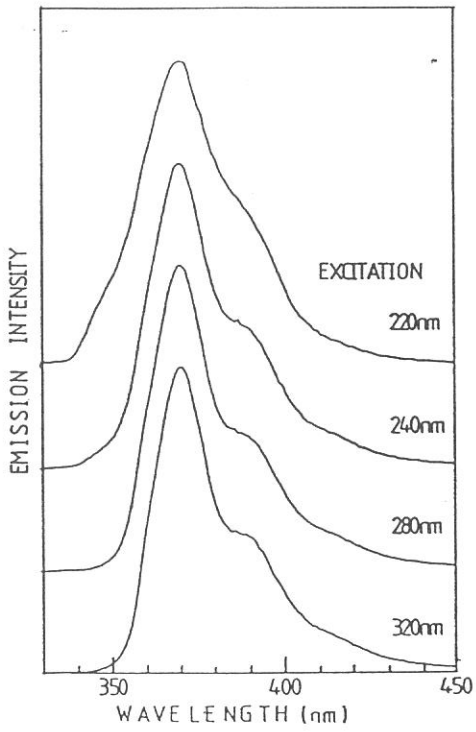

Fig.1 Emission spectra under the various excitations at R.T.

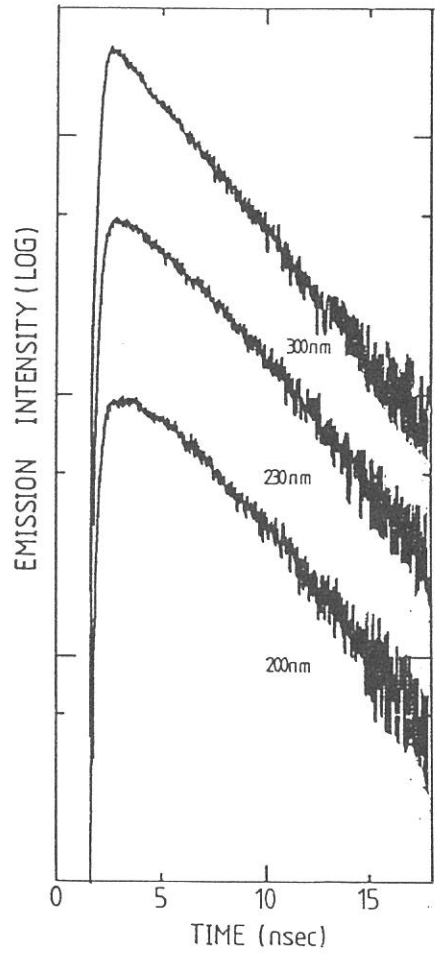

Fig.2 Emission decay cureves under various excitaions at R.T.

TIME- RESOLVED FLUORESCENCE MICROSPECTROSCOPY OF MUSCLE FIBERS USING SYNCHROTRON RADIATION FROM UVSOR

M. Taniguchi, S. Toyonaga, N. Watanabe and K. Osada

Department of Physics, Faculty of Science, Nagoya University
Chikusa-Ku, Nagoya (Japan)

The dynamical properties of muscle fibers in the nanosecond time range is becoming increasingly important for resolving the mechanism of muscle contraction [1]. The intrinsic fluorescence from glycerinated crab muscle was measured in rigor, relax and contraction solutions. We have carried out time-resolved excitation and emission spectroscopic studies of the tryptophan and tyrosine residues of muscle fibers to determine internal rotational motions of these chromophores.

The microspectroscopic apparatus was made and the fluorescence measurements were carried out at beamline 1B or 7B , illustrated schematically in Fig. 1. The excitation and emission spectra were measured using a Seya-Namioka type monochromator for excitation and a Jobin-Yvon HR-320 monochromator or a filter for emission. The emission from the fibers was collected with fused quartz lenses. The fluorescence lifetimes were measured by a single-photon counting apparatus using the single bunch operation of synchrotron excitation. The imaging of the fibers was made by combining with a multichannel plate and a camera.

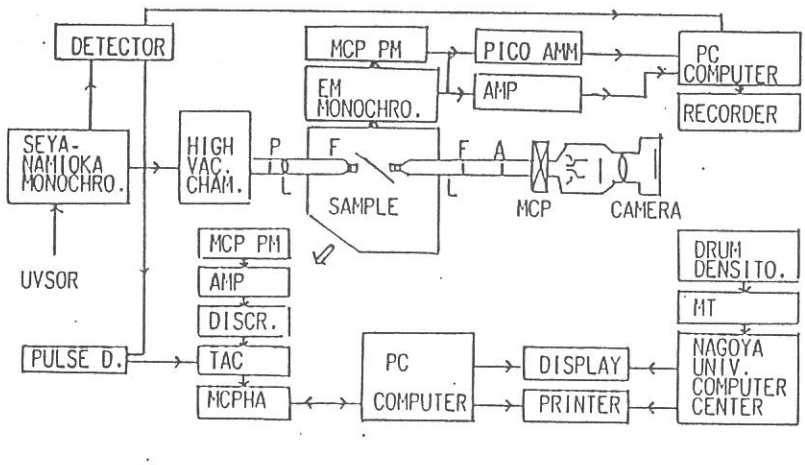

Fig. 1 Block diagram of apparatus for measuring time-resolved fluorescence microspectroscopy and imaging.

The excitation and emission spectra of glycerinated crab fibers were measured at 23.5+0.5°C. The excitation spectrum of the fibers in rigor solution have three bands peaking at 230 nm, 270 nm and 300 nm,

when emitted at 340 nm (Fig. 2). The emission spectrum of the fibers in a rigor solution shows a fluorescence band peaking at 330 nm, when excited at 295 nm. When the rigor solution was changed to relax solution or contraction solution, the second peak near at 270 nm decreased dramatically and increased at 300 nm. The emission maximum did not change in rigor muscle and changed with blue shift in relaxing or contraction muscles, when excited near at 280 nm.

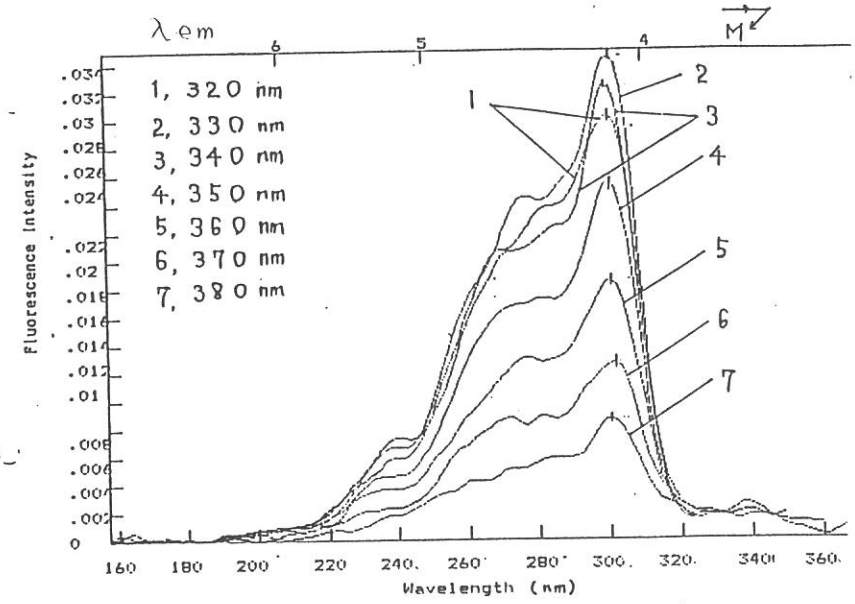

Fig. 2 Excitation spectra of glycerinated crab muscle in rigor solution.

When excited at 300 nm, the fluorescence decay of crab muscle was fitted with three exponentials:the fast component with a lifetime of about 0.4 ns and with a major component of 3.1 ns and a minor component of 12.0 ns, respectively. It was found that the decay curves of the fibers excited at 280 nm was also drastically changed in the relaxing and contracting muscles. Experimental results indicate that proteins undergo rapid fluctuations in the structure of relaxing muscle.

3. Acknowledgments

The authors thank Prof. M. Watanabe and Dr. K. Fukui for the help and encouragements. We are very grateful to Mr. K. Sakai, Mr. O. Matsudo, Mr. J. Yamazaki, Mr. E. Nakamura and the staffs of the Institute for Molecular Sciences for technical assistance. This study was partially supported by a grant in aid from the Ministry of Education, Research and Science in Japan.

1) M. Taniguchi and N. Watanabe, J. Sci. Soc. Press. 305 (1990).

CORE EXCITON SPECTRA IN $CdCl_2$-$CdBr_2$ MIXED CRYSTALS

Masami FUJITA, Hideyuki NAKAGAWA[+], Norio KITAGATA[+], Atsushi FUKUMOTO[+], Hiroaki MATSUMOTO[+], Takeshi MIYANAGA[++], Makoto WATANABE[+++] and Kazutoshi FUKUI[+++]

Maritime Safety Academy, Wakaba, Kure 737
[+]Department of Electrical and Electronics Engineering, Faculty of Engineering, Fukui University, Fukui 910
[++]Department of Physics, Faculty of Education, Wakayama University, Sakaedani, Wakayama 640
[+++]Institute for Molecular Science, Myodaiji, Okazaki 444

Cadmium halides are ionic layer compounds. In 15-17 eV region of the optical spectra, three main peaks with fine structures are observed in $CdCl_2$, while two main peaks are observed in $CdBr_2$ and CdI_2.[1] They are considered to be due to the excitonic transitions from shallow Cd 4d core to Cd 5p level. In the present study, reflection spectra of $CdCl_2$-$CdBr_2$ mixed crystals were measured in order to clarify correspondence between the fine structures in $CdCl_2$ and $CdBr_2$ and to investigate core exciton states in layered ionic crystals. Measurements were made using Seya-Namioka type monochromator at BL1B in UVSOR.

Reflection spectra of cleaved surfaces of mixed crystals at 35 K are shown in Fig. 1 for different compositions. Gross features in 15-17 eV region change continuously from pure $CdBr_2$ to pure $CdCl_2$, indicating that the electronic states relevant to these structures are attributed to the intra-atomic excitation in Cd^{2+} ions. Seven components a-g are observed in $CdCl_2$ and six components a-f are observed in $CdBr_2$. The small peak b in $CdBr_2$ inceases in intensity with increasing concentration of $CdCl_2$. The hump e found in $CdBr_2$-rich crystals is hardly observable in mixed crystals of the concentration between 30 and 50 mole % of $CdCl_2$, but appears as a shoulder in $CdCl_2$-rich crystals. The structure g, which is not clearly observed in $CdBr_2$-rich crystals, becomes discernible with increasing concentration of $CdCl_2$.

In Fig. 2 the energy positions of the fine structures are plotted against the composition. The structures are classified into two groups, (a,b,e) and (c,d,f,g), according to the energy shift. It should be noted that the energy difference between c(d) and f(g) in mixed crystals (0.60-0.67 eV) is almost the same value as the spin-orbit splitting of the Cd 4d core level (0.65 eV) found in photoemission spectrum of CdI_2.[2] The separation between b and e (0.61-0.66 eV) is also nearly this value. Due to the trigonal crystal field around cadmium ions, the Cd 5p state splits into lower level of mainly p_z-like character and upper level of mainly $p_{x,y}$-like character. Therefore the peaks c(d) and f(g) are assigned to the excitonic transitions to the upper

5p level from $4d_{5/2}$ and $4d_{3/2}$, respectively. The peaks b and e are assigned to the transitions to the lower 5p level from $4d_{5/2}$ and $4d_{3/2}$, respectively. Crystal field splitting of Cd 4d core level and electron core-hole exchange interaction should be taken into account in order to explain the splittings of a-b, c-d and f-g.

References
1)M. Fujita, H. Nakagawa, H. Matsumoto, T. Miyanaga, M. Watanabe, K. Fukui, E. Ishiguro, Y. Fujii and Y. Sakisaka, to be published in J. Phys. Soc. Jpn. 59(1990).
2) R. Coehoorn, G. A. Sawatzky, C. Haas and R. A. de Groot, Phys. Rev. B31(1985)6739.

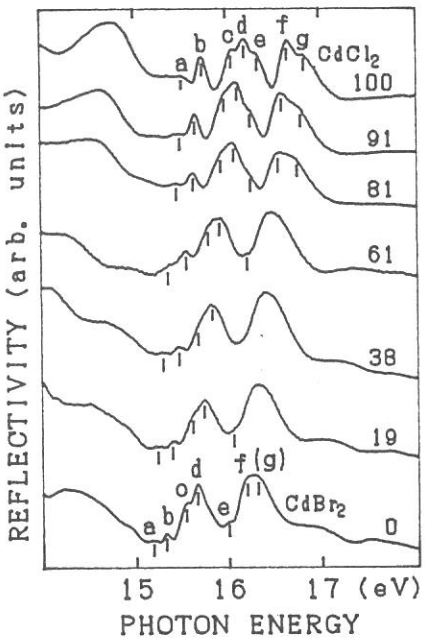

Fig. 1. Reflection spectra of $CdCl_2$-$CdBr_2$ mixed crystals at 35 K. The numbers shown on the right of each spectrum indicate the concentration of $CdCl_2$ in mole percent.

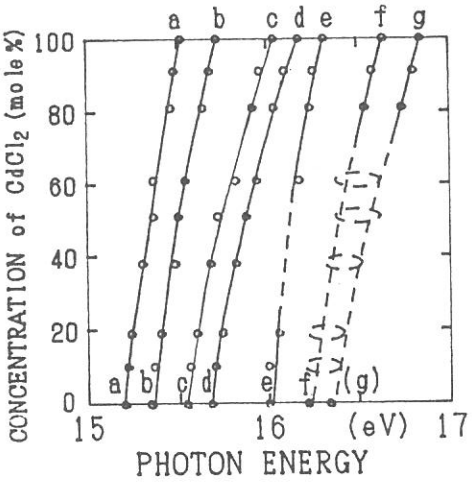

Fig. 2. The energies of the reflection peaks are plotted against the concentration of $CdCl_2$.

Ba $N_{4,5}$ Absorption Spectra of Ba-Compounds

Masao Kamada*, Hiroaki Yamamoto, and Osamu Aita
College of Engineering, University of Osaka Prefecture, Mozu, Sakai, Osaka 591

The localization or delocalization of 4f electrons is of much interest, because it is closely related with the variety of optical, electric, and magnetic properties of rare-earth compounds. Many authors have investigated $4d^9 4f^{n+1}$ excited states produced by 4d-excitation and showed the sharp lines and the giant structures in the $N_{4,5}$ absorption spectra of rare-earths (RE). In recent years, Miyahara et al.[1] have shown that the giant structures due to the $4d^9 4f^1$ excited states of BaF_2 are sensitive to the valency and the crystal structure. This result is very interesting, since the RE $N_{4,5}$ absorption spectra of many rare-earth compounds have been interpreted in the atomic picture. Recent theoretical calculation by Jo also shows the importance of a valence-mixing and a hybridization to explain the sharp lines in the Ce $N_{4,5}$ absorption spectra of some Ce-compounds.[2] The purpose of the present study is to know the localization or delocalization of $4d^9 4f^1$ states of Ba-compounds, where there is no 4f electrons in the ground state but a 4d hole and a 4f electron in the excited state as in the cases of Cs-, La-, and some Ce-compounds.

The experiments were carried out using a 2-m Grasshopper monochromator at BL2B1 beam line of UVSOR. The absorption spectra were obtained with the transmission mode of thin films. Barium halides were prepared on a collodion substrate coated with a thin alminum film by a vaccum-evaporation method. The absorption spectra of total yield mode were also measured on the thin films evaporated on gold. Both absorption spectra are in good agreement except for slight differences in relative intensity of the structures. For a high-T_c $YBa_2Cu_3O_{7-x}$ superconductor, only the absorption spectrum of total yield mode was measured on samples of a disk type.

Figure 1 shows the Ba $N_{4,5}$ absorption spectra of transmission mode for BaF_2, $BaCl_2$, and $BaBr_2$. These spectra consist of sharp lines and broad bands. The spectral shape of

BaF_2 is in good agreement with the existing result by Miyahara et al.[1] Sharp lines are attributed to ^3D and ^3P states, and broad bands are mainly due to the autoionized ^1P states in the atomic picture. However, it should be noted that spectral shapes of the broad bands of $BaCl_2$ and $BaBr_2$ are close to each other, but are much different from those of BaF_2. This difference cannot be explained in the atomic picture. We suppose that this may be interpreted with the difference in the crystal structure, since BaF_2 has a CaF_2-type structure and others have a $PbCl_2$-type structure. Figure 2 shows the Ba $N_{4,5}$ absorption spectrum of total yield mode of $YBa_2Cu_3O_{7-x}$. The spectral shape agrees well with those of $BaCl_2$ and $BaBr_2$, but not with that of BaF_2. This indicates that the local environment of barium ion in $YBa_2Cu_3O_{7-x}$ is closer to those of $BaCl_2$ and $BaBr_2$ than that of BaF_2. Detailed comparison of the absorption spectra with the resonant-photoemission spectra will be given elsewhere.

*present address: Institute for Molecular Science, Myodaiji, Okazaki 444.

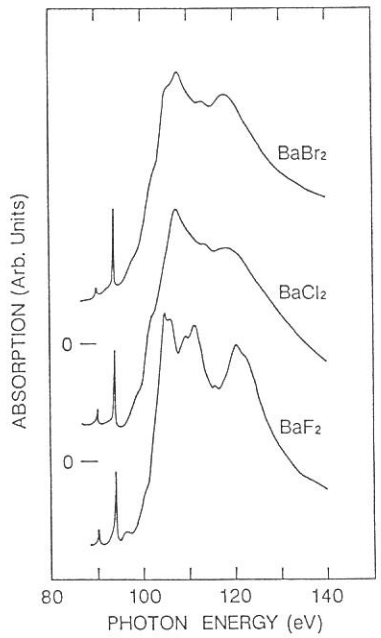

Fig. 1. Ba $N_{4,5}$ absorption spectra of BaF_2, $BaCl_2$, and $BaBr_2$.

References

1) T. Miyahara et al., J. Phys. Soc. Jpn. 55 (1986) 408.
2) T. Jo, J. Phys. Soc. Jpn. 58 (1989) 1452.

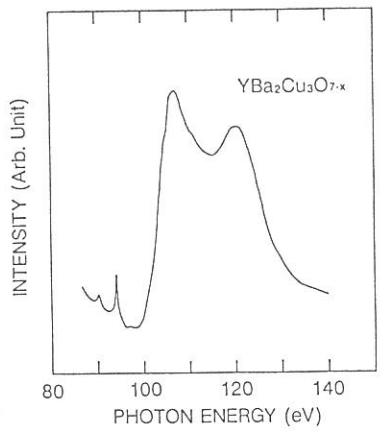

Fig. 2. Ba $N_{4,5}$ absorption spectrum of total yield mode of $YBa_2Cu_3O_{7-x}$.

Pb 5d and Te 4d Absorption Spectra of Crystalline and Amorphous PbTe

Kazutoshi FUKUI, Tadaaki SAITO[1], Shin-ichi KONDO[1]
and Makoto WATANABE

Institute for Molecular Science, Okazaki 444
[1]Department of Applied Physics, Fukui University, Fukui 910

Core absorption spectra of Pb *5d* and Te *4d* levels of PbTe thin films in both crystalline (*c*-) and amorphous (*a*-) phases at about 40 K were measured *in situ* at BL6A2 equipped with a plane grating monochromator (PGM). The *a*-PbTe thin films were deposited by thermal evaporation onto the collodion films kept at about 40 K. The absorption measurement of as-deposit film (*a*-phase) was carried out first, then the film was annealed at room temperature for crystallization. After annealing, it was again cooled to about 40 K, and the absorption measurement on *c*-phase PbTe was made. It was known that the evaporated films of *c*-phase were *n*-type degenerated semiconductor.

Figure 1 shows the absorption spectra of a PbTe thin film in both *a*- and *c*-phases in the energy region from 17 to 26 eV. The curve **a** represents the spectrum in the *a*-phase and **c** represents the spectrum in *c*-phase. These absorption structures correspond to the transition from Pb *5d* core level to the conduction band. The line shape become sharp after crystallization. The structures in *c*-phase are in agreement with those in the previous reflection spectrum on a single crystal[1)] Figure 2 shows the absorption spectra in the energy region from 37 to 49 eV and Te *4d* absorption is observed. Curves **a** and **c** represent spectra in *a*- and *c*-phases, respectively. The broad structures with shoulders can be seen in both *a*- and *c*-phases, and additional structures appear above 4 eV from N_V edge in *c*-phase.

The intensity ratio between the first and the second peaks of the Pb *5d* doublet in Fig. 1 is different from the ratio of statistical weights between O_V and O_{IV} levels (3:2). This means the existence of the strong exchange electron-core-hole interaction so that the transition is *intraatomic*. This is quite consistent with the calculated electronic structure[2)] since the bottom of the conduction band mainly consists of Pb *6p* states. The broad structures of Te N_V and N_{IV} absorptions in Fig. 2 suggest that the electron-core-hole interaction is weak so that they seems to reflect the density of states of the conduction band and transition is *interatomic*. The differences of outermost *d* absorptions between cation and anion are found in the other IV-Te compounds (SnTe, GeTe)[3-4)]. In *c*-SnTe and *c*-GeTe which are *p*-type degenerate semiconductors, there is a small peak below broad structures of Te *4d* absorption, while, there is no small peak (Fig. 2) below broad structures in *c*-PbTe.

Therefore, one possible interpretation is that these small peaks are due to the transition from Te *4d* level to hole states generated by cation vacancies in *p*-type SnTe and GeTe, which are located near the top of the valence band. However, the origin of these peaks is still an open question.

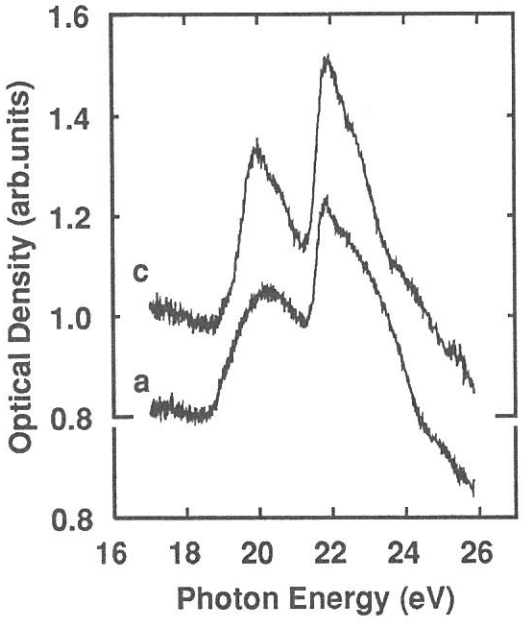

Fig. 1. Pb *5d* absorption spectra of both *a*- and *c*-phase of PbTe thin film in energy region from 17 to 26 eV. Curves a and c show spectra in the *a*- and *c*-phase, respectively.

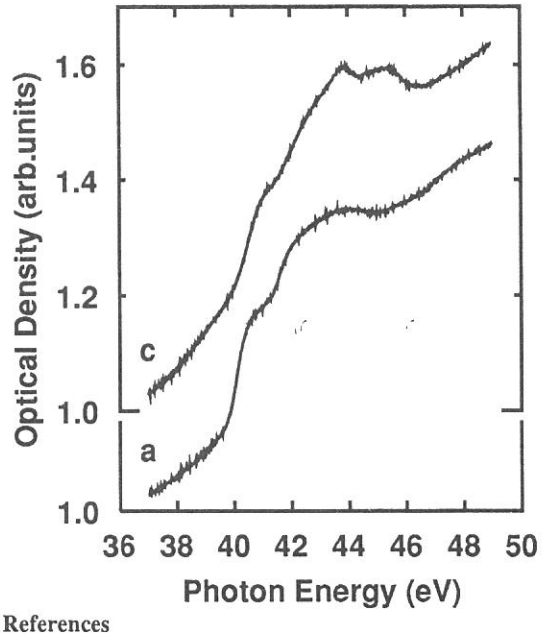

Fig. 2. Te *4d* absorption spectra of both *a*- and *c*-phase of PbTe thin film in energy region from 37 to 49 eV. Curves a and c show spectra in the *a*- and *c*-phase, respectively.

References

1) G.Martinez et al.: Phys. Rev. B **11** (1975) 660.
2) M.Schlüter et al.: Phys. Rev. B **11** (1975) 3808.
3) K.Fukui et al.: J. Phys. Soc. Jpn. **56** (1987) 4196.
4) K.Fukui et al.: UVSOR Activity Report 1988, p.61.

EXAFS study of KH_2PO_4 in the ferroelectric phase and the paraelectric phase.

Takafumi KOSHIBA, Hirofumi KASATANI, Yasuo NISHIHATA,*)
Kiyoshi SAKAUE, Yukio NODA**) and Hikaru TERAUCHI

School of Science, Kwansei Gakuin University, Nishinomiya 662

It is well-known that KH_2PO_4(KDP) undergoes the paraelectric-ferroelectric phase transition at 123K, which is considered to be an order-disorder rearrangement of the proton in the hydrogen-bond. Recently, Tokunaga et al.[1] proposed a new model to explain the Raman scattering data. In the paraelectric phase, the PO_4 tetrahedra have the C_2 site symmetry and distribute statistically. The paraelectric-ferroelectric phase transition is caused by the PO_4 order-disordering. We measured the EXAFS spectra near the P-K edge in order to elucidate the local symmetry of the PO_4 in the paraelectric and ferroelectric phases.

We examined the two samples(#1 and #2) prepared by the different method. The sample #1 was made by the same method as that in the previous experiment.[2] The sample #2 was made by dropping the saturated aqueous solution of KDP into ethanol. The monochromator and the measuring apparatuses were the same as that in the previous experiment. The EXAFS spectra near the P-K edge between 2.06keV to 2.81keV were obtained at room temperature(R.T) and at low temperature(17K) at BL 7-A . The closed cycle cryocooler was used for the low temperature measurement.

Figure 1 shows the EXAFS spectra $k^3\chi(k)$ of #2 measured at R.T(a) and 17K(b), where k is the wavenumber. The spectra of #1 are almost the same as those of #2. Fourier transforms of the spectra from $k=2.57$ Å^{-1} to 13.00 Å^{-1} are shown in Fig.2.(a),(b). The peaks of higher shells become high at low temperature. The results of the curve fitting are given in Table I. The 1-shell model signifies that the site symmetry of the PO_4 is S_4, and the 2-shell model signifies C_2. Even if the least-squares refinement at room temperature data was started with the 1-shell model(c), the 2-shell model(b) had the more reliability. It is conculuded that the site symmetry of the PO_4 tetrahedra is the C_2 symmetry in the paraelectric phase. More detailed analysis is in progress.

The authors thank M. Watanabe, O. Matsudo, K. Fukui and other staffs of the Institute for Molecular Sciences for the help and encouragements.

*) Faculty of Science, Okayama University, Okayama 700
**) Faculty of Science, Chiba University, Chiba 260

1) M. Tokunaga, Y. Tominaga, and I. Tatsuzaki, Ferroeiectlics 63, 171 (1985).
2) Y. Nishihata and H. Terauchi, UVSOR Activity Report,(1988) p.75.

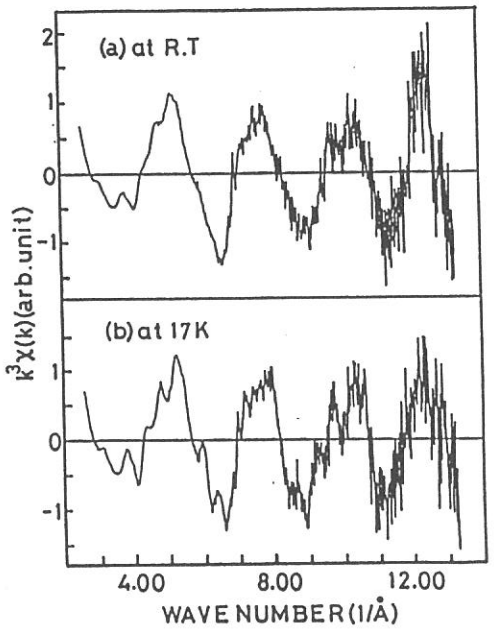

Fig.1 EXAFS spectra $k^3\chi(k)$, vs. wavenumber (a) at R.T (b) at 17k

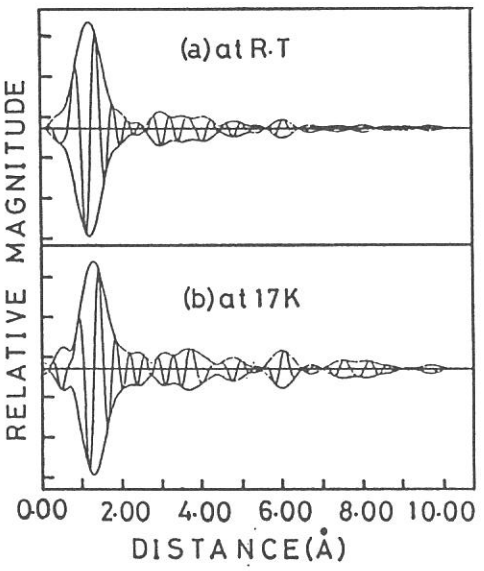

Fig.2 Fourier transform of EXAFS spectra (a) at R.T (b) at 17k

	temperature	model	P-O distance(Å)
(a)	17K	2-shell	1.527(1)
			1.585(2)
(b)	R.T	2-shell	1.504(9)
			1.578(3)
(c)	R.T	1-shell	1.541(2)

Table I The results of the curve fitting of the first peak

Na K-edge XANES/EXAFS Studies on Structure of Sodium Catalyst for Coal Gasification

Hiromi YAMASHITA, Satohiro YOSHIDA*, Akira TOMITA
Chemical Research Institute of Non-Aqueous Solutions,
Tohoku University, Katahira, Sendai 980, Japan.
*Department of Hydrocarbon Chemistry, Faculty of Engineering,
Kyoto University, Kyoto 606, Japan.

Sodium compounds are useful catalysts for coal gasification. Although NaCl is cheap enough to be attractive as a raw material of catalyst for gasification, its activity is generally quite low compared with that carbonate because of the strong affinity between sodium ion and chloride ion. We have found recently that an active sodium catalyst can be prepared from NaCl solution by using the ion-exchanging method[1]. In the present study, structures of sodium catalysts in Na-loaded coals and chars have been investigated by X-ray absorption spectroscopy.

Loy Yang brown coal from Victoria, Australia, was used. NaCl, $Na_2CO_3 \cdot 10H_2O$ were used as precusor salts. Several Na-loaded coals (4 wt% as metal) were prepared by ion-exchanging or imregnation. The coal samples were dried and devolatilized in N_2 in a fluidized bed reactor to prepare char samples. Soft X-ray absorption spectra at Na K-edge were recorded with EXAFS facilities[2] at BL-7A of UVSOR (ring energy: 750 MeV). A beryl two-crystal monochrometer was used. Energy calibration was made by using Al K-edge absorption.

Figure 1 shows the XANES spectra of NaCl (a), $Na_2CO_3 \cdot 10H_2O$ (b), Na-loaded coal (c) and chars prepared by heating at 550°C (d-f). Na atom is surrounded octahedrally by six chlorine atoms in NaCl and surrounded distorted-octahedrally by six oxygen atoms in $Na_2CO_3 \cdot 10H_2O$, respectively[3]. This structural difference reflected obviously on the XANES spectra. NaCl exhibited a sharp main peak at 1077 eV with a sharp sub-peak at 1080 eV (a), while $Na_2CO_3 \cdot 10H_2O$ exhibited a broad main peak at 1078 eV with a shoulder at 1076 eV (b). Anhydrous Na_2CO_3 exhibited very similar spectrum to that of hydrate. The spectra of dried Na-loaded coal prepared by the impregnation with NaCl [ICLdry] (c) and Na-loaded char prepared by heating of ICLdry coal at 550°C [ICL550] (d)

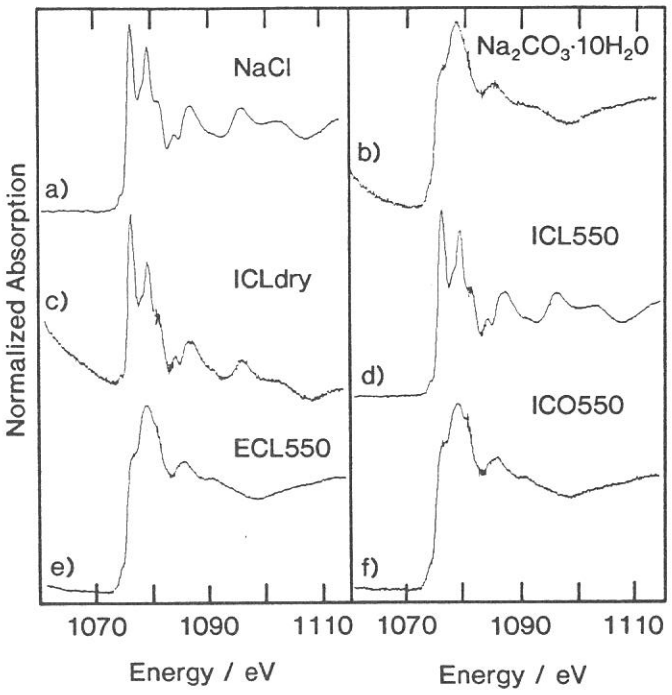

a)NaCl
b)$Na_2CO_3 \cdot 10H_2O$
C)ICLdry: NaCl, impregnation, after drying.
d)ICL550: NaCl, impregnation, after heating at 550° C.
e)ECL550: NaCl, ion-exchanging, after heating at 550° C
f)ICO550: $Na_2CO_3 \cdot 10H_2O$, impregnation, after heating at 550° C.

Figure 1 Na K-edge XANES spectra.

were very similar to that of NaCl. This result indicated that the NaCl crystalline particle existed even after drying of NaCl impregnated coal and decomposition of NaCl crystalline did not occurred after devolatilization at 550° C. On the other hand, Na-loaded coals prepared by ion-exchanging with NaCl [ECL] and by impregnation of $Na_2CO_3 \cdot 10H_2O$ [ICO] exhibited very ambiguous spectra suggesting the Na species in coals had very disordered local structures. Na-loaded chars prepared from ECL [ECL550] (e) and ICO [ICO550] (f) exhibited similar spectra to those of two kinds of Na_2CO_3 salts. This result indicated that Na atom was surrounded by six oxygen atoms distorted-octahedrally and that fine particles of Na_2CO_3 might be formed in these chars.

References

1) T. Takarada, T. Nabatame, Y. Ohtsuka and A. Tomita, Ind. Eng. Chem. Res., **28**, 505 (1989).
2) T. Murata, T. Matsukawa, M. Mori, M. Obashi, S. Naoe, H. Terauchi, Y. Nishihata, O. Matsudo and J. Yamazaki, J. Phys., **47**, C8-135 (1986).
3) T. Taga, Acta Cryst., **B25**, 2656 (1969).

Doping Effect of Sodium and Sodium ion on Magnesium Oxide and Aluminum Oxide

Geng ZHANG, Tsunehiro TANAKA, Hideshi HATTORI
and Kozo TANABE

Department of Chemistry, Faculty of Science,
Hokkaido University, Sapporo 060

It is well known that the doping of alkali metal[1] or alkali metal ion to magnesium oxide significantly improved the basic strength of the matrix oxide. Recently, Na^+-MgO was reported to be effective for oxidative coupling of methane[2]. Na-NaOH-Al_2O_3 system[3] has been found to possess basic sites with H_->35, so-called superbase. In the present work, the chemical states of sodium atom or ions added to matrix have been investigated by X-ray absorption spectroscopy.

NaOH-MgO, NaOH-Al_2O_3 and $NaNO_3$-MgO were prepared by adding aqueous solution of NaOH or $NaNO_3$ to MgO and Al_2O_3, respectively, stirring at room temperature followed by drying at 353K. All the samples were evacuated at 873K prior to X-ray absorption measurements. Sodium metal deposited MgO, *i.e.*, Na-MgO, was prepared as follows. Sodium azide(Na-content 0.05g) evacuated at 473K was added to 0.5g of MgO evacuated at 873K followed by heating at 673K for 1h *in vacuuo*. Na-NaOH-MgO, Na-Al_2O_3 and NaOH-Al_2O_3 were prepared in the similar way.

X-Ray absorption measurement was carried out at beam line 7-A in UVSOR facility. A beryl two-crystal monochrometer was used. Energy calibration was made by using Al K-edge absorption. Mg K-edge and Na K-edge absorption spectra were recorded.

For Mg K-edge absorption, the XANES region of Na atom or Na^+ ion kept unchanged from non-doped MgO up to the range of Na content of 5.56mmol/g-MgO. The analysis of EXAFS oscillations showed that both Debye-Waller factors and distances from Mg to O and from Mg to Mg were in consistence with those of pure MgO. Those results support the conclusion derived from XPS experiment that most of sodium ions aggregate on MgO surface rather than

diffuse into MgO bulk.

Fig.1 showed the XANES spectra at Na K-edge of typical Na^+-MgO, Na^+-Al_2O_3 and Na-NaOH-MgO. We could not identify the structure of Na atom possessed at this stage because of the lack of reference compound. The fact that no significant difference in the spectra was found among NaOH-MgO, NaOH-Al_2O_3 and $NaNO_3$-MgO revealed that Na^+ deposited on MgO and Al_2O_3 in a similar way and Na^+ deposition was hardly affected by the type of starting material.

The deposition of Na metal on NaOH-MgO by decomposition of sodium azide generated a new absorption at 1075eV which was tentatively assigned to the absorption by Na metal. However, with Na-NaOH-Al_2O_3, the fine structure was hidden, probably, due to the strong absorption of Na metal. Although the exact structures of Na^+ or Na species are not clear at this stage, it is considered that the mechanism for generation of strong basic sites is similar for Na-promoted MgO and Al_2O_3.

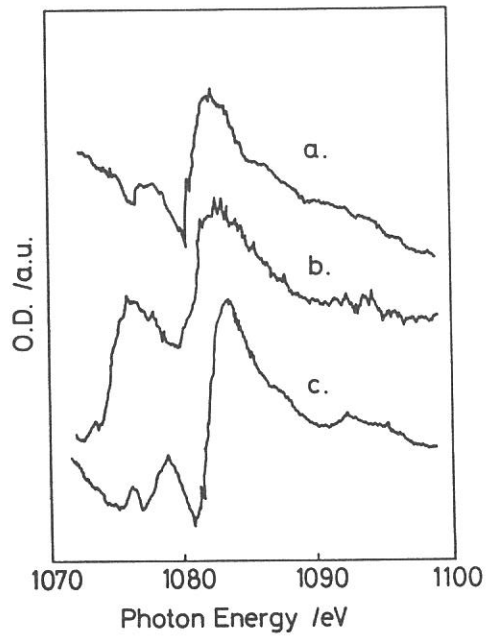

Fig.1 Na K-edge absorption spectra of (a) Na^+(5.56mmol/g)-MgO, (b)Na^+(5.56mmol/g)-Al_2O_3 and (c)Na-Na^+(2.78mmol/g)-MgO.

References:

1. S. Malinowski, J. Kijenski, in *Catalysis* (C. Kemball and D.A.Dawen, eds.) Vol.4, p.130, Royal Soc. Chem.(1981).
2. C.-H. Lin, J.-X. Wang and J. H. Lunsford, *J. Catal.*, 111, 302(1988).
3. G. Suzukamo, M. Fukao and M. Minobe, *Chem. Lett.*, 585, 1987.

Mg K-Edge Absorption Spectra of Magnesium Oxide Species Formed in Mg-Exchanged Y-Type Zeolite. II

Tsunehiro Tanaka, Hideto Tsuji, Geng Zhang, Hideshi Hattori, and Takanori Murata*

Department of Chemistry, Faculty of Science, Hokkaido University, Sapporo 060.
**Department of Physics, Kyoto University of Education, Fushimi-ku, Kyoto 612.*

Previously, we have reported that the fine particle of magnesium oxide is formed in/on Mg-exchanged Y-type zeolite elucidated by means of K-edge absorption spectroscopy. The fine structure of the spectra in the XANES and NEXAFS region was similar to that for magnesium oxide. In the EXAFS region, however, noise hid the fine structure. During the latest experiment, we have tried to accumulate photons as largely as possible to avoid statistical noise. We report here extended results of the spectrum with higher quality.

The samples were prepared by immersing Mg-exchanged Y-type zeolite (MgO/MgY) or SiO_2 (MgO/SiO_2) into a methanol solution of magnesium methoxide under an oxygen- and moisture- free nitrogen atmosphere, followed by evaporation of methanol and calcination in air at 823 K. The presence of MgO crystal was not confirmed by X-ray diffraction technique.

Characterization of the samples was carried out by chemical reactions and it was found that both the MgO/MgY and MgO/NaY exhibit basic properties. The poisoning experiment of 1-butene isomerization at 273 K suggest that magnesium oxide species are formed in supercages in the case of MgO/MgY and not in MgO/SiO_2.

X-Ray absorption experiments have been carried out on the beam line 7-A with UVSOR facilities. A beryl two-crystal monochromator was used.

Figure 1 shows the XANES spectra of MgO, MgO/MgY and MgO/SiO_2. Narrow white lines due to 1s-3p transition found in the vicinity of 1310 eV shows that Mg cations of all the sample are located at symmetrical centers. However, comparing with the heights of three peaks in the region less than 1320 eV, the white lines for MgO/MgY and MgO/SiO_2 is lower than that for MgO. This is caused by the presence of $Mg(OH)_2$ for MgO/MgY and MgO/SiO_2. Figure 2 shows the

Fourier transforms of k-weighted EXAFS of these samples. In the case of MgO/MgY, the height ratio of peak at around 2.5 A to that at around 4 is a little larger than that for the cases of MgO/SiO_2 and MgO and absolute peak heights for the MgO/MgY are smaller than those of the two of others. This suggests that fine particle of MgO is formed in MgO/MgY. Though estimation of the particle sizes is in progress, it is very likely that MgO fine particle is formed in the super cages of MgY combining the result of poisoning experiment.

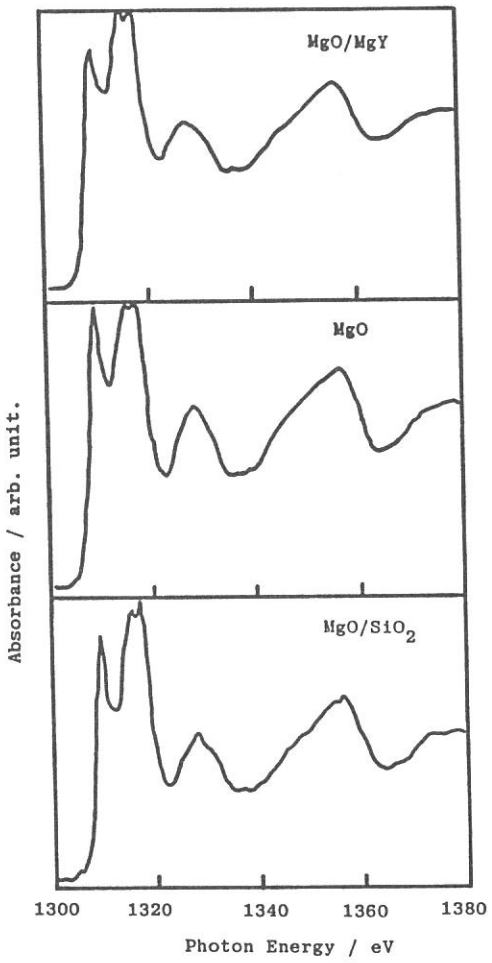

Fig. 1 Mg K-edge XANES spectra of MgO/MgY(top), MgO(middle), and MgO/SiO_2(bottom).

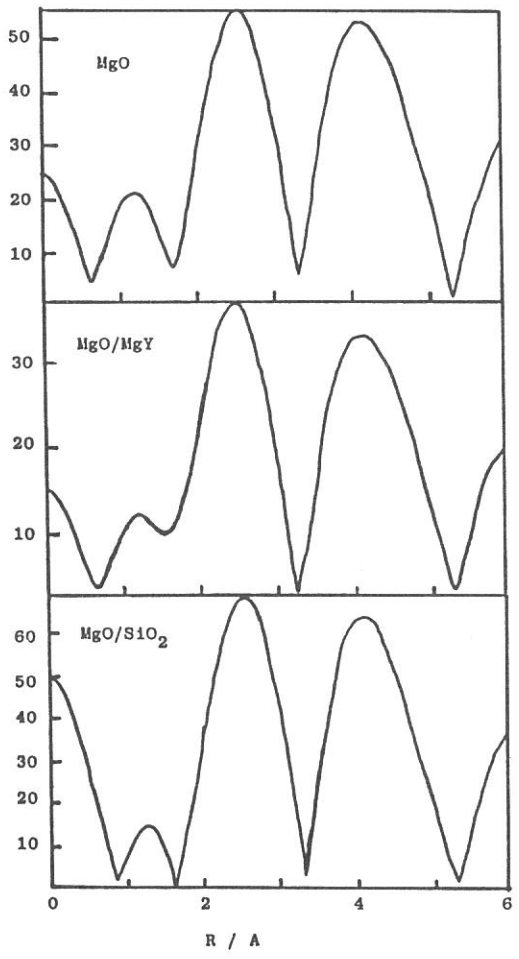

Fig. 2 Fourier transforms of Mg K-edge EXAFS of MgO(top), MgO/MgY(middle), and MgO/SiO_2.

Absorption Coefficients of Al, Ti, Ni, Cu, Ag and Au Thin Films in the 1-5 keV Region

M.Watanabe, O.Matsudo, K.Sakai, J.Yamazaki,
E.Nakamura and K.Fukui
UVSOR, Institute for Molecular Science

Mass absorption coefficients of Al, Ti, Ni, Cu, Ag and Au thin films were measured at room temperature at BL7A equipped with a double crystal monochromator. In the 1-2 keV region, the synchrotron radiation was dispersed by beryl crystals and in the 2-5 keV, quartz crystals. In the below figures are shown the absorption spectra of Al, Ti, Cu and Ag. They are in good agreement with the data of Henke at al.[1] obtained by fitting theoretical calculations to the best available experimental data.

Reference
1) B.L.Henke et al., Atomic Data and Nuclear Data Tables 27, No.1, p,1.

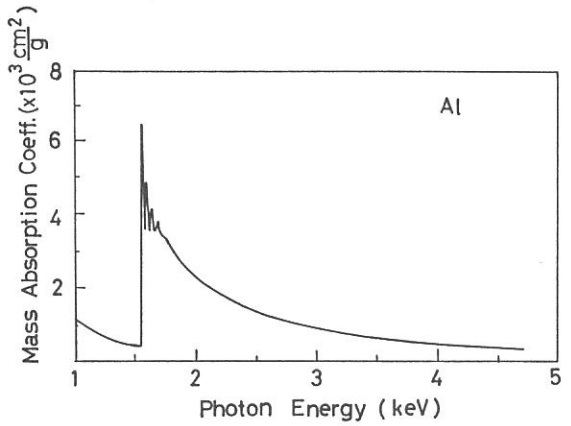

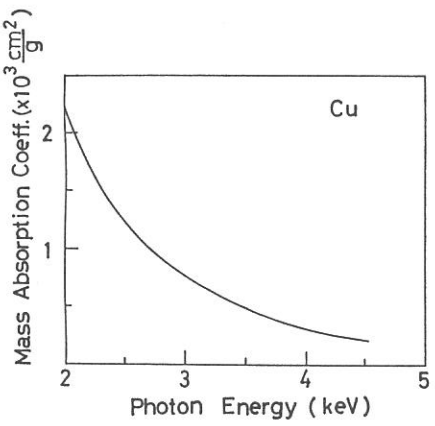

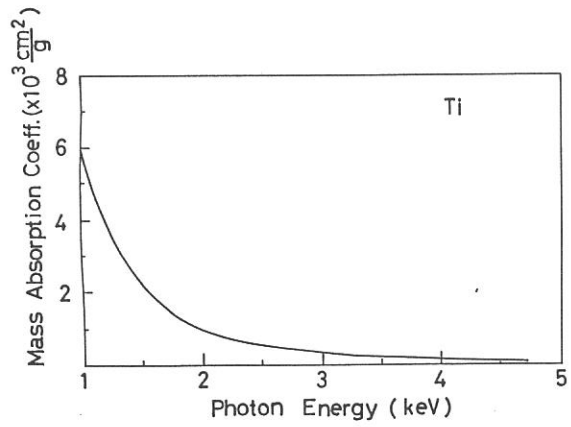

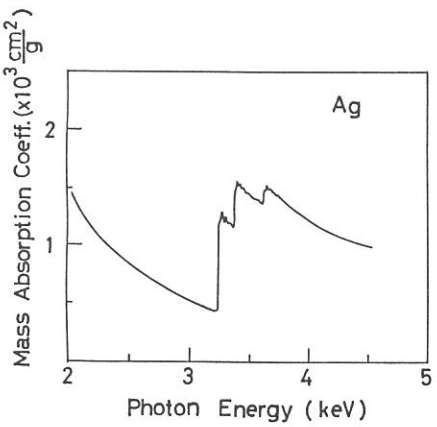

K Absorption Spectrum of Solid Neon

Atsunari HIRAYA, Kazutoshi FUKUI, Poh-Kun TSENG(*National Taiwan Univ.*)
Takatoshi MURATA(*Kyoto Univ. of Education*), **and Makoto WATANABE**

Absorption spectra of solid and gaseous neon were measured in the 850 - 1300 eV region at BL7A equipped with a double crystal monochromator. Beryl crystals were used for this energy range. For the measurement of solid neon a He cryostat was installed in a vacuum chamber at the beam line. Solid neon film was deposited on an Al foil (0.8 μm thickness) mounted on a sample holder at the bottom of the He cryostat. The deposition tempereture was 6.33 ± 0.05K. A gas cell was connected to the exit port of the vacuum chamber. Windows of the gas cell were thin film organic-polymer. Figure 1 shows the spectra of solid and gaseous neon in 860 - 880 eV region. Gas phase spectrum is in agreement with the result of Wuilleumier[1]. Two sharp peaks at 867.6 and 869.3 eV in gaseous neon correspond to the 1s→3p and 1s→4p transitions, respectively. Both two peaks appear at, 868.6 and 870.0 eV, also in solid neon with spectral shift toward high energy. The separation between the first peak and the second peak in gaseous neon becomes small in solid neon (1.7 → 1.4 eV). The width of the first peak becomes broader (1.0 eV) in solid neon, in comparison with that in gaseous neon (0.8 eV). Figure 2 shows the absorption spectrum of solid neon in 830 - 1300 eV region. In solid neon XANES was observed above 880 eV and EXAFS was observed very weakly above 980 eV. Amplitudes and shapes of XANES and EXAFS were found to be altered depending on the deposition temperature. Measurements on the temperature effect are under way.

References 1) F. Wuilleumier, J. Phys. (Paris), Colloq. C4, Supp. 10, **32,** 88 (1971).

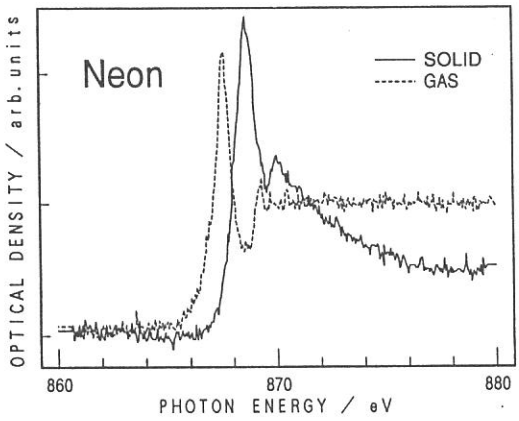

Figure 1 Absorption spectra of solid and gaseous neon. Deposition temperature was 6.37K. Ne gas pressure was 538 mTorr.

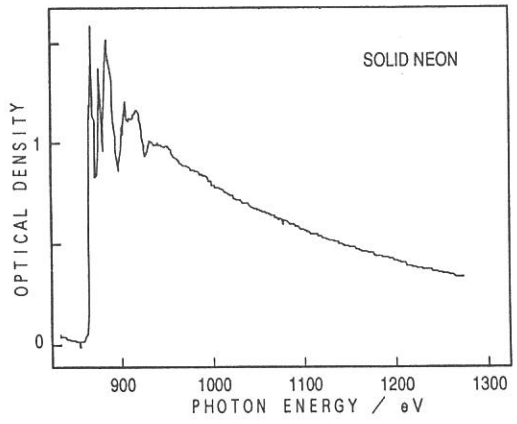

Figure 2 XANES and XEAFS of solid neon.

COMPARATIVE ANGLE-RESOLVED PHOTOEMISSION STUDY OF $Bi_2Sr_2Ca_{1-x}Y_xCu_2O_8$ (x=0.0 AND 0.5)

Hiroyoshi MATSUYAMA, Takashi TAKAHASHI, Koji KAMIYA[A],
Hitoshi FUJIMOTO[B], Kazuhiko SEKI[C], Sigeru SATO, and Hiroo INOKUCHI[A]

Department of Physics, Tohoku University, Sendai, 980
[A]Institute for Molecular Science, Okazaki 444
[B]Department of Chemistry, Kumamoto University, Kumamoto 860
[C]Department of Material Science, Hiroshima University, Hiroshima 730

We have already reported an angle-resolved photoemission study of the high-Tc superconductor $Bi_2Sr_2CaCu_2O_8$[1]. Figure 1 shows the angle-resolved photoemission spectra and the band structure of $Bi_2Sr_2CaCu_2O_8$ determined from the angle-resolved photoemission, where two dispersive bands A and B clearly intersect the Fermi level midway between the center and the boundary of the Brillouin zone, giving a direct evidence for the existence of Fermi surface and resultingly the Fermi-liquid states in the high-Tc superconductor.

Knowlege of the nature and origin of the Fermi liquid states is a key-step toward understanding the high-Tc mechanism. In this viewpoint, it would be very useful to study the difference of the electronic structure between the supercunductor and the non-superconductor. In this report, we present the result of an angle-resolved photoemission study of non-superconducting $Bi_2Sr_2Ca_{0.5}Y_{0.5}Cu_2O_8$ where holes are compensated with electrons by replacing divalent Ca with trivalent Y.

A single crystal of $Bi_2Sr_2Ca_{0.5}Y_{0.5}Cu_2O_8$, typically $3\times3\times0.5mm^3$, was successfully grown with a self-flux technique. The single-crystallinity was checked by an x-ray diffraction measurement and the magnetic-susceptibility measurement showed that the crystal does not become superconductive even at liquid-helium temperature.

Figure 2a shows angle-resolved photoemission spectra of $Bi_2Sr_2Ca_{0.5}Y_{0.5}Cu_2O_8$ for the Γ-X direction in the Brillouin zone measured at the photon energy of $h\omega$=18eV. The most remarkable feature in Fig. 2 is the absence of spectral intensity in the vicinity of the Fermi level in contrast with the case of superconducting Bi_2Sr_2Ca-Cu_2O_8. Figure 2b shows the obtained band sturucture for $Bi_2Sr_2Ca_{0.5}Y_{0.5}Cu_2O_8$. Comparison between the band structures of the superconductor (Fig. 1) and the non-superconductor (Fig. 2) shows that (i) bands A and B which intersect the Fermi level in superconductor disappear in the non-superconductor, (ii) a non-dispersive band at 1.5 eV in the superconductor also disappears in the non-superconductor, instead a new non-dispersive band (band C') emerges at 2.3 eV, and (iii) a small shift by 0.2-0.3 eV toward the high-binding-energy side is observedfor bands D and F in the non-superconductor. The direction of the shift for bands D and F looks reasonable when we suppose a possible rigid shift of the Fermi level upon doping of electrons into the hole-doped superconductor. However it is not the case for bands A and B, which disappear after doping of electrons. This experimentalresult is consistent with an x-ray absorption spectroscopy of $Bi_2Sr_2Ca_{0.5}Y_{0.5}Cu_2O_8$, where the oxygen-K edge is not shifted by electron-doping but only the intensity of the edge-peak changes according to the hole concentration[2].

The observed non-rigid shift of the electronic structure in the vicinity of the Fermi level indicates that the Fermi-liquid state in the high-Tc superconductor is not a simple one-electron state predicted from the band structure caluculation. The experimental result that hole-doping does not necessarily cause a shift of the Fermi level but produces new electronic states near the Fermi level is in favor of a kind of impurity state as an origin of the Fermi-liquid state.

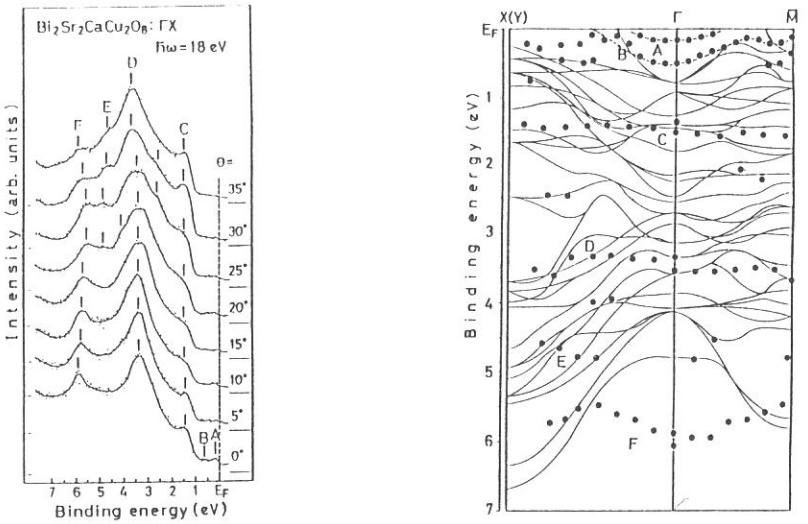

(a) Figure 1 (b)

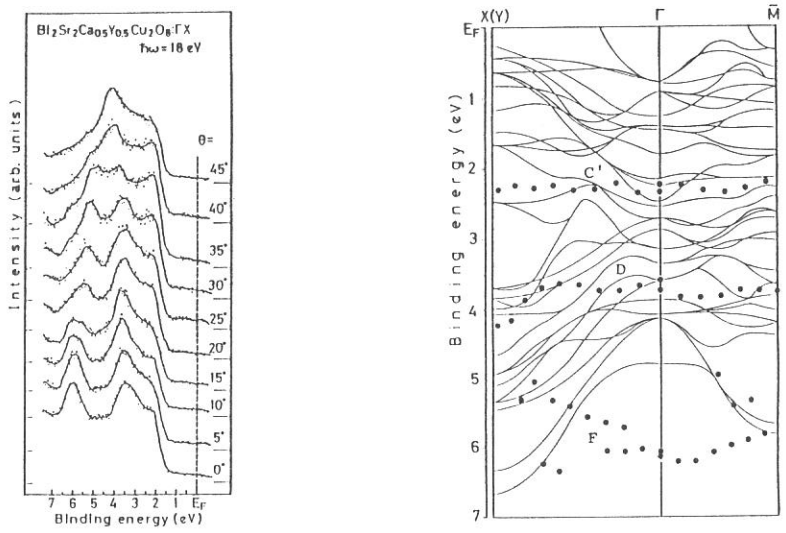

(a) Figure 2 (b)

References

1. T. Takahashi et al.: Nature **334**, 691 (1988).
2. H. Matsuyama et al.: Physica C **160**, 567 (1989).

ARUPS spectra of amorphous and crystalline In_2Se_3

Shuichi KANEKO, Yuichi WATANABE*, Hiroshi KAWAZOE, Masayuki YAMANE,
Hiroo INOKUCHI**, Hitoshi FUJIMOTO***, Koji KAMIYA**

Tokyo Institute of Technology, Meguro, Tokyo 152
*Nagaoka University of Technology, Fukasawa, Nagaoka 949-54
**Institute for Molecular Science, Myodaiji, Okazaki 444
***Kumamoto University, Kurokami, Kumamoto 860

Amorphous In_xSe_{100-x} has attracted much interest because of its anomalous electrical conduction behavior, which is observed especially in the composition of X=40 [1] : The observed activation enthalpy for electrical conduction is far less than a half of the optical band gap. The reasons why the anomaly appears have not been fully discussed. In order to find out the origin of the anomalous conduction, we carried out an energy band calculation on polymorphs of crystalline In_2Se_3 (X=40) using the tight binding method [2] and measurements of photo-conduction. In a present study we obtained ARUPS spectra of amorphous and crystalline In_2Se_3 and compared the spectra with the calculated DOS to establish the relation between the electronic structures of amorphous and crystalline In_2Se_3 and their electrical properties.

Fig.1 shows the representative UPS spectra for amorphous and crystalline In_2Se_3 together with the calculated DOS. The energys of humps of the observed spectra coincide with those of the calculated DOS. The difference between the spectrum of amorphous and that of crystalline seems to be little.

Fig.2 shows the photon-energy-dependence of the spectra for amorphous In_2Se_3. The excitation energy dependence of the relative intensity of the lower binding energy peak (3eV) is similar to that for Se-4p orbital [3]. This fact well agrees with the calculated results; Se-4p orbital is dominating in the upper valence band.

Fig.3 shows the ARUPS spectra for crystalline In_2Se_3. The spectra slightly changed with changing the escape orientation of the photoelectrons with respect to the incident beam. From the calculated E-k diagram, the dispersion in this direction ($\Gamma - M$) is small. It, however, seems that the angle dependence of the spectra resembles the result of energy band calculation.

REFERENCES

1) Ichiro WATANABE and Teiji YAMAMOTO : Jpn. J. Appl. Phys. 24 (1985) 1282
2) Yuichi WATANABE, Shuichi KANEKO, Hiroshi KAWAZOE and Masayuki YAMANE : Phys. Rev. B40(1989) 3133
3) J.J.YEH and I.LINDAU : Atomic Data and Nuclear Data Tables, 32(1985) 1

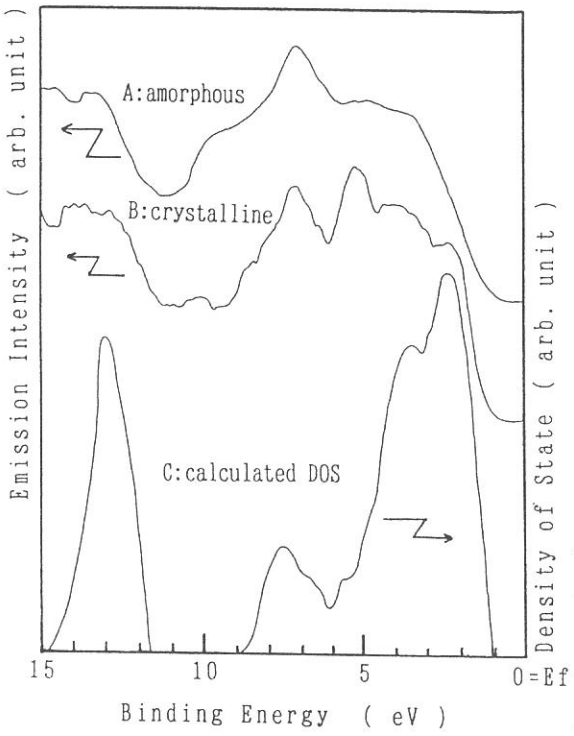

Fig.1 Observed UPS spectra
and calculated DOS

A : UPS spectrum of amorphous In_2Se_3

B : UPS spectrum of crystalline In_2Se_3

C : Calculated DOS

Photon Energy = 50eV

α = 60° θ = 0°

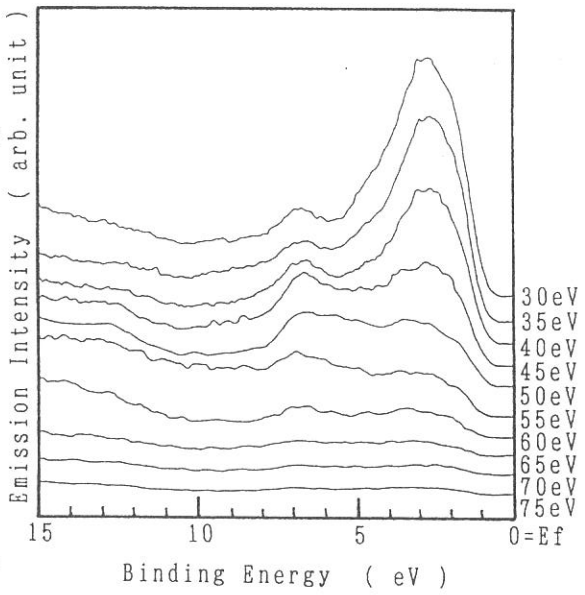

Fig.2 Photon energy dependence of
UPS spectra for amorphous In_2Se_3

α =60° θ =0°

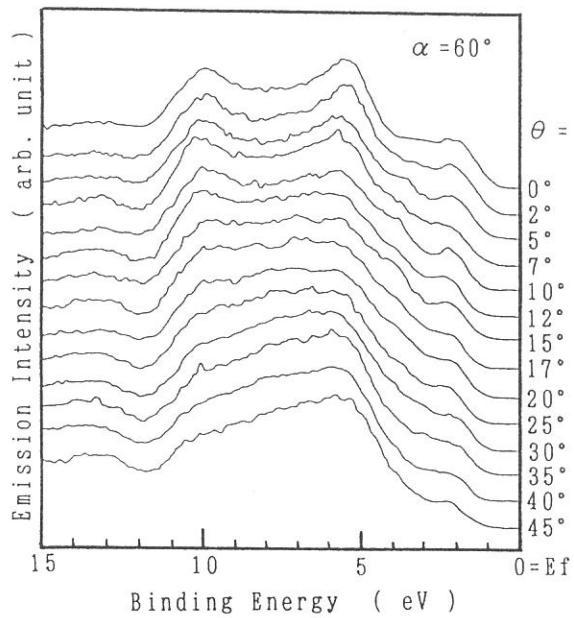

Fig.3 ARUPS spectra for crystalline In_2Se_3

Ultraviolet Photoemission Study of Polythiophene Oligomers (III)

H. Fujimoto,* K. Seki,[a] U. Nagashima, H. Nakahara,[b] J. Nakayama,[b] M. Hoshino,[b] K. Fukuda,[b] and H. Inokuchi

Institute for Molecular Science(IMS), Myodaiji, Okazaki 444, Japan.
[a] *Department of Materials Science, Hiroshima University, Hiroshima 730, Japan.*
[b] *Department of Chemistry, Saitama University, Urawa 338, Japan.*

In our previous work,[1,2] we have reported the results on the electronic structures of oligothiophenes obtained by using the ultraviolet photoemission spectroscopy (UPS). It is shown that (1) the π-band evolution is clearly seen in a series of α-linked oligomers (α_n), and (2) the β linkage shows a strong irregularity on the π-electron systems of polythiophene.

Here, we report the results of the UPS study on the effect of a vinylene introduction into the polythiophene system using oligomers shown in Fig. 1. The observed UPS spectra of these oligomers are discussed in comparison with those of α_n and the results of the semi-empirical MNDO calculations.

Thin films of 50 nm thickness of these compounds were prepared on a polished molybdenum substrate by *in situ* vacuum evaporation in the preparation chamber and transferred to the measurement chamber *in vacuo*.[3] UPS spectra were measured for electrons emitted normal to the sample surface with an incidence angle 60° of the light beam. All theoretical calculations were carried out on an HITAC S-810/10 and an HITAC M-680H computers at the Computer Center of IMS according to our previous paper.[4] The detailed experimental method will be published elsewhere.[5]

The UPS spectra of $\alpha_2V\alpha_2$ and $\alpha_3V\alpha_3$ are shown in Fig. 2. The solid curves show the valence band spectra and the broken ones are the simulated spectra by using a Gaussian function with a width of 0.6 eV to each orbital energies calculated by MNDO (the vertical lines in Fig. 2). The simulated spectra and the orbital energies are shifted down by 6.5 eV to obtain a better fit.

The observed UPS spectra of $\alpha_2V\alpha_2$ and $\alpha_3V\alpha_3$ are similar to those of α_5 and α_7 (shown in Fig. 3), respectively. In particular, the correspondence of the π-band shapes is very good. The π bands of the simulated UPS spectra of these oligomers are also identical to those of the corresponding α_n's. This fact reveals that the π system of vinylene between the α parts does not strongly affect the π-band structures of the host chain. The theoretical results show that the molecular geometries of these oligomers are almost planar and that the π electrons can delocalize over the whole molecule.

In contrast with the π bands, the σ-band shapes of $\alpha_2V\alpha_2$ and $\alpha_3V\alpha_3$ are different from those of the corresponding α_n's, because the skeleton of the

main chain is deformed by the introduction of the vinylene group. This discrepancy is more prominent in $\alpha_2 V \alpha_2$ than in $\alpha_3 V \alpha_3$. This fact confirms that the electronic and geometric structures of these vinylene-containing oligomers are settled by the balance of the π-electron stabilization and the nuclear repulsion of hydrogen atoms.

*present address: *Department of Environmental Science, Kumamoto University, Kurokami, Kumamoto 860, Japan.*

References

1)H. Fujimoto, U. Nagashima, H. Inokuchi, K. Seki, H. Nakahara, J. Nakayama, M. Hoshino, and K. Fukuda, *J. Chem. Phys.*, **89**, 1198 (1988).

2)H. Fujimoto, K. Seki, U. Nagashima, H. Nakahara, J. Nakayama, M. Hoshino, K. Fukuda, and H. Inokuchi, *UVSOR Activity Report*, **15**, 68 (1987); *ibid.*, **16**, 102 (1988).

3)K. Seki, H. Fujimoto, T. Mori, and H. Inokuchi, *UVSOR Activity Report*, **14**, 11 (1986).

4)U. Nagashima, H. Fujimoto, H. Inokuchi, and K. Seki, *J. Mol. Struct.*, **197**, 265 (1989).

5)H. Fujimoto, U. Nagashima, H. Inokuchi, K. Seki, Y. Cao, H. Nakahara, J. Nakayama, M. Hoshino, and K. Fukuda, *J. Chem. Phys.*, in press.

(E)-bis(2,2'-bithiophene-5-yl)ethylene

$\alpha_2 V \alpha_2$

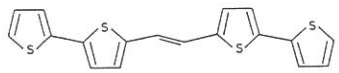

(E)-bis(2,2':5',2''-terthiophene-5-yl)ethylene

$\alpha_3 V \alpha_3$

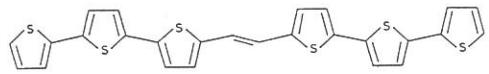

Fig. 1 Oligomers used in this study.

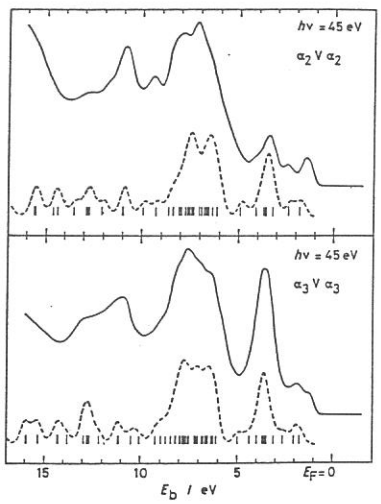

Fig. 2 UPS spectra of $\alpha_2 V \alpha_2$ and $\alpha_3 V \alpha_3$.

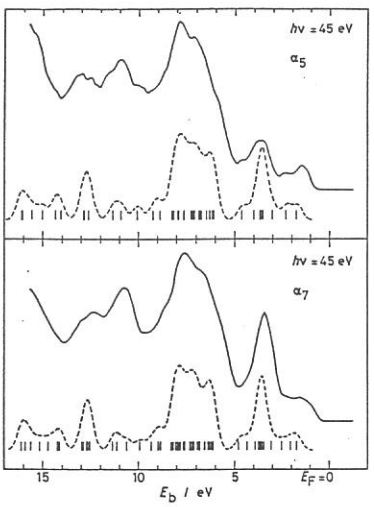

Fig. 3 UPS spectra of α_5 and α_7.

Photoemission Study on the Electronic Structures of Pc_2Lu and $(PcAlF)_n$

M. R. Fahy, H. Fujimoto,* A. J. Dann, H. Hoshi,
Y. Maruyama, and H. Inokuchi
Institute for Molecular Science, Myodaiji, Okazaki 444, Japan.

M. R. Willis
Department of Chemistry, University of Nottingham, Nottingham, UK.

The Phthalocyanine (Pc) class of materials have been the subject of a vast amount of study, both theoretical and experimental.[1] They are the most stable organic materials known, both chemically and thermally and can be sublimed at about 500 °C to form high quality thin films. Most Pc's are, in their intrinsic state, poor semiconductor except for the class of radical Pc dimers of which Pc_2Lu is a typical example. It consists of two Pc rings separated by 2.7 Å and has a single, central, lutetium atom. Pc_2Lu has been the subject of intense recent study because of its excellent electrochromic properties,[2] its high intrinsic conductivity and low band gap of 1.2 eV.[3] A second material that has attracted attention recently is the polymeric Pc, $(PcAlF)_n$ which consists of a stack of AlPc's with fluorine bridges. This material also has a higher than usual conductivity and also has some interesting optical properties.[4] In this study, we will present the results of the UPS study on thin films of Pc_2Lu and $(PcAlF)_n$.

Both materials were prepared as reported[5] and was purified by using gradient sublimation for $(PcAlF)_n$ and by using column chromatography for Pc_2Lu. UPS measurements were carried out at the beamline BL8B2 in the UVSOR Facility. All spectra were taken by using thin films of 100 Å thickness prepared by vacuum evaporation at a slow rate of less than 1 Å/minute.

The UPS spectra of Pc_2Lu and $(PcAlF)_n$ are shown in Fig. 1 along with the spectra for metal free (PcH) and copper (PcCu) Pc's as measured by Battye.[6] As many previous workers have remarked, there is a strong similarity between all the spectra. This is explained by the high ratio of Pc electrons to metal electrons and by the photoionization cross sections of these electrons. The most interesting observation is the energy shift of whole spectral structures to lower energy and the splitting of the lowest energy peak in the Pc_2Lu spectrum. Figure 2 shows the lowest energy peak for Pc_2Lu and $(PcAlF)_n$ and the splitting is clearly seen. This can be explained, in a very simplistic manner, using Fig.3. There is a significant overlap π-electron system of the Pc rings which causes the HOMO orbital to split. Because the Pc_2Lu is a radical, the upper orbital is half filled and this undergoes a further splitting in a way analogous to a Peierls transition in the

solid state of Pc_2Lu.

*present address: *Department of Environmental Science, Kumamoto University, Kurokami, Kumamoto 860, Japan.*

References

1)H. Meier, "Organic Semiconductors-Dark and Photoconductivity of Solids", Verlag-Chemie, 1974 and references therein.

2)G. Corker, B. Grant, and N. Clecak, *J. Electrochem. Soc.*, **126**, 1339 (1979).

3)P. Turek, P. Petit, J.-J. Andre, J. Simon, R. Even, B. Boudjema, G. Guillaud, and M. Maitrot, *J. Amer. Chem. Soc.*, **109**, 5119 (1987).

4)R. Nohr, P. Kuznesof, K. Wynne, M. Kenney, and P. Siebenman, *J. Amer. Chem. Soc.*, **103**, 4371 (1981).

5)T. Permien, R. Engelhardt, C. Feldmann, and E. Koch, *Chem. Phys. Lett.*, **98**, 527 (1983); A. De Cian, M. Moussavi, J. Fischer, and R. Weiss, *Inorg. Chem.*, **24**, 3162 (1985).

6)F. L. Battye, A. Goldmann, and L. Kasper, *Phys. Status Solidi B*, **80**, 425 (1977).

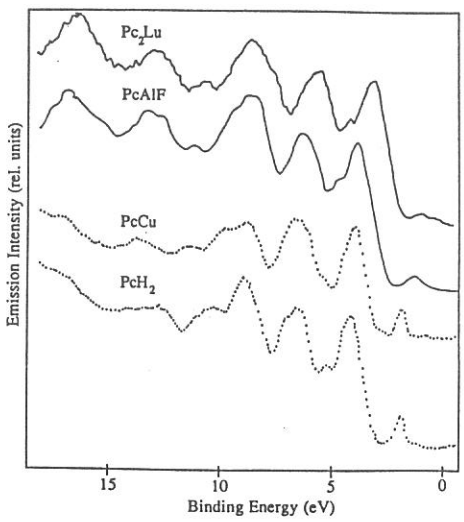

Fig.1 UPS spectra of Pc's.

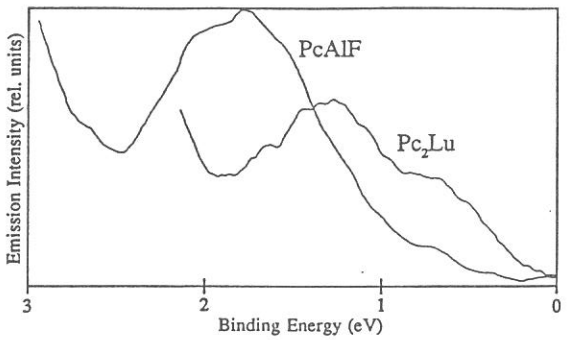

Fig.2 Lowest peaks of Pc_2Lu and $(PcAlF)_n$.

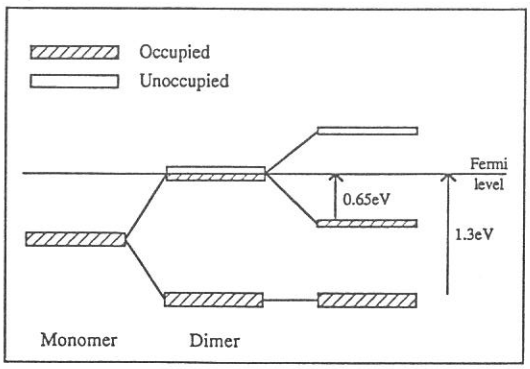

Fig.3 Electronic structure of Pc_2Lu.

UPS FOR VINYLTHIOPHENE OLIGOMER AND ITS LB FILMS.

H.NAKAHARA, J.NAKAYAMA, T.FUJIMORI, M.HOSHINO, K.FUKUDA, H.FUJIMOTO*, H.INOKUCHI* and K.SEKI**

Department of Chemistry, Faculty of Science, Saitama University, Urawa 338,
*Institute for Molecular Science, Myodaiji, Okazaki 444,
**Department of Material Science, Faculty of Science, Hiroshima University, Hiroshima 730.

Previously, we clarified the electronic structures of α-linked oligomers with 4-8 thiophene rings and effect of irregularity on the π-electron system by ultraviolet photoelectron spectroscopy(UPS) together with MNDO-SCF molecular orbital calculation. On the other hand, for the monolayer assemblies containing oligothiophenes mixed with Cd stearate the molecular orientation was reflected in the angle-resolved UPS. In this work, for (E,E,E)-2,2'-vinylenebis[5-[2-(2-thienyl) vinyl]-thiophene][$T(VT)_3$,Fig.1] the elecronic structure and the molecular orientation in LB films with Cd stearate have been investigated by UPS in addition to the polarized electronic spectra.

Figure 1 shows the photon energy dependence of the UPS spectra for the vacuum deposited film of $T(VT)_3$, which was normalized at the intensity σ band of 6.6 eV in the photon energy region of 30 - 60 eV. These spectra are almost similar to those for the α-linked oligothiophenes. The peak at E_b= 8 eV is relatively weakened with increasing the photon energy, while the band at 3.3 eV increases with hν. These facts seem to be attributed to the hν dependence of photoionization cross section. By reference to the results of UPS for α-oligothiophenes, the band at E_b=3.3 eV and its lower side band can be assigned to the non- and anti-bonding π bands, respectively.

The polarized electronic absorption spectra obtained with normal and 45° incidence for the LB film of $T(VT)_3$ mixed with Cd stearate are shown in Fig.2, as compared with the solution spectrum. The strong visible band at 365 nm assigned to the electronic transition polarized along the long-axis of the molecule exhibits a blue shift and is weakened in the LB film,

indicating the almost vertical orientation of the molecular axis. This is also supported by a dichroism in the polarized spectra. The bands in the longer wavelength region of 400-550 nm may be due to the intermolecular charge transfer.

Figure 3 shows the UPS spectra of the LB film (5 layers) containing $T(VT)_3$ mixed with Cd stearate at different angles (θ = 0,40°) of the photoemission with the 60° incidence of the photon ($h\nu$ = 45 eV), compared with that of the vacuum-deposited film. The bands A and B below E_b= 5 eV assigned to the π bondings are relatively intensified by increasing the angle θ and reversely the C_{2s} band due the alkyl chain is weakened. These results support the vertical orientation of $T(VT)_3$ and Cd stearate in the LB films.

Reference:
H.Fujimoto, U.Nagashima, H.Inokuchi, K.Seki, Y.Cao, H.Nakahara, J.Nakayama, M.Hoshino and K.Fukuda, J. Chem. Phys. in press (1990).

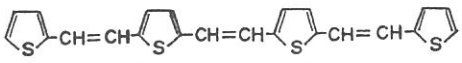

Fig.1. $T(VT)_3$, mp.216°C, λ_{max}=460 nm in $CHCl_3$ soln.

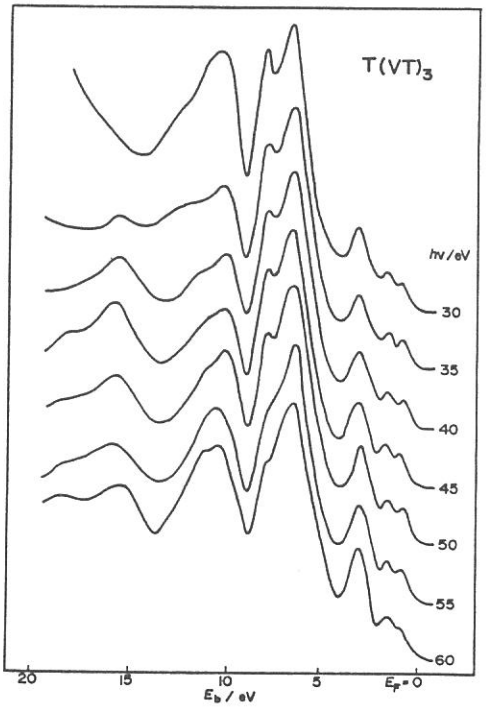

Fig.2. Photon energy dependence of UPS for vacuum deposited $T(VT)_3$.

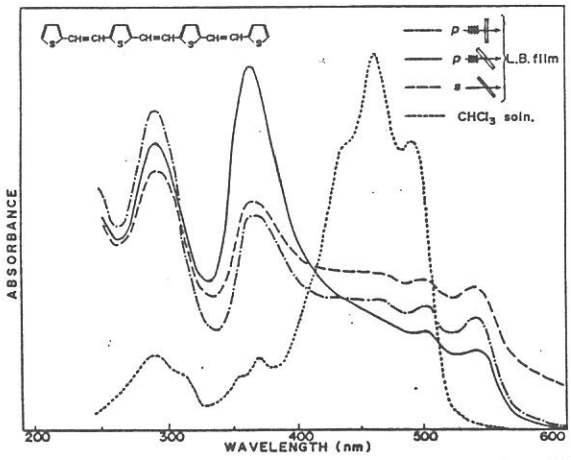

Fig.3. Polarized electronic spectra for LB film of $T(VT)_3$ mixed with Cd stearate, as compared with solution spectrum.

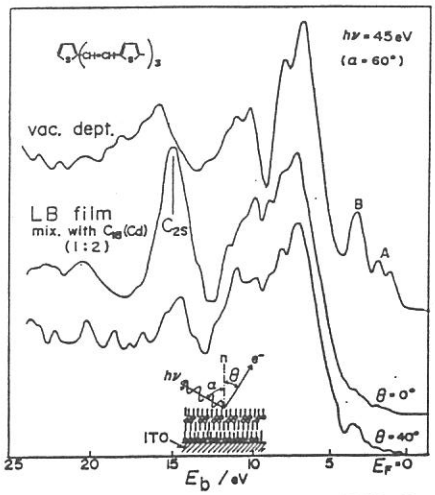

Fig.4. Angular dependence of UPS for LB film containing $T(VT)_3$ [$h\nu$ = 45 eV].

UV PHOTOELECTRON SPECTROSCOPY OF POLY(TETRAFLUOROETHYLENE) $\{CF_2\}_n$

Kazuhiko SEKI[*,***], Hiroshi TANAKA[*], Toshiaki OHTA[*], Yuriko AOKI[**], Akira IMAMURA[**], Hitoshi FUJIMOTO[***], and Hiroo INOKUCHI[***]

[*]Department of Materials Science, Faculty of Science, Hiroshima University, Hiroshima 730
[**]Department of Chemistry, Faculty of Science, Hiroshima University, Hiroshima 730
[***]Institute for Molecular Science, Myodaiji, Okazaki 444

Poly(tetrafluoroethylene) (PTFE) $\{CF_2\}_n$ is a fundamental polymer, but its electronic structure is not yet well clarified. An XPS spectrum of good quality was reported, but it has not been fully interpreted due to the poor reliability of theoretical calculations [1]. In this work we have studied it by UV photoelectron spectroscopy (UPS) with UVSOR as the exciting light source, and interpreted the results with ab-initio band calculations for an isolated PTFE chain. Combining the results with those from electronic absorption spectra [2], XANES [3,4], and electron transmission spectroscopy [4], a detailed picture of the electronic structure of PTFE has emerged [2].

UPS spectra were measured with the angle-resolving UPS system at the beamline 8B2 of UVSOR with a plane-grating monochromator. The specimen were evaporated films of oligomers with a mean n = 172 supplied from Central Glass Co. Ltd. These oligomers are sufficiently long to be treated as a polymer.

The band calculations were performed on a STO-3G basis set using a program POLYGAUSS-74 modified by us at Computer Center of Institute for Molecular Science. For simplicity, a planar-zigzag conformation was assumed instead of the reported helical structure. The validity of this simplification was confirmed by the little difference between the calculated results for oligomers with these two conformations.

In Fig. 1 (a) we show the UPS spectrum at $h\nu$ = 101.2 eV. For comparison, we also show the reported XPS spectrum [4] (b), UPS spectrum of an oligomer n-C_8F_{18} [5]. We see a good correspondence among the experimental data, confirming that electronic structures of oligomers of carbon number of $\geq$ 8 already simulate that of a polymer. We note that the topmost region of the UPS spectrum is more clearly observed than that in the XPS spectrum.

In Fig. 2 we show the calculated band structure. In Fig. 1(d) we show the density of states derived from Fig. 2. We see a good correspondence with the observed spectra with the calculated density of states, which enables the assignments of the observed features in the UPS spectrum as follows. The features A , D. and E are derived from the combination of F2p and C2p orbitals, B and C from the F2p lone pair orbitals, F and G from the C2s orbitals, and H from the F2s orbitals. These assignments are confirmed by the photon energy dependence of the relative peak intensities between the UPS and XPS spectra. The topmost part A has a wavefunction extended along the molecular chain, as in the corresponding state in polyethylene (PE) $\{CH_2\}_n$ [5]. The ionization threshold energy 10.6 eV is ca. 2 eV larger

than that of PE, and the highest value observed for a polymer.

REFERENCES

[1] J.J. Pireaux, J. Riga, R. Caudano, J.J. Verbist, J.M. Andre, J. Delhalle, and S. Delhalle, J. Electron Spectrosc., 5, 531 (1974).

[2] K. Seki, H. Tanaka, T. Ohta, Y. Aoki, A. Imamura, H. Fujimoto, H. Yamamoto, and H. Inokuchi, Phys. Scripta, in press.

[3] T. Ohta, K. Seki, T. Yokoyama, I. Morisada, and K. Edamatsu, Phys. Scripta, in press.

[4] I. Ishii, R. McLaren, A.P. Hitchcock, K.D. Jordan, Y. Choi, and M.B. Robin, Can. J. Chem., 66, 2104 (1988).

[5] M.B. Robin, private communication.

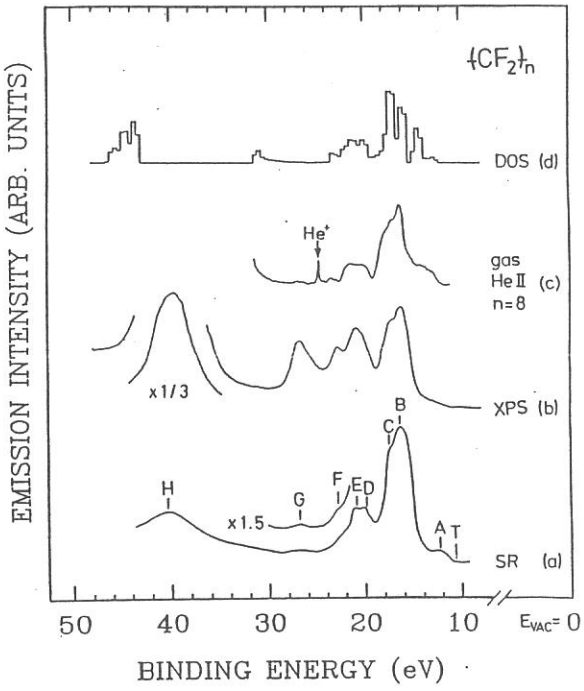

Fig. 1 (above) UV Photoelectron spectrum of PTFE at $h\nu$ = 101.2 eV (a) compared with the reported XPS spectrum [1], UPS spectrum of n-C_8F_{18} vapor [5], and (d) density of states derived from the calculated band structure in Fig. 2.

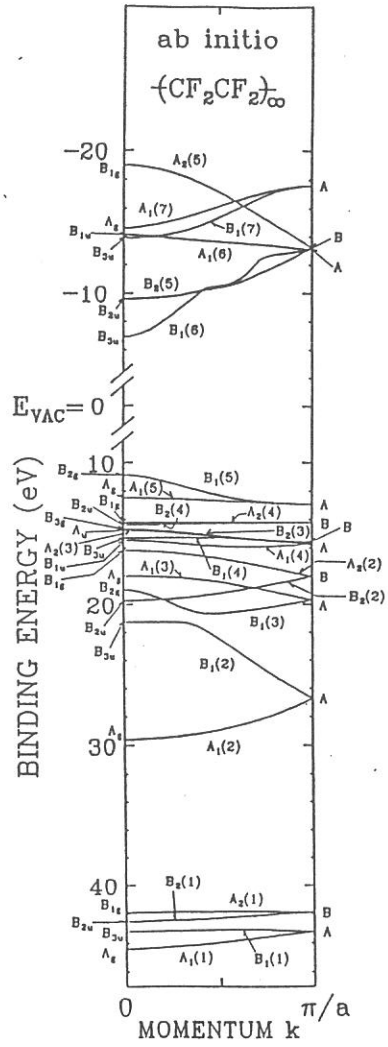

Fig. 2 (right) Band structure of PTFE by ab initio calculation.

ANGLE-RESOLVED PHOTOELECTRON SPECTROSCOPY ON LANGMUIR-BLODGETT FILMS OF COPPER TETRAKIS(n-BUTOXYCARBONYL)PHTHALOCYANINE

N. UENO[a], K. KAMIYA[b], M. TAKAHASHI[c], H. NAKAHARA[c], K. OGAWA[d], H. YONEHARA[d] K. FUKUDA[c], K. SEKI[e] AND H. INOKUCHI[b]

[a]Department of Image Science and Technology, Faculty of Engineering, Chiba University, Yayoi-cho, Chiba 260

[b]Institute for Molecular Science, Myodaiji, Okazaki 444

[c]Department of Chemistry, Faculty of Science, Saitama University, Urawa 338

[d]Kawamura Institute of Chemical Research, Sakado, Sakura 285

[e]Department of Materials Science, Faculty of Science, Hiroshima University, Hiroshima 730

The interest in studying angle resolved ultraviolet photoemission spectroscopy (ARUPS) is partly due to its capability of obtaining information on the angular parts of wave functions for the valence electrons , since the differential cross section of photoelectron is determined by them. This in turn means that the molecular orientation in ultrathin films of organic molecules can be proved by investigating a valence band of a definite orbital symmetry with this technique.

Langmuir-Blodgett films of phthalocyanine (Pc) derivatives can be considered as one of the most useful films for organic devices due to their thermal stability and the existence of Pc rings. Among these, LB films of copper tetrakis(n-butoxycarbonyl)phthalocyanine [$(BuCOO)_4CuPc$] were recently found to show that the molecular planes (Pc rings) are nearly perpendicular to the surface and also to the dipping direction for thick films (40 layers) with polarized UV-visible absorption spectra [1].

We measured ARUPS spectra of 8L LB films of $(BuCOO)_4CuPc$ deposited on copper substrates with synchrotron radiation in order to study the molecular orientation of the CuPc rings in the films. The experimental parameters are shown in Fig. 1.

The ARUPS spectra are shown in Fig. 2 as a function of angle ϕ at $h\nu$=40 eV, α=0° and θ=45°. The feature A corresponds with the top valence band of evaporated CuPc and can be ascribed to π electron band localized on the ring with 8 nitrogen atoms in the molecules [2]. The ϕ dependence of the intensity of the band A is shown in Fig. 3. In the figure, the ϕ dependences of photoelectron intensities of evaporated gold are also shown for a

check of the instrumental function in the measurements of the ϕ dependence of the spectra. It is clearly found that the intensity of the band A increases with increase in ϕ from -30° to 10°, decreases above $\phi \simeq 10°$, and gives a maximum around $\phi \simeq 10°$. The present results suggest that the CuPc rings in the films are oriented as their planes almost perpendicular to the dipping direction. Further studies are still in progress.

References

[1] K.Ogawa, S.Kinoshita, H.Yonehara, H.Nakahara and K.Fukuda, J.Chem.Soc., Chem.Commun. 478 (1989).

[2] R.Engelhardt, R.Dudde, E.E.Koch and N.Ueno, 8th Int. Conf. Vacuum Ultraviolet Radiation Physics, VUV-8, 8/4-8/8 (1986), Lund, Sweden, p.632 and references therein.

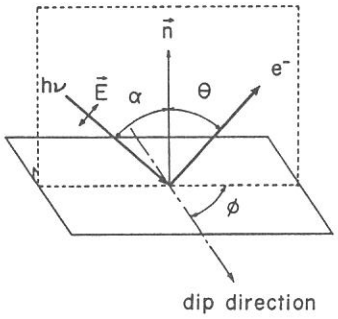

Fig. 1 Experimental parameters in the angle-resolved photoemission experiments.

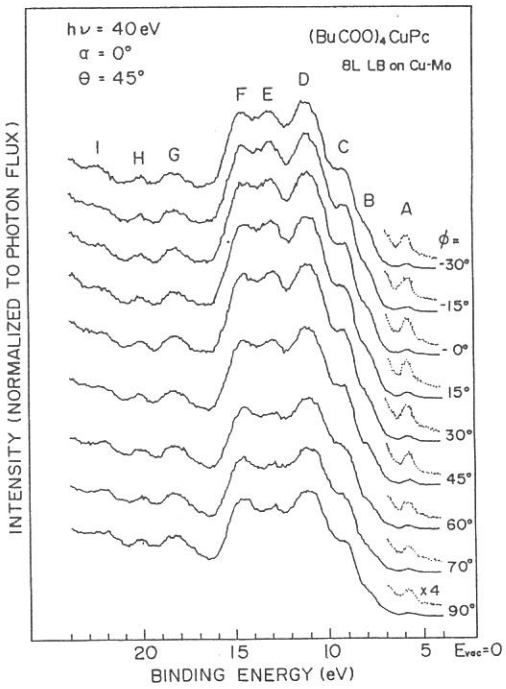

Fig. 2 ϕ dependence of the photoemission spectra

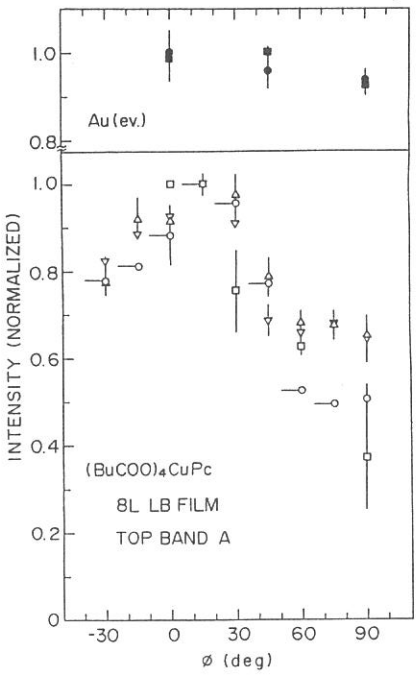

Fig. 3 ϕ dependence of the intensity of the band A. ○, △, ▽: obtained for 8L LB film on Cu-evaporated Mo. □ : obtained for 8L LB film on Cu plate. Upper panel shows the ϕ dependences of photoelectron intensities at 2.8 eV (●) and 6.4 eV (■) below the Fermi level for an evaporated gold.

SURFACE CN^- CENTERS ON KCl CRYSTALS

Hideyuki NAKAGAWA, Atsusi FUKUMOTO, Hiroaki MATSUMOTO, Masami FUJITA*, Takeshi MIYANAGA**, Kazutoshi FUKUI***, and Makoto WATANABE***

Department of Electrical and Electronics Engineering, Fukui University, Fukui 910
* Maritime Safety Academy, Wakaba, Kure 737
** Department of Physics, Faculty of Education, Wakayama University, Sakaedani, Wakayama 640
*** Institute for Molecular Science, Okazaki 444

Creation of CN^- centers in/on the crystal surfaces of some alkali halide has been investigated extensively with various methods, that is, with light-ion (H^+ or He^+) bombardment[1,2], with ion implantation[3] of C^+ and N^+, with electron beam irradiation[2,4] and with extreme ultraviolet undulator light (UL) irradiation[5,6,7]. It has been concluded from the the CN^- growth rate experiments on KCl with UL irradiation in N_2 and/or CO_2 ambient gases that the surface CN^- centers are created through two photochemical processes, the one is photo-dissociation of gas speacies and photo-synthesis to form CN radicals in the ambient gas phase, and the other is photo-induced surface reaction to incorporate the CN radicals as the CN^- centers into the crystal surface region. With UL irradiation, the created CN^- centers produce molecular luminescence bands in the region from 3.5 to 5.8 eV which are almost identical with those observed on the bulk CN^- centers doped in KCl[8]. In the present study, life-time measurements have been performed on the surface CN^- luminescence in KCl in order to compare the results with those of the bulk CN^- in KCl. For the decay measurements, the UL was chopped with a cylindrical light chopper which was rotated with an appropriate velocity around an axis perpendicular to the direction of UL.

Figure 1 shows a decay curve obtained at 300 K. The decay curve consists of two exponential components as indicated with two straight lines, τ_1 = 80 ms and τ_2 = 30 ms, the sum of which reproduces the observed decay curve. As shown in Fig. 2, the temperature dependences of these components can be fitted to the well-known formula, $\tau = \tau_r / \{1 + \tau_r \nu \exp(-\Delta E / kT)\}$. The values of fitting parameters are given in Table I together with those for the bulk CN^- centers doped in KCl[9]. The main component, τ_1, in the present case corresponds to the decay time of the doped CN^-, while the τ_2 component appears only for the surface CN^-. The observation of two decay components for the surface CN^- indicates the participation of two closely lying excited states in the decay process. The $a^3\Pi$ state, which is considered as the intial state of the CN^- luminescence, may

split into two levels through mixing of the bulk states due to the surface potential.

The temperature dependence of the CN^- luminescence intensity, I, is also shown in Fig. 2. The behavior can be understood in terms of enegy transfer from the bulk to the CN^- centers below 350 K and non-radiative thermal decay above 350 K. Illuminating the crystal with UL may produce many electrons, holes and excitons in the bulk. At low temperatures below 200 K, electrons and holes would be self-trapped or trapped at various defects and the energy transfer would be dominated by the exciton diffusion process. It would be difficult for excitons, however, to reach the surface CN^- centers because of the presence of the surface dead layer against excitons. At higher temperatures, thermally released electrons and holes can migrate through the crystal and to reach the surface region to excite the CN^- centers.

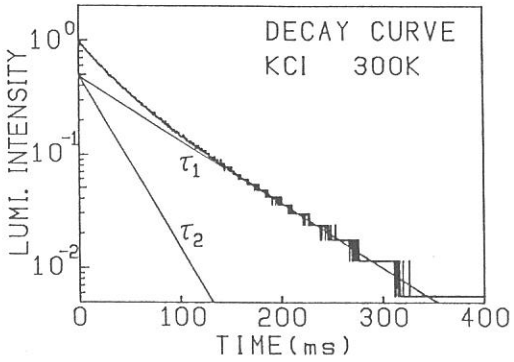

Fig. 1. A decay curve of the CN^- luminescence of KCl at 300K.

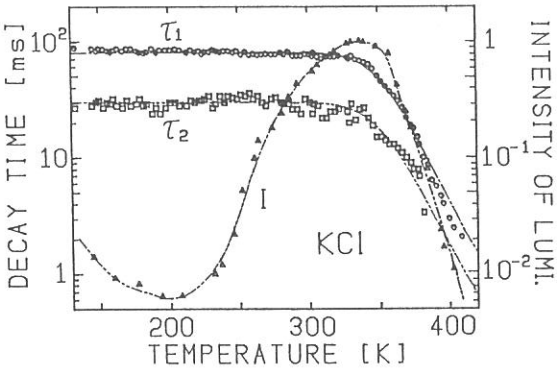

Fig. 2. Temperature dependences of the decay times and the intensity of the CN^- luminescence of KCl.

Table I. Parameters obtained from the fitting of the temperature dependence of the decay time. The values for τ' are those for the doped CN^- centers.

	τ_r [ms]	ΔE [eV]	ν [1/s]
τ_1	80	0.79	2×10^{12}
τ_2	30	0.76	2×10^{12}
τ'	90	0.86	2×10^{13}

1) A.I.Bazhin et al.: J. Chem. Phys. **65** (1976) 3897.
2) D.Cherry et al.: Nucl. Instrum. & Methods B13 (1986) 533.
3) W.A.Metz et al.: Nucl. Instrum. & Methods 194 (1982) 505.
4) M.Kamada et al.: J. Phys. Soc. Jpn. **58** (1989) 4228.
5) H.Nakagawa et al.: J. Phys. Soc. Jpn. **58** (1989) 2605.
6) M.Watanabe et al.: Proc. 9th Int. Conf. on Vacuum Ultraviolet Radiation Physics, honolulu, 1989, to be published.
7) H.Nakagawa et al.: Proc. of the US-Japan Seminar, Nagoya, 1989, to be published.
8) M.Mendenhall et al.: Chem. Phys. Lett. **147** (1988) 59.
9) S.S.Camargo et al.: Phys. Status Solidi b153 (1989) 757.

SYNCHROTRON RADIATION EXCITED CHEMICAL VAPOR DEPOSITION OF HYDROGENATED AMORPHOUS SILICON FILMS

Haruhiko OHASHI*, Akira YOSHIDA*
and
Kosuke SHOBATAKE**

* Toyohashi University of Technology, Toyohashi, Japan 440
** Institute for Molecular Science, Okazaki, Japan 444

Photochemical vapor deposition (Photo-CVD) has been playing very important roles in modern semiconductor technology [1]. Synchrotron radiation (SR) is now expected to be a suitable light source for photochemical processes [2)-4)]. In this study, hydrogenated amorphous silicon (a-Si:H) films were deposited on Si and SiO_2 substrates by SR-CVD using Si_2H_6 gas at room temperature. The effects of high energy photons upon the density of formed silicon films are investigated.

Experimental The SR light through an aperture and a Ni mesh (64% transmittance) was irradiated upon the substrate perpendicularly to the surface as illustrated in Fig.1. Pure Si_2H_6 gas was used and the gas pressure in the reaction chamber was kept at 0.2 Torr. The substrate temperature was fixed at room temperature.

Results and Discussion The surface roughness of the deposited film is shown in Fig.2. The right part of Fig.2 shows the film surface which was not treated by KOH enchant after deposition, and the left one shows the same film surface after KOH treatment. Though the SR light was irradiated through Ni mesh, the un-etched part of the surface (the right part of Fig.2) exhibits only shallow dips. The surface treated with KOH solution exhibits distinct steps (the left part of Fig.2). The former finding suggests that the precursors of deposition are produced in the gas phase, since the films were deposited in the un-irradiated area around the irradiated area. The latter fact suggests that the SR light is effective for increasing of the film density.

Figure 3 shows the wavelength dependence of the transparent light intensity ratio I/I_0 at the substrate surface. Since some photons were absorbed by Si_2H_6 gas between the aperture and substrate surface in the reaction chamber, only high energy photons (>10eV) arrived at the surface. Therefore photons with energies higher than 10 eV are effective for the forming high density films.

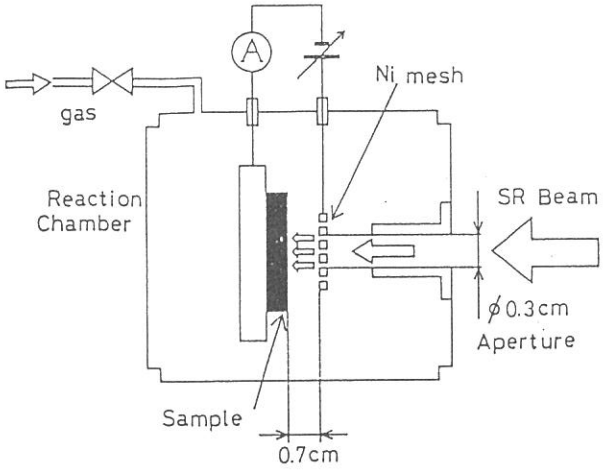

Fig.1

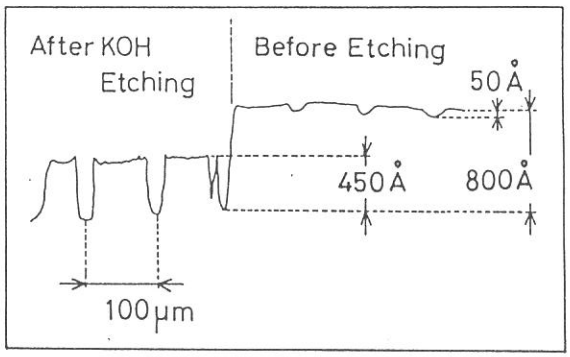

Fig.2

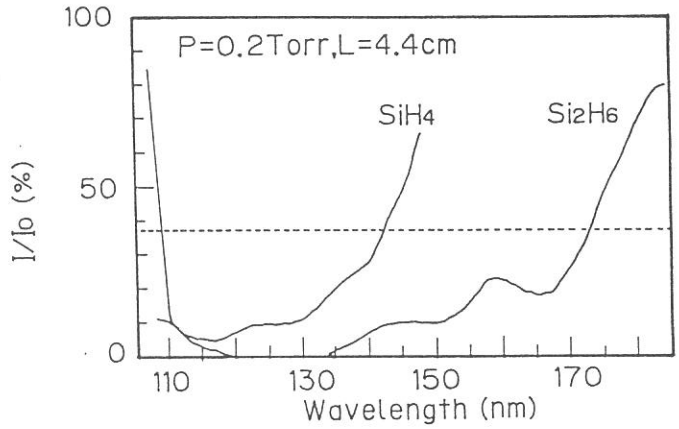

Fig.3

References

1) D.J.Ehrlich and J.Y.Tsao, J.Vac.Sci.Technol. **B1**, 969(1983).
2) H.Ohashi, K.Inoue, Y.Saito, A,Yoshida, H.Ogawa and K.Shobatake, Appl.Phys.Lett. **55**, 1644(1989).
3) N.Hayasaka, A.Hiraya and K.Shobatake, Jpn.J.Appl.Phys. **26**, L1110(1987).

VUV-assited silicon epitaxy using silane

Maki SUEMITSU, Fumihiko HIROSE, Kazuhiro CHIBA, Hitoshi SAKAMOTO,
Jiro Ishibe, Michio NIWANO, and Nobuo MIYAMOTO

Research Institute of Electrical Communication
Tohoku University, Sendai 980

In order to investigate effects of VUV photons on silicon epitaxy using silane, a photo-stimulated desorption (PSD) from Si(100) surface in an ambiance of 5.0×10^{-5} Torr Silane was observed. VUV photons of its energy 50eV were utilized. Desorbed ions were detected by a quadrupole mass spectrometer with its ionizing filament off. Figure 1 shows a spectrum obtained for the substrate temperature of $400^{\circ}C$. The peak at m/e=1 corresponds to the ionized hydrogen atom and a broader one peaked at m/e=30 corresponds to a set of ionized fragments of silane molecules. No ions were detected without the VUV irradiation.

An evidence that these ions, if not all, are created at the substrate surface is given by the substrate-temperature dependence of the m/e=1 peak shown in Fig. 2. This plot was obtained by normalizing the peak height in Fig. 1 with the ring current ranged from 36 to 118 mA. The normalized intensity shows a monotonous increase with the increasing substrate temperature until it saturates above $600^{\circ}C$. The presence of the temperature dependence indicates that at least part of the hydrogen ions are desorbed (PSD) from the intermediate or final products of the surface reactions which proceeds thermally. This temperature dependence in Fig. 2 evokes the one obtained in our previous study[1] for the growth rate using silane without VUV irradiation (Fig. 3). There we found that the growth rate Arrhenius plot presents a break around at $600^{\circ}C$, separating the lower- and the higher-temperature regions. This similarity suggests that the PSD observed in our present experiment arises from the silane or sub-silane molecules just being incorporated into the crystal. In the growth rate Arrhenius plot, the two regions were assigned to be rate-limited by silane adsorption process for the higher- and hydrogen desorption process for the lower-

temperature region, respectively. Therefore, the change in the PSD rate at 600°C might probably reflects the change in the growth kinetics at the surface.

Reference

1)F. Hirose, M. Suemitsu, and N. Miyamoto, Jpn. J. Appl. Phys. 28 (1989) L2003.

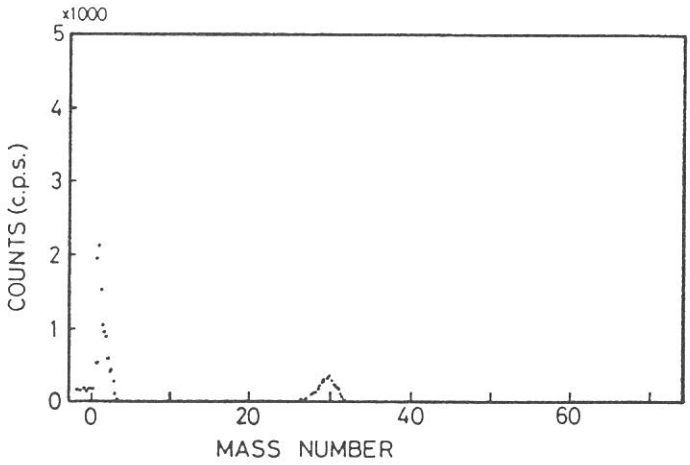

Fig.1 PSD mass spectrum obtained from Si(100) surface at 400°C in an ambiance of 5.0×10^{-5} Torr silane.

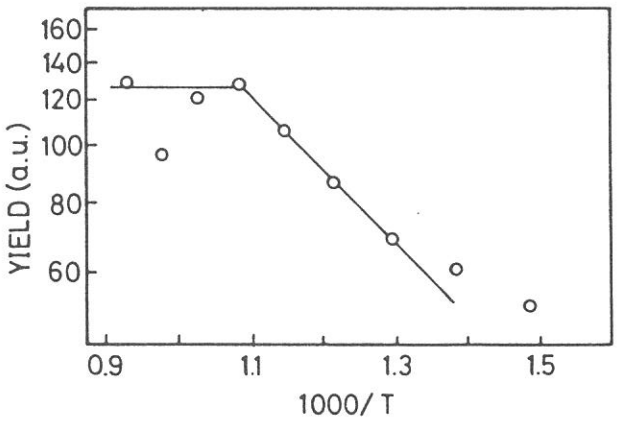

Fig.2 PSD yield of m/e=1 peak as a function of the substrate temperature.

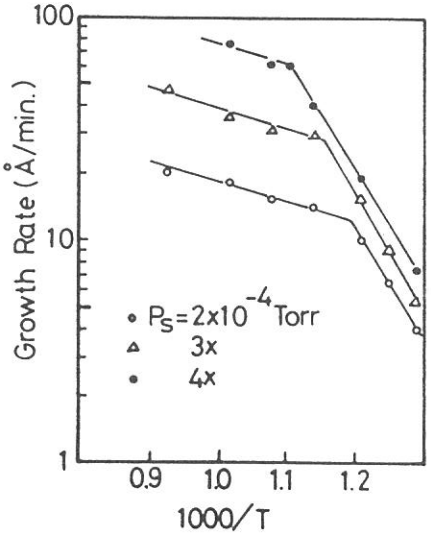

Fig.3 Growth rate Arrhenius plot without VUV irradiation.(ref.1)

Patterned Polymerization of Styrene by SR-CVD

T.Hayakawa T.Tashiro H.Yamada* S.Morita S.Hattori**
H.Ohashi*** K.Shobatake****

Dep. of Electronic Mechanical Eng. Nagoya Univ..
Furo-cho. Chikusa-ku. Nagoya 464-01
* MEITEC Corporation.
2-20-1. Koseidori. Nishi-ku. Nagoya 481
** Industrial Science Research Institute of Nagoya Municipal. 3-4-41. Rokuban-cho. Atsuta-ku. Nagoya 456
*** Visiting Student at Institute for Molecular Science from Toyohashi Univ. of Technology.
**** Institute for Molecular Science.
Myodaiji. Okazaki 444

Chemical vapour deposition (CVD) is performed through reactions of vapour monomers by using thermal. plasma. or photo activation. Recently. X-rays have been highlighted as an excitation source for the CVD process because large flux X-ray sources became available such as synchrotron radiation (SR). plasma focus X-ray source and so on. Among newly developing X-ray sources. SR is the most suitable one for the CVD because of its large flux. stability and controllability. This new CVD method is named synchrotron radiation chemical vapour deposition (SR-CVD).

A preliminary investigation of the properties of polymerized styrene film and the patterned polymerization by SR-CVD has been reported[1]. If the direct pattern formation can be realized. it is expected that SR-CVD can present a new dry resist coating method in place of plasma polymerization for an all vacuum lithography. Also. if the polymerized styrene film has enough resistivity to Si etchant. this method can be applied to Si process such as micro-machining technology.

In this study the direct fine pattern formation was investigated. Then the resistivity of the polymerized styrene film to Si etchant (CF_4 plasma) was investigated and the transfer of the pattern profile to the Si substrate was performed.

Experiments were carried out using the beam line BL-8A. The diameter of the beam was 4mm. For the direct pattern formation. a Ni mesh having 5x5 μm square windows was set in front of Si substrate. The pattern profile was observed by an scanning electron microscope (SEM). In order to obtain the high resolutive patterns. the removal of the film at the unirradiated area was tried by O_2RIE or a benzene washing.

Observing by SEM, such a profile as shown in Fig.1 was typically obtained. The change of pattern feature after O_2RIE

or a benzene washing is shown in Fig.2 and Fig.3, respectively. By O_2RIE, the removal of the film at the unirradiated area could not be accomplished perfectly, and more etching could not improve the profile any more. By a benzene washing, however, the film at the unirradiated area was easily removed. As a result, only the film at the irradiated area remained very clearly.

The transfer of the polymerized styrene pattern to Si substrate was performed using CF_4 gas with a parallel plate type plasma etching device at a frequency of 13.56 MHz. The polymerized styrene film has enough resistivity to CF_4 plasma and the borderline between the styrene film and Si substrate could be easily recognized as shown in Fig.4.

[1] H.Yamada, M.Nakamura, H.Katoh, T.Hayakawa, S.Morita and S.Hattori, UVSOR ACTIVITY REPORT 1988, 106.

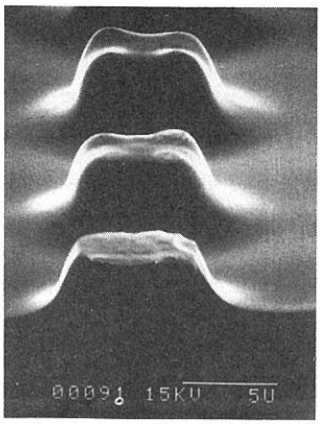

Fig.1 as deposited

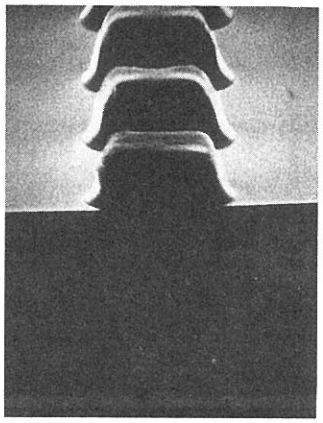

Fig.2 after O_2RIE

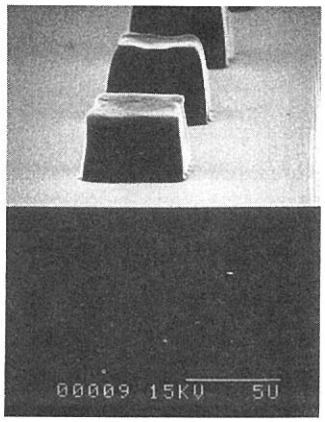

Fig.3 after benzene washing

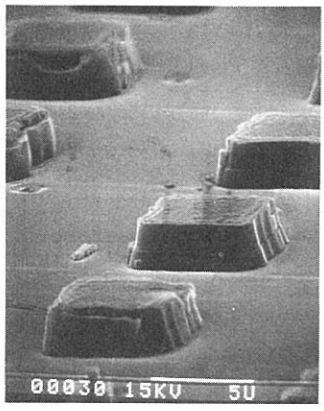

Fig.4 Si pattern transferred from polymerized styrene pattern

GROWTH OF SiO_2 THIN FILM BY PHOTO-CVD USING SYNCHROTRON ORBITAL RADIATION

Masanori OKUYAMA, Masakazu NAKAMURA and Yoshihiro HAMAKAWA

Department of Electrical Engineering, Faculty of Engineering Science,
Osaka University, Toyonaka, Osaka, 560

SiO_2 thin films have been grown from Si_2H_6 and O_2 on Si and MgF_2 crystals by photo-CVD using the SOR. The SOR light from the storage ring was applied to substrate surface through a hole of diameter 3mm without any spectroscopic system. The substrate temperatures were changed from room temperature to 200°C. Incident photon flux is estimated to be 6.7×10^{14} photons/sec at beam current of 100mA. O_2 was introduced to the whole chamber and Si_2H_6 was flown to the substrate. The total pressure in the reaction chamber was fixed to be 0.2Torr and flow rate ratio of Si_2H_6 to O_2 was 0.052. SiO_2 thin films grew much on the irradiated circle of diameter 3mm, and their surfaces were very flat.

Figure 1 shows deposition rates on the irradiated area & on the nonirradiated area just outside the irradiated and refractive indices as a function of the substrate temperature. The deposition rates are normalized by the electron beam current of the storage ring. The deposition rate on the irradiated area changes little up to 100°C, decreases a little at 150°C and increases again at 200°C. The difference of the rates of the films on and outside the irradiated changes little below 100°C, decrease at 150°C and diminishes at 200°C. The refractive indices change a little in the substrate temperature up to 150°C, but decreases very much at 200°C. The indices of the nonirradiated are less than 1.25 and their densities seem to be very low. It is considered that the source gases are dissociated in vapor phase and the reacted species are adsorbed on the substrate at low temperature. But, the source gases begin to react above about 150°C, and the films can grow even on the nonirradiated. So the density of the film deposited at 200°C might be rather low. The ultraviolet and visible light transmission spectra were also measured in the film deposited on the MgF_2. Two absorption peaks are observed near about 3.3 and 5eV, and increase with increasing the deposition temperature.

Figure 2 shows IR transmission spectra of the film deposited at room temperature by photo-CVDs using SOR, a Kr-He resonance lamp and a deuterium(D_2) lamp. Two peaks assigned to Si-O bond are found commonly in all spectra near 1060-1070cm^{-1} and 460-480cm^{-1}. Absorption peaks assigned

to Si-H bond are found near 2260 and 880cm^{-1} in the films deposited by the photo-CVD using the Kr-He and D_2 lamps, but not found in the film by the photo-CVD using the SOR. Absorption peak assigned to Si-OH is not also found in the film by that of the SR light, but is found near 3600cm^{-1} in the other films.

Electrical properties were measured in MOS diodes made of the SiO_2 film deposited on the (100)n-Si/n^+-Si wafer. Figure 3 shows a typical C-V characteristic of the MOS diode using the SiO_2 film(710Å thick) deposited at 150°C. Fixed-oxide-charge density, N_{ox}, estimated from the flat band voltage, is 1.6x10^{11}cm^{-2} in the film of thickness 92nm deposited at room temperature. Interface state density, N_{ss}, has been obtained by DLTS measurement and the minimum is 1.1x10^{11}eV^{-1}cm^{-2} in the film deposited at 150°C. These values are pretty low in comparison with those of the films deposited by the other CVD methods.

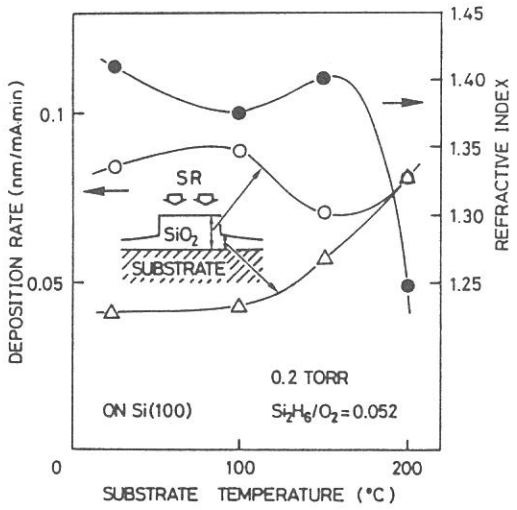

Fig. 1. Deposition rate at the irradiated area(open circles), just outside the irradiated(open triangles) and refractive index (closed circles) as a function of substrate temperature.

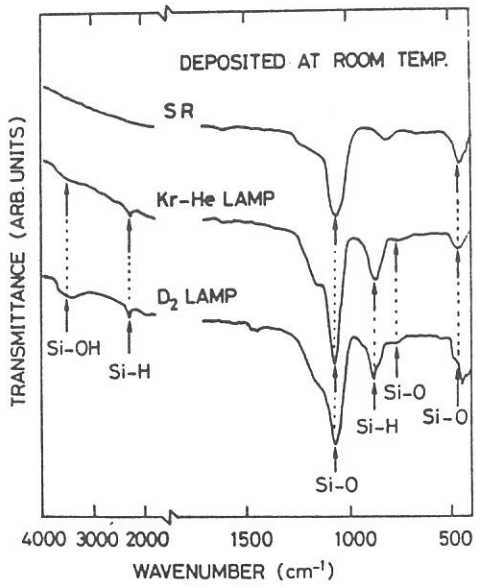

Fig. 2. Infrared transmission spectra of the photo-CVDs using SOR, a Kr-He lamp and a D_2 lamp

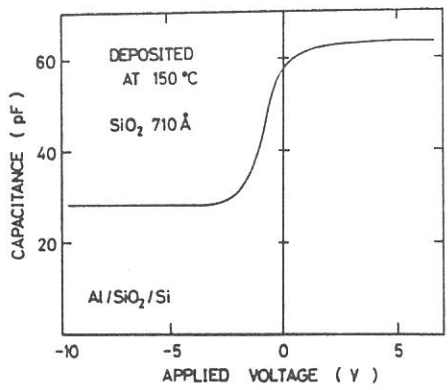

Fig. 3. C-V characteristic of an MOS diode using SiO_2 film deposited at 150°C.

DEFECTS IN HYDROGENATED AMORPHOUS SILICON FILMS INDUCED BY SYNCHROTRON IRRADIATION

Yoji SAITO and Akira YOSHIDA
Toyohashi University of Technology, Toyohashi 440

We have investigated[1] the rapid degradation in hydrogenated amorphous silicon (a-Si:H) films induced by irradiation of vacuum ultra violet (VUV) light from synchrotron radiation (SR). In this work, the degradation mechanism and the properties of the defects are investigated.

Undoped a-Si:H films with the thickness of about 0.7 μm were deposited onto glass substrates at 250°C, using rf glow discharge technique.

First, the a-Si:H samples were irradiated by SR light through a Be filter of 15μm thickness, through which only the light of wavelength less than 10Å can penetrate, in order to clarify the rapid degradation of the films induced only by the high energy photons. Figure 1 shows the dependence of photo-conductivity σ_{ph} of the films as a function of the exposure, when the power of illumination is $50mW \cdot cm^{-2}$. The initial value of σ_{ph} was about $2X10^{-4}Scm^{-1}$. In this figure, the data for direct SR light are also shown. The σ_{ph} of the samples using the filtered light are 30 times as large as those for the direct light. From this result, it is estimated that the wavelength of the light which contributes to the rapid degradation is less than 25Å for the direct light irradiation, if the density of induced defects is proportional to the density of the absorbed photons in the films. This implies that the degradation mechanism relates to the inner-shell excitation and relaxation processes[2,3].

Second, we examined the properties of the induced defects by electron spin resonance (ESR) measurement. The ESR signal was observed with g-value of 2.0055, corresponding to the silicon dangling bonds. The intensity of the signal, which is proportional to the defect density, decreases in the

thermal annealing. According to the bi-molecular model[4], the decay of the defect density N_{ind} is described as,

$$[N_{ind}(t_a)]^{-1}-[N_{ind}(0)]^{-1}=v_o\exp(-E_a/k_BT_a)t_a, \qquad (1)$$

where t_a, E_a, T_a, and v_o, are the annealing time, an activation energy, annealing temperature, and a constant. Figure 2 shows the decay of the defect density, calulated from the experimental data according to this model. From the slope of straight lines, E_a is found about 1.0eV. This value is almost the same as that for the visible light induced defects[5]. Therefore, the defects due to SR irradiation consist mainly of the Si dangling bonds.

References
1. Y.Saito, K.Inoue, A.Yoshida, J.Appl.Phys.65, 2552(1989).
2. M.L.Knotek, P.J.Feibelman, Phys.Rev.Lett.40, 964(1978).
3. D.Menzel, R.Gomer, J.Chem.Phys.41, 3311 (1964).
4. C.Lee, W.D.Ohlsen, P.C.Taylor, H.S.Ullal, G.P.Ceasar, Phys.Rev.B31, 100(1985).
5. M.Stutzmann, W.B.Jackson, C.C.Tsai, Phys.Rev.B32, 23(1985).

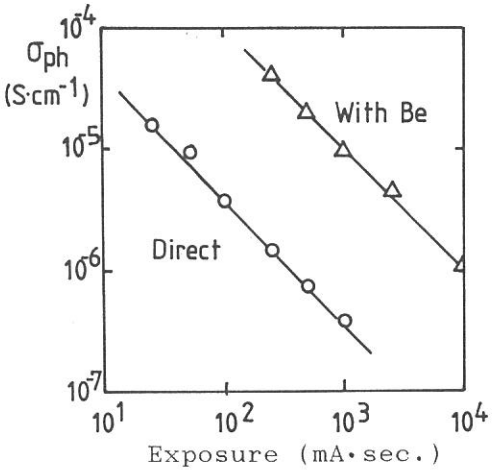

Fig.1 Dependence of σ_{ph} as a function of exposure

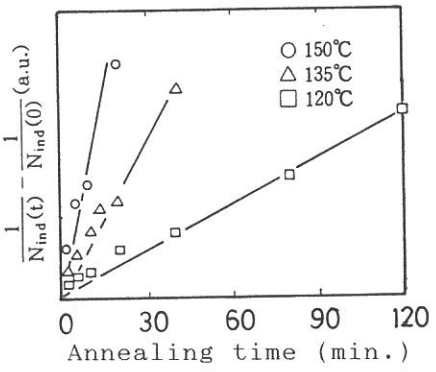

Fig.2 Decay of density of the defect

X-RAY REFLECTIVITY OF GOLD MIRROR IN 1.7-5KEV REGION

Koujun YAMASHITA, Shunji KITAMOTO, Isamu Hatsukade, Masayuki OHTANI, Keisuke TAMURA, Isao YAMADA* and Yoichi HASHIMOTO**

Department of Physics, Osaka University, Toyonaka 560
*Ion Beam Engineering Experimental Laboratory, Kyoto University, Kyoto 606
**Manufacturing Development Laboratory, Mitsibishi Electric Corporation, Amagasaki 661

A thin gold layer deposited on supersmooth surface is useful for the reflector of grazing incidence X-ray optic systems, since it shows high X-ray reflectivity and is chemically stable. However the X-ray reflectivity around Au M-edge has not been well investigated, which depends on deposition methods, surface roughness of substrates and the thickness of deposited layers.

We carried out the measurement of X-ray reflectivities of Au mirror in the energy region of 1.7-5keV on BL-7A. The incident X-ray beam is monochromatized by InSb double crystal spectrometer, collimated in 0.1-0.4mmϕ by a pinhole and introduced to a reflectometer which has θ-2θ rotation system controlled by a microcomputer. A thin window proportional counter is mounted on the rotation arm. The incident flux is adjusted to less than 10^4c/s for proper operation of the counter by the thickness of Al filter and the size of pinhole. X-ray reflectivities are measured as a function of X-ray energy at fixed incidence angle and vice versa. Samples thus measured are Au and Au+Ni mirror, multilayers(Mo/C+Au, Ni/C and W/Si) and graphite crystal. Au mirror with layer thickness of 230A, 500A and 1100A is deposited by ICB method in Kyoto University(1) and Mitsubishi Electric Corporation and that with 500A thick by EB method.

Here we only present results of Au mirror. Fig.1 shows X-ray

reflectivities of Au mirror(d=230A) deposited by ICB method against X-ray energy. Incidence angle is written on each curve. Reflectivity is discontinously reduced at Au M_V absoption edge(E=2.22keV) and gradually decreases to higher energy, depending on incidence angle. These observed values are systematically higher than those calculated from optical constants, which means that ICB method can synthesize high density and supersmooth layer on the substrate. The surface roughness is out of question, so that we have to reevaluate optical constant of this kind of thin layer. On the other hand, reflectivities of Au mirror deposited by EB method are consistent with calculated values. Reflectivities gradually decrease with increasing of the layer thickness in d>300A.

(1) I. Yamada and T. Takagi, IEEE Trans. Electron Devices, ED-34, 1018(1987).

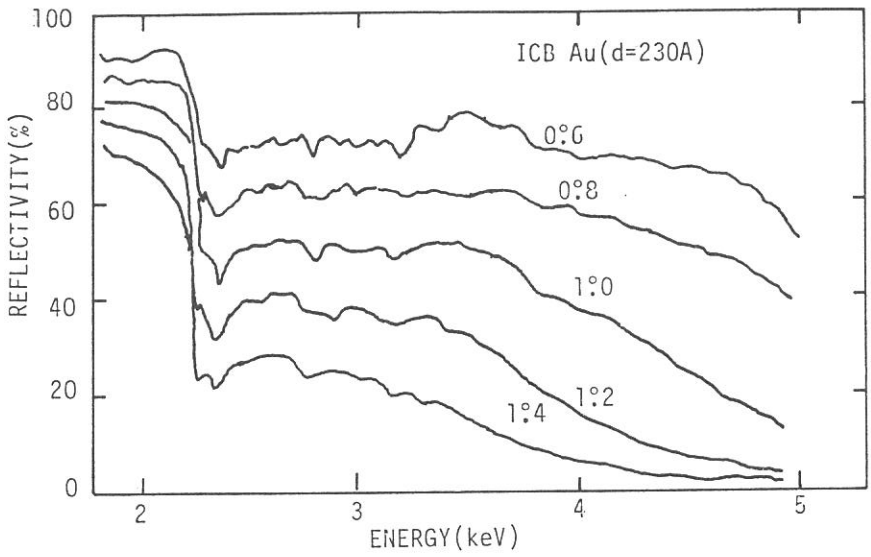

Fig.1 X-ray reflectivity of Au mirror deposited by ICB method

Soft X-ray Microscope with Zone Plates at UVSOR

Norio Watanabe[1], Mieko Taniguchi[1], Yoshio Shimanuki[2], Kenzo Kawasaki[2], Yutaka Watanabe[3], Yoshinori Nagai[4], and Hiroshi Kihara[5]

1) Department of Physics, Faculty of Science, Nagoya University, Nagoya 464, Japan
2) Department of Oral Anatomy, School of Dental Medicine, Tsurumi University, Tsurumi 2-1-3, Yokohama 230, Japan
3) Canon Research Center, CANON INC., Morinosato-Wakamiya 5-1, Atsugi, Kanagawa 243-01, Japan
4) College of General Education, Azabu University, Fuchinobe, Sagamihara, Kanagawa 229, Japan
5) Jichi Medical School, School of Nursing, Minamikawachi, Tochigi 329-04, Japan

We have been developing soft X-ray imaging microscopy with zone plates. In our previous report[1], We showed results for soft X-ray microscopy with two free-standing zone plates, one of which was masked as a condenser(CZP) and another without a mask as an objective(OZP). We found, however, CZP was damaged seriously by irradiaion through experiments of 4 weeks.

Therefore, as a next step, we have fabricated zone plates with support film of PIQ to avoid radiation damage of CZP. The present characteristics of zone plates are :n=250, f=55.6 mm, at 4.5 nm light, the outermost zone width dr_n=0.5 μm, and Au thickness=300 nm on 300 nm polyimide substrate with a central mask of 100 μmφ as CZP and OZP.

Experiments were done at BL8A(750 MeV) with the geometry shown in Fig.1. In this year, we improved the system at two points as well as the improvement of the zone plate fabrication. One is to put a pinhole(PH1) at the most upstream, located 2803 mm upstream from CZP. PH1 was put because of reducing the source size and then reducing the image size of the source at the focal point. The other is to place a filter in front of CZP to cut unnecessary light of longer and shorter wavelength. We used Ti 100 nm and C 10 nm thick foil on 80 % transparent mesh as a filter. The source image(800 μmφ) of 4.74 nm light is demagnified to 9.6 μmφ at a pinhole(PH2) plane. We selected PH2 of 34 μmφ or 12 μmφ. Samples were placed 5 mm downstream from PH2. OZP was set at 54 mm distant from a sample plane. Detectors(MCP with a single layer) were located 2361 mm from OZP, which had a magnification ratio of 43.7. Obtained images were monitored on fluorescent screen, which was usually accumulated with SIT camera for averaging.

With these set-ups, we have tested imagings of Cu #1000 mesh and a free-standing zone plate(n=312, f=150 mm at 8 nm light, dr_n=0.98 μm, Au thickness=2 μm), which was reported in one of previous paper[2]. These images were shown in Fig.2 and Fig.3. We also tested several biological specimens such as diatoms and ground sections of tooth.

Acknowledgement

The authors are grateful for the help and encouragements from Prof. M. Watanabe, K. Fukui, O. Matsudo and other staffs of the

Institute for Molecular Sciences. Use of MCP and SIT camera was realized by a kind offer of Hamamatsu Photonics, in part which is also greatly appreciated.

References

1. H.Kihara, Y.Shimanuki, K.Kawasaki, N.Watanabe,M.Tamiguchi,H. Tsuruta, Y.Nagai, Y.Watanabe, and S.Ogura (1989) in UVSOR activity report 1988 120-121
2. Y. Nagai, Y. Nakajima, Y. Watanabe, S. Ogura, K. Uyeda, Y. Shimanuki, and H. Kihara (1987) in "X-ray Microscopy" (ed. by P.C.Cheng and G.J.Jan), pp. 263-288, Springer-Verlag, Berlin

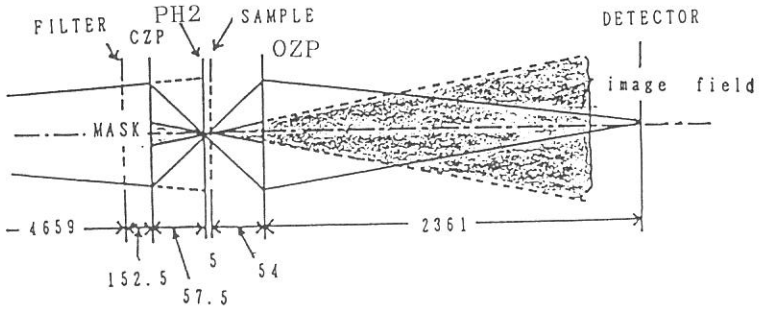

Fig. 1. A diagram of the Soft X-ray microscope with two zone plates without a monochromator. CZP;condenser zone plate with a central mask, PH2; pinhole (34 μmø or 12 μmø), OZP; objective zone plate with a central mask.

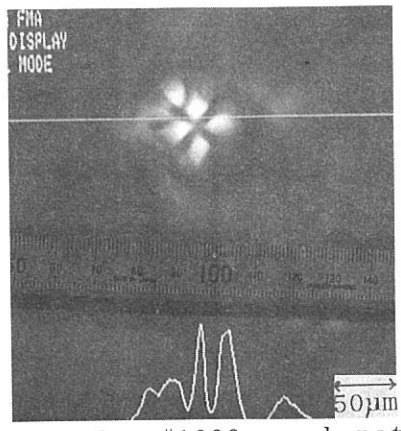

Fig. 2. Cu #1000 mesh pattern in the monitor screen. PH2 of 34 μmø was used. The image on the fluorescent screen of MCP was monitored with SIT camera(4 s accumulation).The horizontal scan intensity along the white line is also shown.

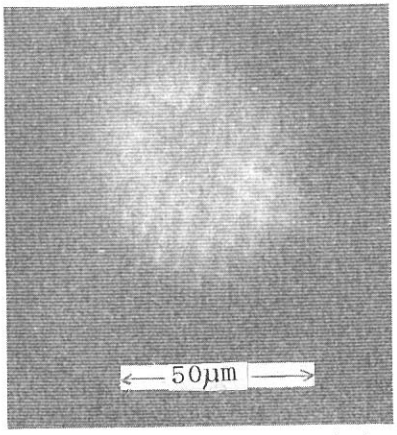

Fig.3. Zone plate image taken by the same way of Fig.2.

FAR-INFRARED ABSORPTION BY METAL MICROCRYSTALS

Shōsuke MOCHIZUKI and Kimihiro ISHI*

Department of Physics, College of Humanities and Sciences, Nihon University, 3-25-40 Sakurajosui, Setagaya-ku, Tokyo 156

*The Research Institute for Scientific Measurements, Tohoku University, 2-1-1 Katahira, Aoba-ku, Sendai 980

The far-infrared absorption by metal microcrystals has been interest for more than ten years because of a direct observation of the quantum-size effects on the conduction electrons predicted by theorists. Although many measurements using metal smokes produced by evaporation in noble gas atmosphere were made by many workers, the results were affected by unwanted anomalous absorption enhanced by several orders of magnitude with respect to the prediction of the simple electromagnetic model. Such enhanced absorption is explained by the clustering, size-distribution, and surface-oxidation of microcrystals, but it is not easy to confirm the validity of these explanations. The purpose of this work is to examine the universality of such explanations. In the report [1], we reported already the preliminary results on far-infrared absorption by nickel- and copper microcrystals embedded into polyethylen. In the present study, the effects of the metal volume fraction and the oxidation on far-infrared absorption were studied in detail.

The experimental results on the nickel- and copper microcrystals/polyethylen composites may be summarized as follows.

(1) Far-infrared absorptions of these composites are linear in the metal volume fractions ranging from 0.001 to 0.03.

(2) Far-infrared absorptions of these composites are almost independent on temperature ranging from 15 K to room teperature.

(3) Progress of the oxidation of metal microcrystals scarcely enhances the far-infrared absorption in these composites and the absorption is scarcely dependent on the different kinds of oxide coating on the surface of the microcrystals.

These results suggest that the anomalous far-infrared absorption does not come from the oxide coating, but comes from some kind of electron-tunneling interaction between adjacent microcrystals.

A more detailed study of the far-infrared properties on nickel- and copper microcrystals/polyethylen composites will be made in a separate paper [2].

References

[1] S. Mochizuki and K. Ishi, UVSOR ACTIVITY REPORT 1988, p. 124

[2] S. Mochizuki, K. Ishi, and A. Johgo, submitted to "physica status solidi (b)" on 3 Nov. 1989.

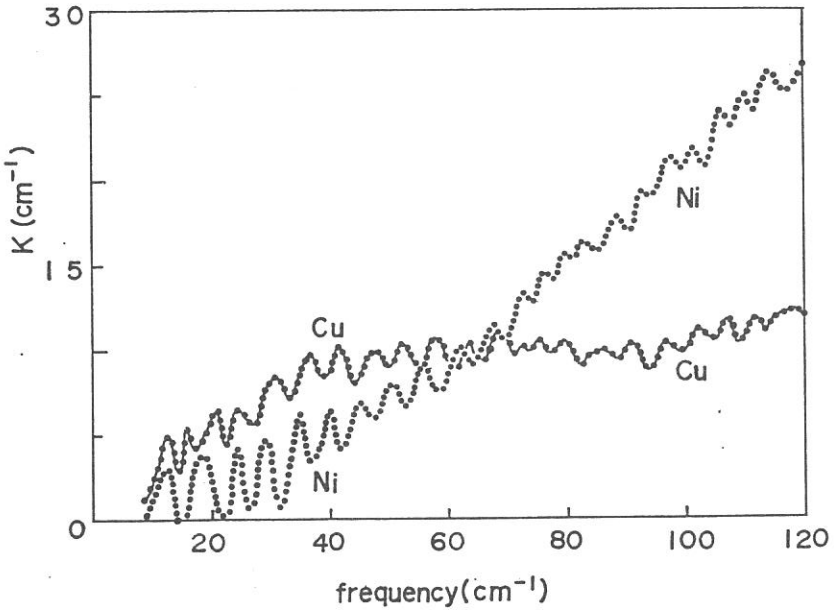

Fig. 1 Far-infrared absorption spectra of naturally-oxidized microcrystals/polyethylen composites with the metal-filling factor of 0.01. These spectra were almost independent on temperature ranging from 15 K to room temperature and on oxide-coating. The nickel- and copper microcrystals are quasi-spheres with the average radius of 10.5 and 25.0 nm, respectively.

FAR-INFRARED SPECTRA OF HYDROGEN-BONDED FERROELECTRICS KH_2PO_4(KDP) AND $PbHPO_4$(LHP)

Shik SHIN, Yuki CHIBA, Astushi SUGAWARA, Yasuhisa TEZUKA, and Mareo ISHIGAME

Research Institute for Scientific Measurements,
Tohoku University, Aobaku, Sendai 980

The phase transition mechanism of the hydrogen-bonded ferroelectrics KH_2PO_4(KDP) and $PbHPO_4$(LHP) has been studied by a lot of experiments.[1] The Raman spectra show the soft modes for both compounds in the very low frequency region, while relaxational central modes are also seen in the Raman spectra. On the other hand, hyper-Raman spectra show only relaxational central modes. In this study, our aim is to observe the soft modes and central modes for both compounds by means of infrared measurement. From the selection rule,[1] infrared measurement will show the similar results as the hyper-Raman measurements, rather than the Raman measurements.

The far infrared spectra of KDP and LHP were measured at the beam-line BL6A in the frequency region from 5 to 250 cm^{-1}.

Figure 1 shows the reflectivity spectra of LHP which were measured in the temperature below the phase transition temperature(T_c). It is found that the lattice mode below 100 cm-1 becomes soft, as the temperature decreases. By the Kramers-Kronig analysis, the frequency(ω_I) becomes low from about 60 cm-1 at 260 K to 40 cm-1 at 300 K, as shown in Fig.2.[2] These results are consistent with the results of Raman measurement(ω_R, open circles) and spontaneous polarization P_s measurement(small closed circles),[3] but are inconsistent with the hyper-Raman measurements. It is curious that the strong central modes which are seen in the hyper-Raman spectra can not been found in the infrared spectra.

Figure 3 shows the reflectivity spectra of KDP. These spectra are consistent with the spectra which have been measured by many workers.[4] The reflectivity spectra below 100 cm^{-1} show the central modes. These spectra have been analyzed by the over-damped mode.[4] However, the hyper-Raman spectra[5] suggest that these spectra are the relaxational type central modes. The ε spectra were also obtained by the Kramers-Kronig analysis in this study. However, it is not clear whether the ε spectra of KDP show the relaxational mode or the over-damped lattice mode. The careful line shape analysis will be needed for the ε spectra.

References

1.S.Shin and M.Ishigame, Solid State Physics(in Japanese), 24(1989)297.
2.D.J.Lockwood, N.Ohno, M.H.Kuok and H.Arend, J.Phys.C19(1986)L233.
3.S.Shin, M.Ishigame, K.Deguchi and E.Nakamura, Solid State Commun.65(1988)749.
4.for example, P.Simon, F.Gervais and E.Courtens, Phys.Rev.B37(1988)1969.
5.S.Shin, A.Sugawara, Y.Tezuka and M.Ishigame, Solid State Commun.71(1989)685.

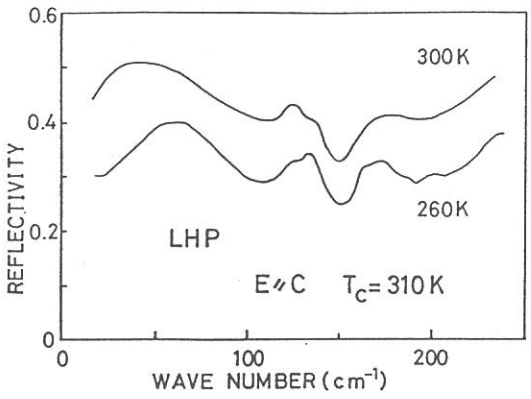

Fig.1

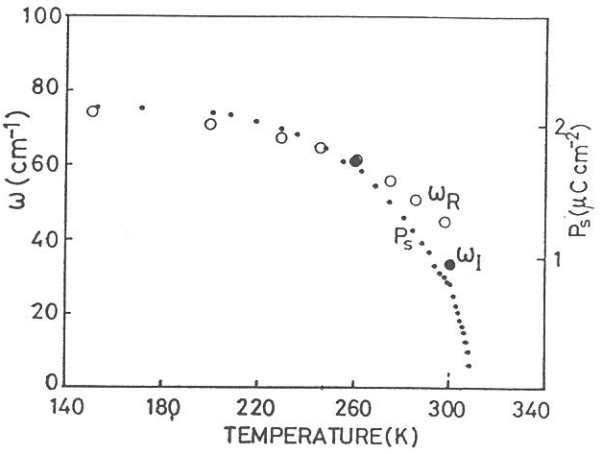

Fig.2

Fig.1
The reflectance spectra of LHP measured at 260 K and 300 K.

Fig.2
The temperature dependence of the soft-mode frequency which are measured by the infrared reflection and the Raman[2)] scattering.

Fig.3
Temperature dependence of the reflectance spectra of KDP.

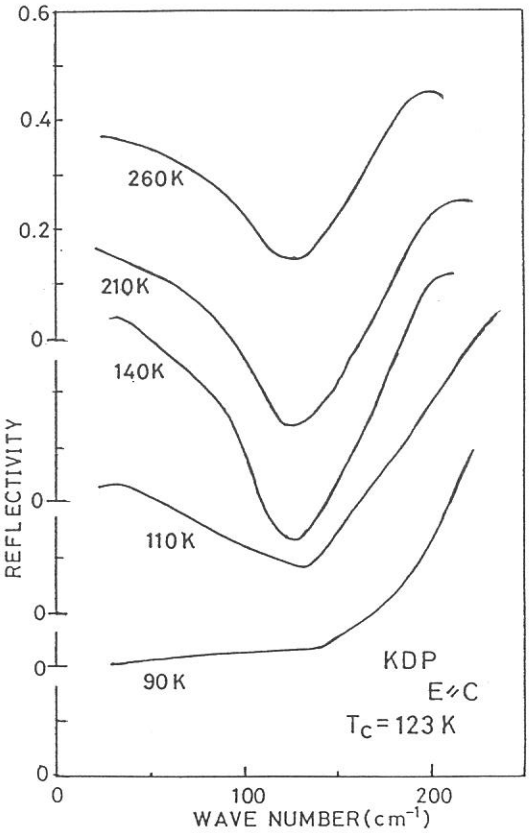

Fig.3

EFFECT OF PRESSURE ON THE INTERACTION-INDUCED FAR-INFRARED ABSORPTION OF LIQUID CARBON TETRACHLORIDE AND LIQUID BENZENE

Yoshitaka FUJITA and Shun-ichi IKAWA

Department of Chemistry, Faculty of Science, Hokkaido University, Sapporo 060

Transient dipole moments that are induced during molecular collisions in the liquid state give rise to absorption of radiation in the far-infrared region. It provides the major part of far-infrared absorption of non-dipolar liquids. Effect of pressure on these spectra will be useful for elucidating how the transition dipole moment is induced and how it decays with time.

In this study, we have measured the far-infrared absorption of liquid carbon tetrachloride and liquid benzene at pressures from 1 bar to 1.1 kbar at 25°C. The pressure cell used was described previously.[1] Figure 1 shows examples of spectra of carbon tetrachloride at 1 bar and 1.1 kbar. The absorption coefficients, α, were obtained from the observed transmission spectra by correcting for the effect of multiple reflection inside the cell. Broad bands around 45 cm^{-1} are assigned to the collision-induced absorption. On their high frequency side, wings of intramolecular vibrational bands overlap. This overlap was resolved by least square fitting, representing the collision-induced band and the intramolecular bands by a function $\nu^2/(a+b\nu^2+c\nu^4+d\nu^6)$ and Lorentzian functions, respectively. The collision-induced bands obtained were shown by broken lines in Fig. 1 and their moments were plotted against pressure in Fig. 2. The zeroth moment is proportional to the mean square amplitude of the transition dipole moments and the second moment is related to their decay, which is induced by the translational and rotational motion of molecules. Both moments increase approximately linearly with increasing pressure.

Figure 3 shows observed spectra of liquid benzene at several pressures. Recently, Mrozek et al.[2] reported that the far-infrared absorption of liquid benzene under pressure possessed a structure resembling that of the solid. Their spectra showed marked peaks around 68, 87, and 112 cm^{-1}. On the contrary, the present spectra do not show any structure like theirs. The shoulder around 135 cm^{-1} is due to crystalline quartz used as a window of a bolometer detector. Correction for the multiple internal reflection and moment analysis on the benzene spectra are now in progress.

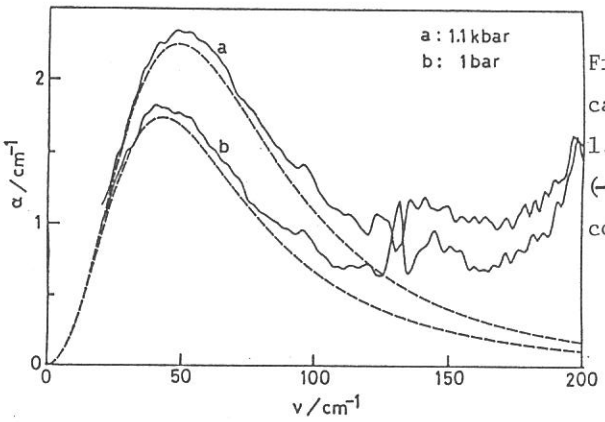

Fig. 1 Far-infrared spectra of carbon tetrachloride at 1 bar and 1.1 kbar. (——) experimental and (- - -) calculated absorption coefficients.

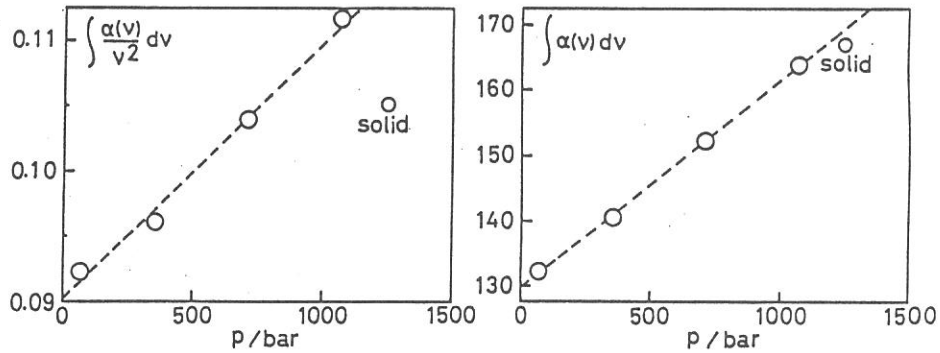

Fig. 2 Zeroth(left) and second(right) moments of the collision-induced spectra of liquid carbon tetrachloride plotted against pressure.

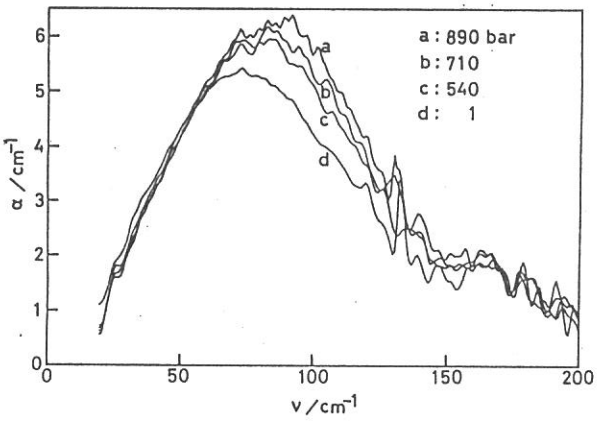

Fig. 3 Far-infrared spectra of liquid benzene at several pressures.

References

1) Y. Fujita, T. Ohba and S. Ikawa, UVSOR Activity Report 1988, p122.

2) R.C.F. Mrozek, W.F. Sherman and G.R. Wilkinson,Mikrochim. Acta, II, 349 (1988).

REFLECTIVITY OF HIGH T_c SUPERCONDUCTOR $Bi_2Sr_2Ca_{1-x}Y_xCu_2O_8$

Xiao-lei WANG, Takao NANBA, Toshiharu TAKAHASHI, Shigeru YASUDA, Fumitaka ARAI, Mikihiko IKEZAWA, Hiroshi YOSHIDA, Takashi TAKAHASHI, Takashi SUZUKI and Tadao KASUYA

Department of Physics, Tohoku University, Sendai 980, Japan

We have grown single crystals of $Bi_2Sr_2Ca_{1-x}Y_xCu_2O_8$ with the Y concentrations of x=0, 0.15, 0.25, 0.50, 0.75 and 1.00. The concentrations of free carriers in the crystals were found to be controlled well by doping of Y and the observed dc conductivity of these crystals was as follows: The sample of x=0 was an ordinary high T_c superconductor with T_c at about 85 K and the temperature dependence of the conductivity was metallic above T_c. The samples with $x \geq 0.5$ were semiconductors and the conductivity decreased at low temperature. The temperature dependences of the conductivity of the samples of x=0.15 and 0.25 were complicated and above 85 K they showed an intermediate behavior between those of the metal and the semiconductor.

The reflectivity spectra were measured at room temperature in the far-infrared region at BL6A1 and also in the photon energy region from 0.01 to 30 eV. A part of the results are shown in Figs.1 and 2. The spectra of the samples of x=0, 0.15 and 0.25 show a sharp rise at about 1 eV. On the other hand, spectra of $x \geq 0.5$ are semiconductor-like, which showed some structure due to phonons in the infrared region but are almost flat in the far-infrared region. The result shows that the carrier concentrations in these samples were so small that the Drude edge of the reflectivity is not seen even in the far-infrared region.

By the Kramers-Kronig analysis of the reflectivity spectra, absorption spectra were calculated. At about 1.8 eV in the visible region, an absorption peak was found to grow with the concentration of Y. The absorption is interpreted to be due to the transition of the charge transfer type between the orbitals of Cu and O.

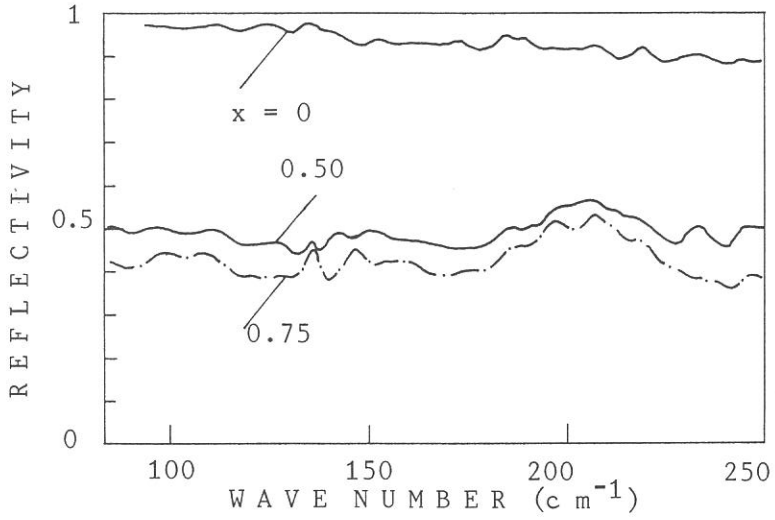

Fig.1 Reflectivity spectra in the far-infrared region.

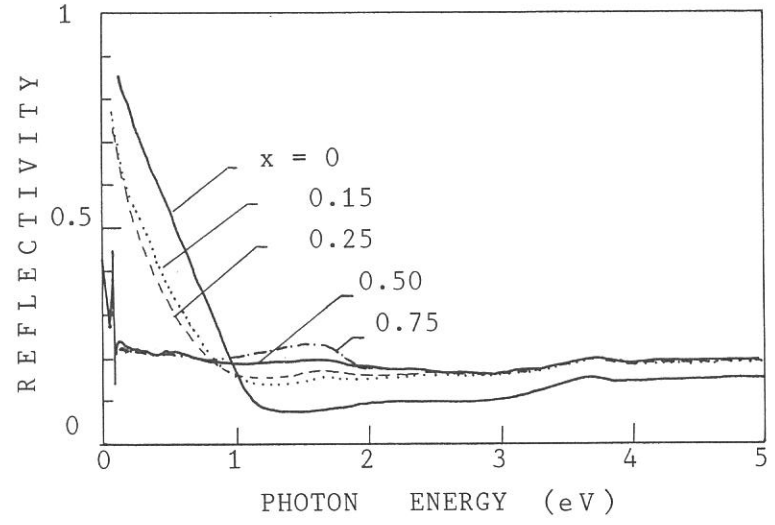

Fig.2 Reflectivity spectra in infrared and visible regions.